MANUFACTURED NANOPARTICLES: ASSESSING THE MOBILITY OF A FUTURE CLASS OF CONTAMINANT IN GROUNDWATERS

by

BRYONY JANE ANDERSON

A thesis submitted to the University of Birmingham for the degree of
DOCTOR OF PHILOSOPHY

School of Geography, Earth
& Environmental Sciences
University of Birmingham
October 2014

ABSTRACT

Estimating manufactured nanoparticle mobility using fast, simple methods could form a useful part of a risk assessment tool. The aim of this work was to investigate whether zeta potential could be used for this purpose.

Using a new surface zeta potential measurement technique, the surface zeta potential of a 50m sandstone sequence was found to vary little with lithofacies when chemical conditions were kept constant. A surface area modified linear mixing model was able to describe the sandstone zeta potential, suggesting that clay minerals are the dominant control on bulk properties.

The sandstone and silica nanoparticle zeta potentials were sensitive to the chemical composition and pH of the surrounding fluid, which was influenced by ion exchange and carbonate dissolution. The zeta potential of the sandstone and nanoparticles can be used to qualitatively describe the relative mobility under different chemical conditions.

Calculations using DLVO and colloid filtration theory (CFT) can reproduce the equilibrium concentration (C'/C_0) values observed experimentally, however the significant tailing in the breakthrough curve is not described by this traditional particle transport model. Further work is required to determine whether DLVO and CFT can be used as part of a mobility screening tool, as this initial study suggests.

ACKNOWLEDGEMENTS

TABLE OF CONTENTS

LIST OF FIGURES

LIST OF TABLES

Nomenclature

Symbols

a	Particle diameter
$a_i\,a_j$	radii of differently sized particles, i and j
a_c	Porous media grain (collector) radius
a_p	Particle radius
A_{132}	Hamaker constant
A_S	Neighbouring grains parameter $= 2(1 - \gamma^5)/(2 - 3\gamma + 3\gamma^5 - 2\gamma^6)$
c	Molar concentration of ion
C	Effluent concentration
C_0	Influent concentration
d_c	Porous media grain (collector) diameter
D	Diffusion coefficient $= kT/(6\pi\mu a_p)$
e	Electron charge
E	Electrical field strength
E_S	Streaming potential
$f(\kappa a)$	Henry correction factor
F	Faraday's constant
g	Acceleration due to gravity
h	Separation distance
I	Ionic Strength $= \frac{1}{2}\sum cz^2$
k	Boltzmann constant
k_{att}	Attachment/deposition rate constant
k_{det}	Detachment rate constant
L	Column length
n	Number of particles per unit volume
N_A	Avogadro's constant
N_G	Dimensionless gravity number $= 2a_p{}^2(\rho_p - \rho_f)g/(9\mu U)$
N_{LO}	Dimensionless London van der Waals number $= A_{132}/(9\pi\mu a_p{}^2 U)$
N_{PE}	Dimensionless Peclet number $= U(2a_c)/D$
N_R	Dimensionless relative size number $= a_p/a_c$
P	Pressure
r	Radius
R	Gas constant
S	Particle concentration attached to the solid
T	Absolute temperature
u	$2h/(a_i + a_j)$

u_E	Electrophoretic mobility
u_{EO}	Electro-osmotic mobility
U	Fluid approach velocity
v	Average particle velocity
v_{eo}	Electro-osmotic velocity
V_{EDL}	EDL interaction energy
V_{max}	Energy barrier height
V_{vdW}	van der Waals interaction energy
V_T	Total interaction energy
W	Stability ratio
x	Transport distance
z	Ionic charge number or valence

Greek letters

α	Collision efficiency
α_D	Dispersivity
γ	$(1-\theta)^{1/3}$
ε_0	Permittivity of free space
ε_r	Relative permittivity
ζ	Zeta potential
η	Collector efficiency
θ	Porosity
κ	Debye parameter
κ^{-1}	Debye length
λ	Characteristic wavelength
λ_0	Solution conductivity
λ_S	Surface conductivity
μ	Fluid viscosity
ρ_b	Dry bulk density
ρ_f	Fluid density
ρ_p	Particle density
ψ	Potential at the Stern plane
ω	$\sqrt{v + 4k_{att}D}$

List of abbreviations

CFT   Colloid filtration theory
EDL   Electrical double layer
ppm   parts per million
SS-EFM   Single Surface Electro-osmotic Flow Mapping
vdW   van der Waals

Glossary of key terms

Collector efficiency   The likelihood of a particle in a given dispersion approaching a porous media grain (collector)

Collision efficiency   The fraction of collisions between a particle and collector which are 'successful' and form an attachment

Debye length   Thickness of the electrical double layer

Electrical double layer System produced in an electrolyte solution around a charged particle; consists of the charged surface and a diffuse layer of counter-ions

Electro-osmotic mobility The velocity per unit electrical field strength of the liquid parallel to a solid surface upon which a current is being applied

Electrophoretic mobility The velocity per unit electrical field strength of a particle dispersion upon which a current is being applied

Hamaker constant   A value used in describing the van der Waals interaction energy, derived from the summation of molecular forces between all atoms of the interacting materials

Laser Doppler velocimetry Measuring particle velocity using the Doppler shift in a laser beam passing through a dispersion

Nanoparticle   Particles with at least one dimension in the size range 1-100nm

Shear plane   Surface of separation between the bulk fluid and the stationary fluid around a dispersed particle

Zeta potential   Potential at the shear plane

1 INTRODUCTION

1.1 Background

Manufactured nanoparticles are particles with at least one dimension in the size range 1-100nm which have been developed and produced for a specific purpose. At the nanometre scale materials display different properties than those of the bulk material, and these specialist properties are of interest to many industries, from sports equipment to medicine and electronics. Over 1800 products containing nanotechnology are currently listed in the Wilson Centre Consumer Products Index, and with global investment already in the multiple billions of US dollars and development, production and use set to rise considerably in the coming decades, manufactured nanoparticles are almost certainly an important part of our future (Roco and Bainbridge, 2005).

With this increase in production comes an increased risk of accidental release into the environment, including the subsurface environment. The level of risk to public health and ecosystems is linked to nanoparticle toxicity and mobility. Recent reviews of exposure studies indicate that manufactured nanoparticles can cause biological effects in microbes and algae, aquatic invertebrates and fish, in some cases at ppm concentrations (Navarro et al., 2008, Scown et al., 2010). It is therefore important to assess the potential mobility of this potential class of contaminant in groundwater in order to protect drinking water resources and indigenous bacterial communities.

Transport studies have been undertaken by many researchers to assess the likelihood of nanoparticle mobility under controlled conditions. The majority of studies have been undertaken using artificial porous media (often glass beads, for example Elimelech and

O'Melia, 1990a, b; Franchi and O'Melia, 2003; Hahn et al., 2004, or clean quartz sand, e.g. Zhuang et al., 2005; Pelley and Tufenkji, 2008) packed into columns, with very few studies using intact natural material. Chemically cleaned, packed material is a simplified porous medium that allows the main transport and retention mechanisms to be investigated conveniently; however it is vital to begin to understand nanoparticle mobility in real rock systems where the increased heterogeneity and presence of natural fabrics could have a significant effect on transport. A number of studies comparing laboratory column breakthrough to field tests found that the most significant factor affecting column study results was the packing of aquifer material, with one finding that there was increased straining in repacked columns (Harvey et al., 1993, Bales et al., 1997, Higgo et al., 1993). Mobility in the environment may be more closely predicted using intact aquifer material in laboratory studies.

Intact rock has been used in a small number of studies (e.g. Neukum et al., 2014), with some of this previous work having been undertaken at the University of Birmingham on redbed sandstone columns (e.g. Rahman, 2006; Anderson, 2008; McMillan, 2010). This previous work has focussed on the interaction of individual nanoparticles with a rock column. While this type of study is very important, there are such a huge number of manufactured nanoparticle types that assessing the mobility of each one with different geologies would be impossible. Therefore a screening method, perhaps based on models developed on artificial porous media, would be useful for a first look at mobility.

Due to its importance to nanoparticle interaction, aggregation and attachment to porous media, zeta potential, a measure of the electrical potential of particle and other surfaces, could provide a good way to estimate the likely mobility, perhaps as part of a transport

2

calculation (e.g. using Colloid Filtration Theory [CFT] calculations, see Chapter 2). It may also offer a method of assessing if nanoparticle surface properties change with time and after contact with rock material, which is important as current models often consider the interaction energy between particles and porous media to be constant.

The zeta potential of both the nanoparticle and the aquifer material surface are needed in order to determine interactions. This study coincides with the development of a new technique to measure the zeta potential of solid surfaces by Malvern Instruments (Corbett et al., 2012). The new Single-Surface Electroosmotic Flow Mapping (SS-EFM) technique measures the surface zeta potential at a smaller scale than previously possible, allowing assessment of zeta potential heterogeneity at a millimetre scale.

As this is a new technique untested on environmental materials, this study would need to 1) show that the new method was applicable to rock surfaces; 2) acquire a dataset and then 3) test predictions made using these measurements on real rock systems.

1.2 Overall aim, and objectives

The overall aim of this study is to determine if zeta potential can be used as the basis for assessing the mobility of nanoparticles in sandstone groundwaters. To achieve this, the following objectives must be met:

1. evaluation of the dependence of nanoparticle mobility on zeta potential according to current theories

2. assessment of the applicability to rocks of a new Malvern Instruments method for measuring the zeta potentials of surfaces

3. measurement of the variation in rock surface zeta potential through an example rock

4. determination of the dependencies of particle and rock surface zeta potentials on chemical conditions

5. testing of traditional nanoparticle transport theory on transport of nanoparticles through rock intact rock columns using measured zeta potential and other properties.

1.3 Approach

The structure of the project is indicated by the objectives listed in Section 1.2. Initially the dependencies of the CFT will be explored, with an emphasis on sensitivity to zeta potential values. Next the methods used will be described, including an assessment of whether the new Malvern Instruments surface zeta potential technique is applicable to rock surfaces. Following this, the zeta potential of a typical redbed sandstone sequence will be determined under a range of possible chemical conditions, focussing on chemical composition of the solution. These zeta potential measurements will lead to predictions of likely transport behaviours, which will be tested using laboratory transport experiments (as field experiments are not allowed in the UK, as decided by the Environment Agency following the suggestions made by Royal Society and the Royal Academy of Engineering, 2004). This work will consider whether zeta potential can be used to assess nanoparticle mobility in a typical sandstone aquifer and if so, what other research needs to be carried out before the technique can be employed.

1.4 Thesis Structure

A brief background to the theory of particle transport models developed on artificial materials will be presented in Chapter 2; this will provide a theoretical basis for the following chapters, and quantify the importance, as indicated by colloid filtration theory,

of zeta potential and other variables to nanoparticle mobility in porous media. In Chapter 3 the SS-EFM technique is introduced and tested on mica surfaces, moving onto sandstone and the assessment of zeta potential of a single sandstone bed. In Chapter 4 the measurements of sandstone surface zeta potential are extended to a full sequence, with samples of various lithofacies taken from a 50m length of sandstone core. Following this, sandstone zeta potential is measured under a range of chemical conditions. Chapter 5 describes the results of intact sandstone column studies and discusses mobility of particles in sandstone with reference to zeta potential measurements taken during the experiments and in previous chapters. The transport models are tested here using surface and nanoparticle zeta potential in an attempt to predict particle behaviour in a rock column. The thesis is concluded in Chapter 6 with a summary of the results gained and recommendations for further research.

2 THEORETICAL BACKGROUND

2.1 Introduction

There is a large and increasing investment in manufactured nanoparticle development, which could lead to a huge variety of nanoparticle types being used more frequently. The use of nanoparticles increases the risk of exposure of the subsurface environment to this potential contaminant. It is important to know if nanoparticles are mobile in groundwater, however an individual assessment of each particle type with different geologies is not possible before industrial scale production and use is likely to begin. Therefore, it is important to investigate the potential for a nanoparticle mobility screening method.

As zeta potential is important in determining the type of interaction particles may experience with other particles and with porous media surfaces, it could form the basis for this screening method. The method could also be based in traditional particle modelling developed over the past decades. These modelling attempts use theories of particle interaction and transport which are important to introduce before continuing.

2.2 Aims

- To present the background theory to nanoparticle transport modelling;
- To demonstrate that zeta potential is an important parameter within this theory and could, therefore, form the basis of a mobility assessment method.

2.3 The solid-liquid interface

2.3.1 The electrical double layer

When a solid surface comes into contact with an aqueous electrolyte solution a surface charge develops. This can occur by several means, the principle methods being from mineral lattice imperfections, ionisation of surface groups and ion adsorption or dissolution due to differences in affinity of the solid or liquid phase for particular ions (Stumm et al., 1992, Elimelech et al., 1995, Hunter, 1981).

The surface charge must be balanced by a charge in the solution so counter-ions are attracted towards the surface, with thermal motion distributing these counter-ions in a diffuse manner (Stumm et al., 1992). A double layer system is then formed, of a charged surface and a diffuse layer of counter-ions. The potential distribution in this diffuse layer was first and most simply described by the Gouy-Chapman model, as an exponential decrease from the surface potential to the potential of the bulk solution. Later additions to this theory by Stern take account of the finite size of ions in solution and specify inner and outer parts of the diffuse layer. There is a decrease in potential in the inner Stern layer, where only specific adsorption may occur, to that of the Stern plane, where follows an exponential decay of potential in the outer part of the diffuse layer (as in the Gouy-Chapman model, Elimelech et al., 1995; Shaw, 1992). There are several limiting assumptions of these models, one being that the surface is flat and infinite.

The Poisson-Boltzman expression is solved analytically to quantify the potential at a point from the surface, and there is an analytical solution for a spherical particle interface with an electrolyte, and where the Debye length is small compared to the

particle radius the calculations for a flat surface system can be used (Elimelech et al.,
1995).

The Debye length, often known as the double layer thickness, can be calculated using:

$$\kappa^{-1} = \sqrt{\frac{\epsilon_r \epsilon_o RT}{2F^2 I}} = \sqrt{\frac{\epsilon_r \epsilon_o kT}{2e^2 N_A I}}$$
Equation 2-1

where ϵ_r is the relative permittivity, ϵ_o the permittivity of free space, R is the gas
constant, k is the Boltzmann constant, T is absolute temperature, F is Faraday's constant,
e is electron charge, N_A is Avogadro's constant and I is ionic strength (Shaw, 1992,
Hunter, 1981).

2.3.2   Electrokinetic phenomena

When a charged solid moves relative to an electrolyte solution, a surface of shear
develops, within which there is a fixed part of the double layer that moves with the solid.
The shear plane is generally considered to be slightly further from the solid surface than
the Stern plane, somewhere in the outer diffuse part of the double layer (Figure 2-1)
(Elimelech et al., 1995, Shaw, 1992). The potential at this surface is the zeta potential.
The zeta potential is particularly important as it is the best description of the "effective
potential", the potential at the start of the diffuse layer which will most directly affect
particle interactions with other particles and surfaces (Hunter, 1993).
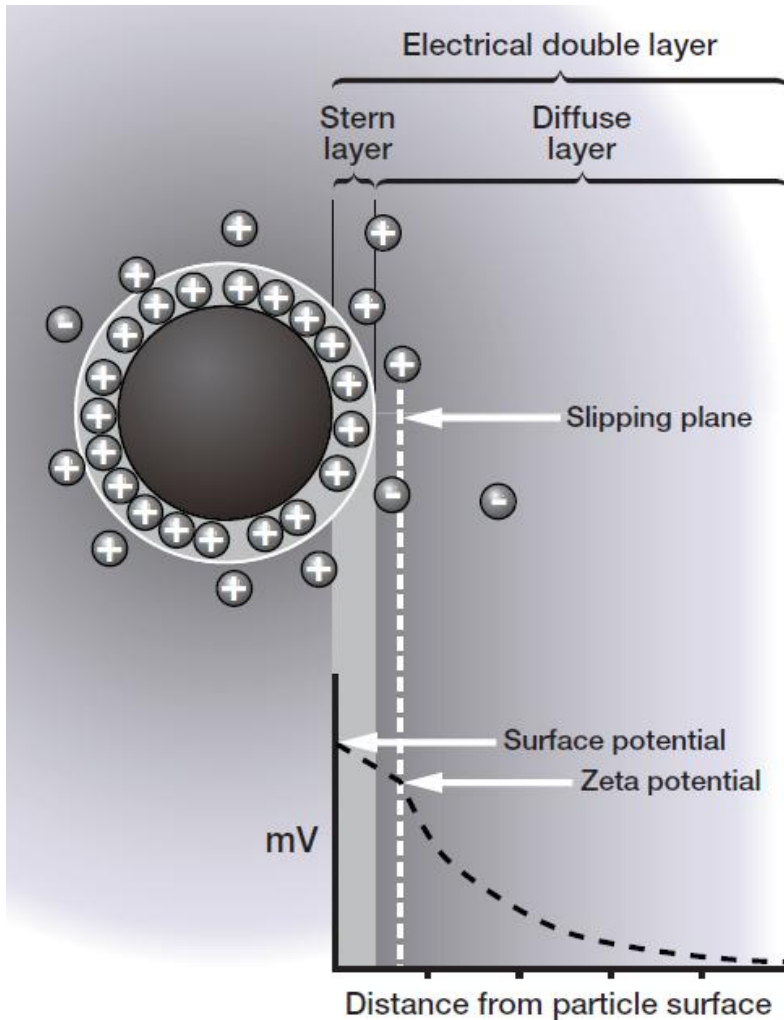
Figure 2-1 A diagram of the electrical double layer showing the relative position of the shear plane (called the slipping plane here) and the zeta potential (Malvern Instruments, 2013).

There are three main electrokinetic phenomena (Delgado et al., 2007):

1. Electro-osmosis, where a current is applied across an immersed surface sample and the movement of fluid under the influence of the surface charge of the solid is measured;

2. Streaming potential, where the fluid is forced to move along the surface and the induced potential difference or current is measured; and

3. Electrophoresis, where a charge is applied across a particle dispersion and the movement of charged particles within this dispersion is observed.

In electro-osmosis, the electro-osmotic velocity is measured; the electro-osmotic velocity (v_{eo}) is the velocity of the liquid parallel to a solid surface upon which a current is being applied. It can be related to zeta potential (ζ) by:

$$\frac{v_{eo}}{E} = u_{EO} = \frac{\varepsilon_r \zeta}{\mu} \qquad\qquad \text{Equation 2-2}$$

where E is the electric field strength applied (calculated from measured values of current and electrolyte conductivity); ε_r is the relative permittivity of the electrolyte; and μ is the fluid viscosity. u_{EO} is electro-osmotic mobility, or electro-osmotic velocity per unit applied electrical field strength (Hunter, 1981, Elimelech et al., 1995, Hunter, 1993). This equation is valid when κa >>1 (Delgado et al., 2007), where κ is the reciprocal of the Debye length and a is particle diameter.

Streaming potential is often used to measure the zeta potential of porous media. The derivation of the relationship is based on fluid being forced through a single capillary which causes a potential difference between the two ends of the capillary to develop. This potential difference is called the streaming potential (E_S) and is related to zeta potential using:

$$\frac{E_S}{\Delta P} = \frac{\varepsilon_r \zeta}{\mu(\lambda_0 + 2\lambda_S/r)} \qquad\qquad \text{Equation 2-3}$$

where ΔP is the pressure difference between the two ends of the capillary, λ_0 is solution conductivity, λ_S is surface conductivity and r is the tube radius (Hunter, 1981, Elimelech et al., 1995, Hunter, 1993).

During an electrophoresis measurement the electrophoretic mobility of charged particles is measured, which is the induced particle velocity per unit applied electric field strength. Zeta potential can be calculated from the electrophoretic mobility using:

$$u_E = \frac{2\varepsilon_r \zeta}{3\mu} f(\kappa a)$$
Equation 2-4

where $f(\kappa a)$ is the Henry correction factor. $f(\kappa a)$ ranges from 1 to 1.5 as κa scales from 0 to ∞ (Hunter, 1981, Elimelech et al., 1995, Hunter, 1993).

If the double layer thickness is small compared with the particle diameter, i.e. $\kappa a \gg 1$, then the Smoluchowski approximation can be used:

$f(\kappa a)=1.5$
Equation 2-5

This is usually the case for the particle and electrolyte combinations encountered during this study. In a very low ionic strength solution the double layer thickness can increase to the point where κa approaches zero and the Huckel approximation should be used, where:

$f(\kappa a)=1$
Equation 2-6

In Equations 2-4, 2-5 and 2-6, κ is the reciprocal of Debye length, or double layer thickness (see Chapter 2), and a is particle diameter.

It is assumed during the derivations of the above calculations that the solution permittivity and viscosity are constant and equal to the bulk solution values (Hunter,

1981). In the measurements carried out during this study the viscosity value is assumed to be equal to that of water at the appropriate temperature.

2.4 Interactions between particles and particles with surfaces

2.4.1   DLVO

Traditional DLVO theory (named after the two groups of investigators who proposed the theory, Deryagin and Landau in 1941 and Vervey and Overbeek in 1946-48) describes the interaction of particles and of particles with surfaces in terms of interaction energy with distance of approach. Nanoparticle stability is described quantitatively as the sum of the van der Waals (vdW) and electric double layer (EDL) interactions (Petosa et al., 2010), i.e.:

$$V_T = V_{vdW} + V_{EDL}$$ Equation 2-7

2.4.2   van der Waals (vdW) interaction energy

van der Waals forces arise from electromagnetic interactions between bodies; they are independent of the zeta potential of the surfaces and ionic strength of the solution (Stumm and Morgan, 1996). Under most circumstances, van der Waals forces are attractive (they can, however be repulsive for some rare conditions where negative Hamaker constants are observed, e.g. Lee & Sigmund, 2001). A number of different calculations to estimate vdW interactions are available in the literature (e.g. Elimelech et al., 1995); Equation 2-8 can be used to calculate the vdW interaction energy between a sphere and a flat plate:

$$V_{vdW} = -\frac{A_{132} a_p}{6h(1+14h/\lambda)}$$ Equation 2-8

where A_{132} is the Hamaker constant for the particle-solution-surface system, a_p is the particle radius, h is the separation distance and λ is the characteristic wavelength (Hahn and O'Melia, 2004, Petosa et al., 2010, Gregory, 1981).

The theory states that the Hamaker constant of a system can be estimated using the geometric mean of the Hamaker constants of the individual materials and separating medium measured in a vacuum (Petosa et al., 2010, Farmakis et al., 2006):

$$A_{131} = \left(A_{33}^{1/2} - A_{11}^{1/2}\right)^2 \hspace{4cm} \text{Equation 2-9a}$$

$$\boldsymbol{A_{132}} = \left(\boldsymbol{A_{11}^{1/2}} - \boldsymbol{A_{33}^{1/2}}\right)\left(\boldsymbol{A_{22}^{1/2}} - \boldsymbol{A_{33}^{1/2}}\right) \hspace{2cm} \text{Equation 2-9b}$$

where Equation 2-9a is used to estimate the constant for aggregation of the same material and Equation 2-9b the constant for one material depositing on another. Subscript 1and 2 refer to the relevant materials of differing composition and 3 is the separating medium. A_{xx} is the constant for a single material in a vacuum.

2.4.3 Electric double layer (EDL) interaction energy

As two particles approach or a particle approaches a surface, the two diffuse double layers interact. If the surfaces have charges of the same sign a repulsion will develop: this is the most likely scenario in groundwater systems as most solids are negatively charged under typical freshwater conditions (Elimelech et al., 1995).

As with vdW interactions, there are a number of different calculations to evaluate the EDL interaction energy that can be found in the literature (e.g. Elimelech et al., 1995). Equation 2-9 can be used to calculate the EDL interaction energy between a sphere and a flat plate:

$$V_{EDL} = \pi\epsilon_0\epsilon_r a_p \left\{ 2\psi_1\psi_2 ln \left[\frac{1+exp(-\kappa h)}{1-exp(-\kappa h)}\right] + (\psi_1^2 + \psi_2^2)ln[1 - exp(-2\kappa h)]\right\}$$

<div align="right">Equation 2-10</div>

where ψ is a 'reduced' surface potential, which represents the potential at the Stern plane. Assumptions of this model include surface potentials of between +/-60mV, $\kappa\alpha$>5 and a symmetrical electrolyte (Hahn and O'Melia, 2004, Hogg et al., 1966).

Zeta potential measurements form an integral part of determining the EDL repulsion, as they are commonly used as a replacement for ψ in Equation 2-10, as the latter is difficult to measure (Hunter, 1993). This is supported by zeta potential measurements giving a very good indication of the particle dispersion stability to aggregation, which would be determined by the repulsive forces between the particles (Hunter, 1981).

2.4.4   *Effect of zeta potential on the energy diagram*

The total energy diagram is the total interaction energy (Equation 2-7) plotted with separation distance of two interacting bodies. It is conventional to present energy in units of kT, which is the interaction energy in joules divided by the Boltzmann constant and absolute temperature. The diagram has three significant parts; 1) the energy barrier, 2) the primary minimum and 3) the secondary minimum, all of which are demonstrated in Figure 2-2 which was calculated using Equations 2-7, 2-8 and 2-10. Not all systems have an energy barrier or secondary minimum. The primary and secondary minima exist due to a dominance of the vdW attractive forces at that separating distance and are points where aggregation or attachment can occur. The energy barrier in the Figure 2-2 example indicates that EDL repulsion is dominant at intermediate separation distances (Overbeek, 1977) and is a barrier to movement into and out of the primary

minimum. The primary minimum is so deep that attachments made here are often

considered permanent, while attachments in the secondary minimum are considered

reversible, as attachments made here can be easily overcome and the secondary

minimum can be removed by lowering the ionic strength (Hahn et al., 2004, Hahn and

O'Melia, 2004).

The interaction energy is sensitive to zeta potential, amongst other factors. For example,

in the case of Figure 2-2, a change of 10mV in zeta potential of both the particle and

surface causes a dramatic difference in the total energy curve, with the energy barrier to

attachment increasing as the zeta potential becomes more negative.
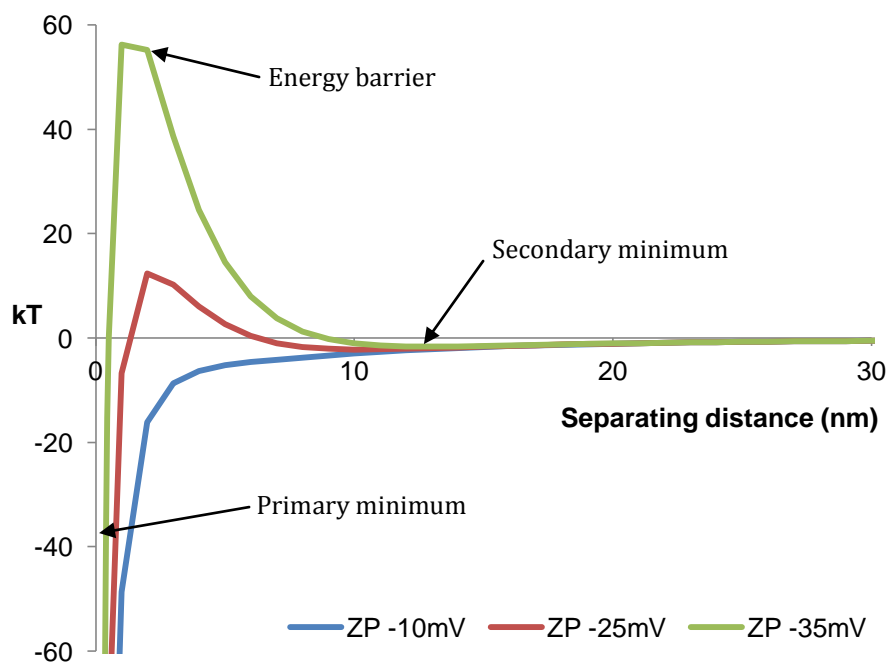
Figure 2-2 Total interaction energy for three zeta potentials with a 20mM ionic strength, particle radius of 100nm and Hamaker constant of 2E-20J

The ionic strength of the electrolyte solution and the valence of the constituent ions also

have an important role in particle-particle and particle-surface interactions. They both

influence the double layer thickness and the zeta potential; as ionic strength and valency

increase, the double layer thickness decreases and zeta potential values move closer to zero. The EDL forces are reduced by these phenomena, with an associated decrease in the energy barrier and increase in the size of the secondary minimum. The secondary minimum in the total interaction energy diagram is not observed at all at low ionic strengths (Hahn and O'Melia, 2004, Hahn et al., 2004).

The shape of the energy interaction curve is also significantly affected by the Hamaker constant, as an increase in the Hamaker constant will linearly increase the vdW attractive force, which means a decrease in the height of the energy barrier and a deepening of the secondary minimum (Hahn and O'Melia, 2004, Hahn et al., 2004).

2.4.5   Non-DLVO forces

DLVO theory considers only vdW and EDL forces in describing interactions between two bodies, however under some conditions there are other measureable forces which contribute to these interactions. These additional interactions include steric interaction, due to the adsorption of polymers or surfactants, and hydration forces, where there is a fluid layer around the particle, both causing additional repulsion (Elimelech et al., 1995). While it is understood that these forces could be present in the transport of silica through a sandstone column, they will not be considered during this project both to simplify the analysis and due to a lack of information on the effects of non-DLVO forces in this system.

2.5 Describing nanoparticle transport and deposition

2.5.1 *Collisions between particles and particles and surfaces*

Aggregation and deposition rates depend on the number of inter-particle or particle-surface collisions which occur, then on the fraction of collisions which successfully produce attachment. Aggregation is important to nanoparticle mobility as aggregates with larger diameters are more likely to be removed from solution by physical straining.

Under favourable conditions, where there is no energy barrier, every collision is successful, or results in attachment. Where the electrical double layer (EDL) interaction energy dominates, attachment will be limited by the size of the total energy barrier. The fraction of successful collisions is often represented by the collision efficiency, α.

2.5.2 *Particle aggregation*

The frequency of particle collisions depends on the physical conditions of the system. In aggregation, particles can collide under the influence of their Brownian motion (perikinetic), as a result of advection and velocity gradients which develop during fluid flow (orthokinetic) or under differential sedimentation of particles (Elimelech et al., 1995, Stumm et al., 1992).

In aggregation, the frequency of collisions can be represented by a second-order rate constant. If the rate constant is expanded and the full Stokes-Einstein equation substituted for the Brownian diffusion coefficient then the kinetics of aggregation of a monodisperse suspension can be represented by Equation 2-11:

$$-\frac{dn}{dt} = \alpha \frac{4kT}{3\mu} n^2 \qquad \qquad \text{Equation 2-11}$$

where n is the number of particles per unit volume of dispersion and t is time (Stumm et al., 1992, Shaw, 1992). Aggregation rates increase with increasing particle size heterogeneity (Stumm et al., 1992).

The collision efficiency represents a reduction in rate and when this is due to van der Waals (vdW) and electrical double layer (EDL) interactions then it is conventional to use the stability ratio, which is the reciprocal of α and given by the Fuchs equation:

$$W = \frac{1}{\alpha} = 2 \int_0^\infty \frac{exp\left(\frac{V_T}{kT}\right)}{(u+2)^2} hu \qquad \text{Equation 2-12a}$$

where:

$$u = \frac{2h}{(a_i+a_j)} \qquad \text{Equation 2-12b}$$

h is the separation distance between particles and a_i and a_j are the radii of particles of unequal size (arising through an initially polydisperse nanoparticle population, aggregation or interactions between different particle populations, e.g. contaminant and indigenous particles) (Elimelech et al., 1995).

A simple approximation to Equation 2-12a can be used to calculate a theoretical value for the collision efficiency (α):

$$\alpha \approx \kappa\left(a_i + a_j\right) exp\left(-\frac{V_{max}}{kT}\right) \qquad \text{Equation 2-13}$$

where V_{max} is the energy barrier height (Elimelech et al., 1995). This value is very sensitive to the height of the energy barrier, and so to the zeta potential, as shown in section 2.4.4.

2.5.3 Particle deposition

Collisions occur between moving particles and a static porous medium surface as a result of three processes: interception due to the particle size; gravitational sedimentation (although this will be less important for individual nanoparticles it may become more important if there is aggregation during transport) and by diffusion towards the grain (Yao et al., 1971). If the collisions are successful then particle attachment will occur, which can either be permanent or reversible.

This particle transport and attachment/detachment can be described using the convective dispersive transport equation:

$$\frac{\partial C}{\partial t} + \frac{\rho_d}{\theta}\frac{\partial S}{\partial t} = D\frac{\partial^2 C}{\partial x^2} - v\frac{\partial C}{\partial x} \qquad\qquad \text{Equation 2-14a}$$

where the kinetics of attachment and detachment are described using first order rate constants k_{att} and k_{det}:

$$\frac{\rho_b}{\theta}\frac{\partial S}{\partial t} = k_{att}C - \frac{\rho_b}{\theta}k_{det}S \qquad\qquad \text{Equation 2-14b}$$

In Equations 2-14a and 2-14b C is particle concentration in the fluid and S is particle concentration attached to the solid, ρ_b is the dry bulk density, θ is porosity, D is the diffusion coefficient, x is transport distance and v is the average particle velocity (Tufenkji, 2007).

2.5.4 Colloid filtration theory (CFT)

Colloid filtration theory (CFT) was produced to describe particle mass transport and deposition under a particular set of circumstances, which include irreversible attachment. In CFT, the rate constant for deposition (k_{att}) is proportional to the product

of the collector efficiency (η) and the collision efficiency (α), where η represents the

mass transport step and α reflects the attachment to the surface:

$$k_{att} = \frac{3(1-\theta)v}{2d_c}\eta\alpha \qquad\qquad\qquad \text{Equation 2-15}$$

where d_c is the collector (porous media grain) diameter (Tufenkji, 2007, Tufenkji et al.,

2003).

Experimental results are often used in the prediction of α under these circumstances,

the measured equilibrium concentration (C'/C_0) at the end of a packed column of length

L is used to determine a value retrospectively for a particular system (Petosa et al., 2010,

Ryan and Elimelech, 1996, Yao et al., 1971, Hahn and O'Melia, 2004):

$$\alpha = -\frac{2d_c}{3(1-\theta)^{1/3}\eta L}\ln(C'/C_0) \qquad\qquad \text{Equation 2-16}$$

It is assumed that the α calculated here from experimental results is comparable to that

estimated in Equation 2-13. The collector efficiency (η) is evaluated assuming conditions

favourable for deposition.

There are a number of correlation equations for predicting the collector efficiency,

which have been derived from multiple simulations in idealised particle-porous media

systems (Nelson and Ginn, 2005, Nelson and Ginn, 2011, Tufenkji and Elimelech, 2004a,

Hahn and O'Melia, 2004). The equation presented by Rajagopalan and Tien (1976) and

amended by Nelson and Ginn (2005) was chosen for this study, as it most closely

describes the accepted definition of the collector efficiency in terms of geometry:

$$\eta \approx \gamma^2\left[A_S N_{LO}^{1/8} N_R^{15/8} + 0.00338 A_S N_G^{1.2} N_R^{-0.4} + 4A_S^{1/3} N_{PE}^{-2/3}\right] \qquad \text{Equation 2-17}$$

where the dimensionless parameters used are defined in Table 2-1. Further description of these parameters can be found in Nelson and Ginn (2005).

The choice of equation for η (Equation 2-17) meant a slight adjustment had to be made to the definition of α in Equation 2-16 (Nelson and Ginn, 2005, Logan et al., 1995).

Parameter	Definition	
γ	$(1-\theta)^{1/3}$	
A_S	$2(1-\gamma^5)/(2-3\gamma+3\gamma^5-2\gamma^6)$	
N_{LO}	$A_{132}/(9\pi\mu a_p{}^2 U_x)$	U_x is fluid approach velocity
N_R	a_p/a_c	
N_G	$2a_p{}^2(\rho_p-\rho_f)g/(9\mu U_x)$	ρ_p is particle density ρ_f is fluid density g is acceleration due to gravity
N_{PE}	$U_x(2a_c)/D$	D is the Brownian diffusion coefficient
D	$kT/(6\pi\mu a_p)$	

Table 2-1 Definition of the parameters used in the calculation of the collector efficiency

In this study, the Ogata-Banks solution to the convective dispersive equation with linear sorption and first order decay was used to model particle breakthrough:

$$C(x,t) = \frac{C_0}{2}\left[e^{\frac{x}{2D}(v-\omega)}erfc\left(\frac{x-\omega t/R_f}{2\sqrt{Dt/R_f}}\right) + e^{\frac{x}{2D}(v+\omega)}erfc\left(\frac{x+\omega t/R_f}{2\sqrt{Dt/R_f}}\right)\right] \qquad \text{Equation 2-18a}$$

where:

$$\omega = \sqrt{v+4k_{att}D} \qquad\qquad\qquad \text{Equation 2-18b}$$

C and C_0 are effluent and influent particle concentration in the fluid, x is transport distance, D is the diffusion coefficient and R_f is the retardation factor (Ogata and Banks, 1961, Van Genuchten and Alves, 1982). D is calculated using the equation in Table 2-1 and k_{att} using Equation 2-15.

2.6 Sensitivity of transport calculations to input parameters

The sensitivity of the equilibrium breakthrough concentration (C'/C_0) calculated using colloid filtration theory (CFT) to variations in the input parameter values of zeta potential, Hamaker constant, particle size, porous media grain size and ionic strength is considered here. Numerous calculations using the Ogata-Banks solution to the convective dispersive equation (Equation 2-18a) were carried out in Microsoft Excel, each with slight changes to the parameter under investigation.

The Ogata-Banks solution includes a value for the depositional rate constant (k_{att}), found using Equation 2-15, with the collector efficiency and theoretical collision efficiency calculated using Equations 2-17 and 2-13 respectively.

The general parameters used are reported in Table 2-2 and were informed by the conditions of the column experiments carried out in Chapter 5. The C'/C_0 value reported after each calculation was plotted against the parameter under investigation to illustrate the predicted change in breakthrough.

Parameter	Symbol	Value	Unit
Porosity	θ	0.2	-
Particle radius	a_p	50	nm
Collector radius	a_c	0.055	mm
Absolute temperature	T	293	K
Ionic strength	I	0.0055	mol/kg
Hamaker constant	A_{132}	1.5E-20	J
Velocity	U_x	0.00005	m/s
Column length	L	0.06	m
Dispersivity	α_D	0.0025	m

Table 2-2Parameter values used in the CFT calculations illustrated below

2.6.1 Sensitivity of CFT calculations to zeta potential

In the CFT calculations α is used to represent the chemical interactions between the particle and surface, with the theoretical α value being evaluated from the maximum height of the energy barrier (Equation 2-13). The magnitude of the EDL interaction energy will determine the energy barrier height, and this is sensitive to the zeta potential of the interacting particle and collector grain (Equation 2-10). Here the zeta potential of the particle and grain are assumed to be equal.

The C'/C_0 is very sensitive to the zeta potential (Figure 2-3), and using the parameters listed in Table 2-2 it would take a minimum change in zeta potential of 5mV to switch between a C'/C_0 of 1 to 0. The sensitivity of the calculations to zeta potential do not change with changing Hamaker constant, with all other parameters remaining constant.
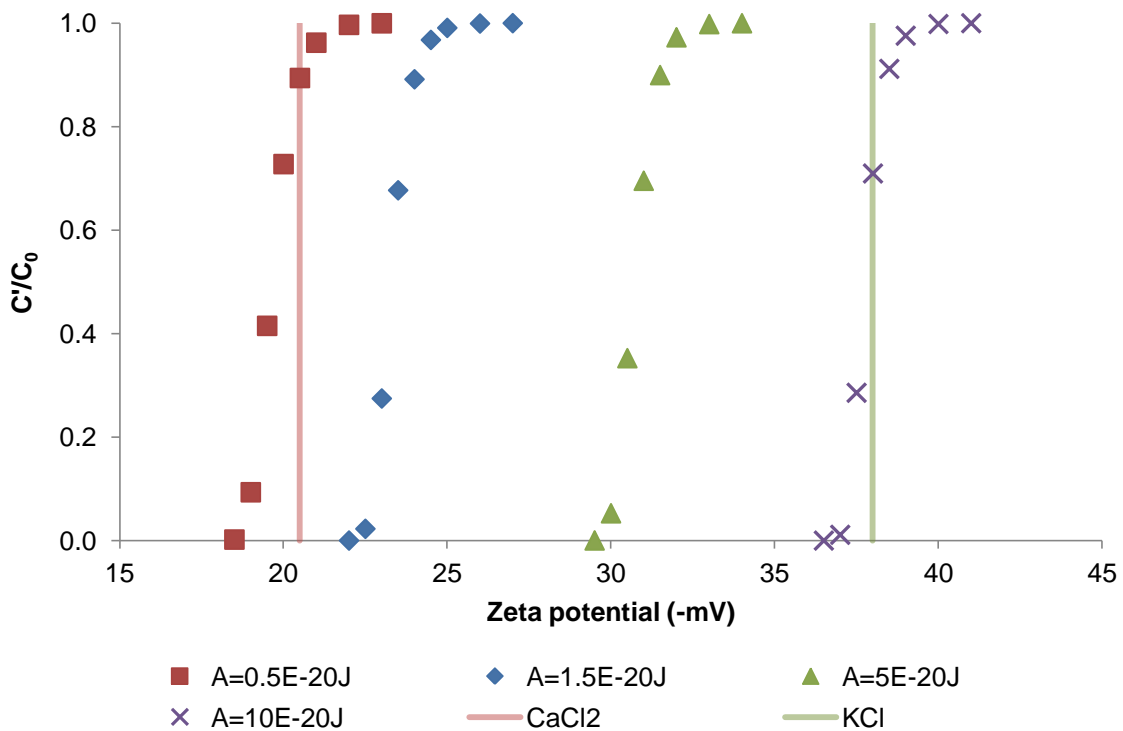
Figure 2-3 Sensitivity of C'/C$_0$ to changing zeta potential over a range of Hamaker constants. The zeta potential of silica in CaCl$_2$ and KCl at pH6 measured using electrophoresis is indicated by the vertical lines.

2.6.2   Sensitivity to calculation parameters: the impact of zeta potential

The sensitivity of C'/C_0 from CFT calculations to particle and grain size, Hamaker

constant and ionic strength is illustrated in Figures 2-4 to 2-7.

The particle and collector grain radii (a_p and a_c) are used in the calculation of both

theoretical α and η. From Figure 2-4 it can be seen that smaller particles are less mobile

than larger particles at the same zeta potential. Then particles of the same size are less

likely to be removed by larger collector grains (Figure 2-5), due partly to a decrease in

collisions via diffusion and interception. With a more negative zeta potential, the C'/C_0

becomes more sensitive to the particle and grain size.
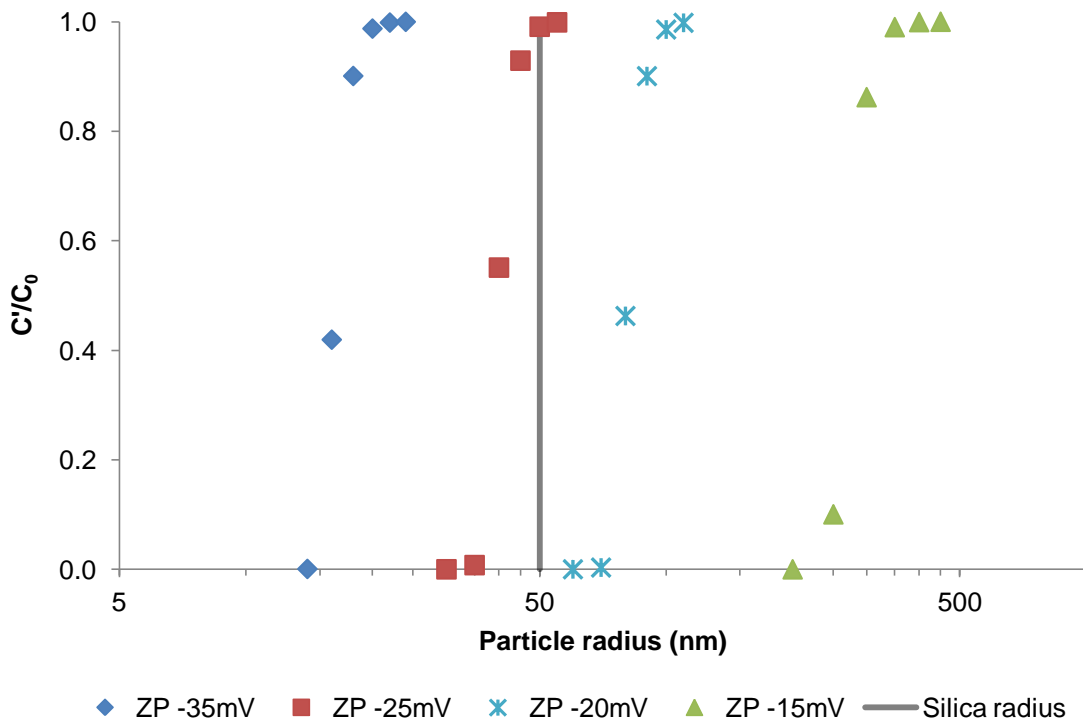
Figure 2-4 Sensitivity of C'/C_0 to changing particle radius over a range of zeta potential from -15 to -35mV. The radius of the silica particles used throughout this study is indicated by a vertical line.
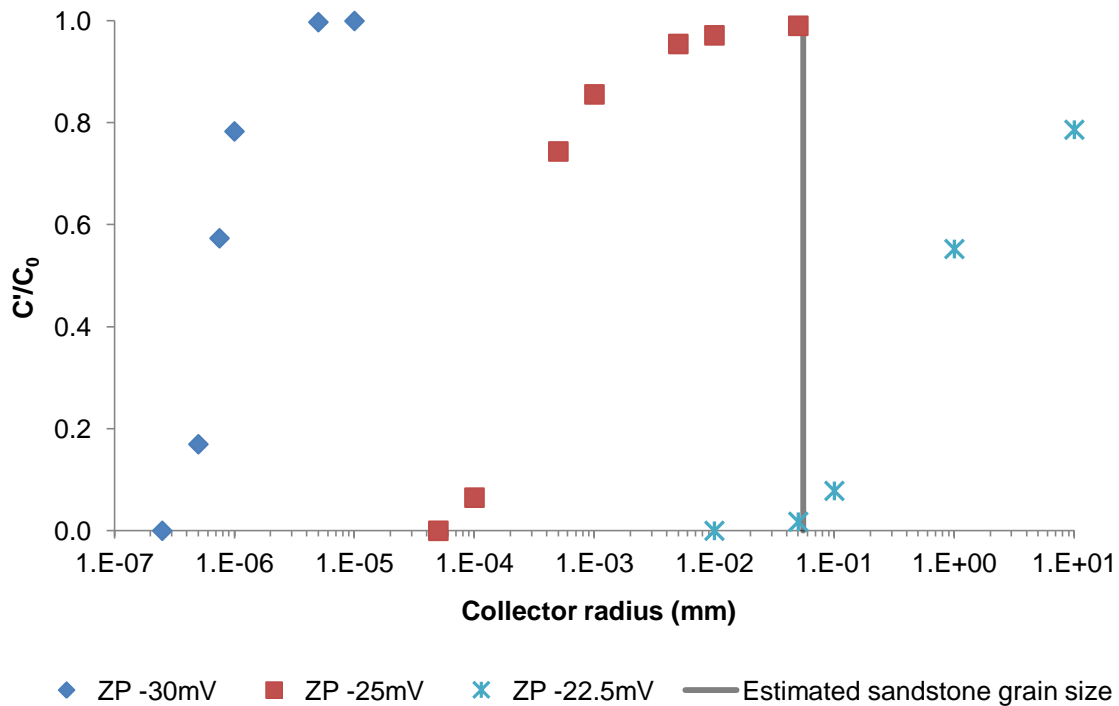
Figure 2-5 Sensitivity of C'/C₀ to changing collector grain radius over a range of zeta potential from -22.5 to -30mV. The estimated radius of the grains in the sandstone used here in column studies is indicated by a vertical line.

The Hamaker constant, like zeta potential, impacts on the maximum height of the energy barrier, in this case due to a linear relationship with the vdW interaction energy. With an increasing Hamaker constant there is decreasing mobility (Figure 2-6), as the attractive interaction forces are greater. With a more negative zeta potential there is a reduced sensitivity to the Hamaker constant. However, with the difficulties in quantification of this parameter, the predictions across all zeta potential values are considered to be highly sensitive to its value.
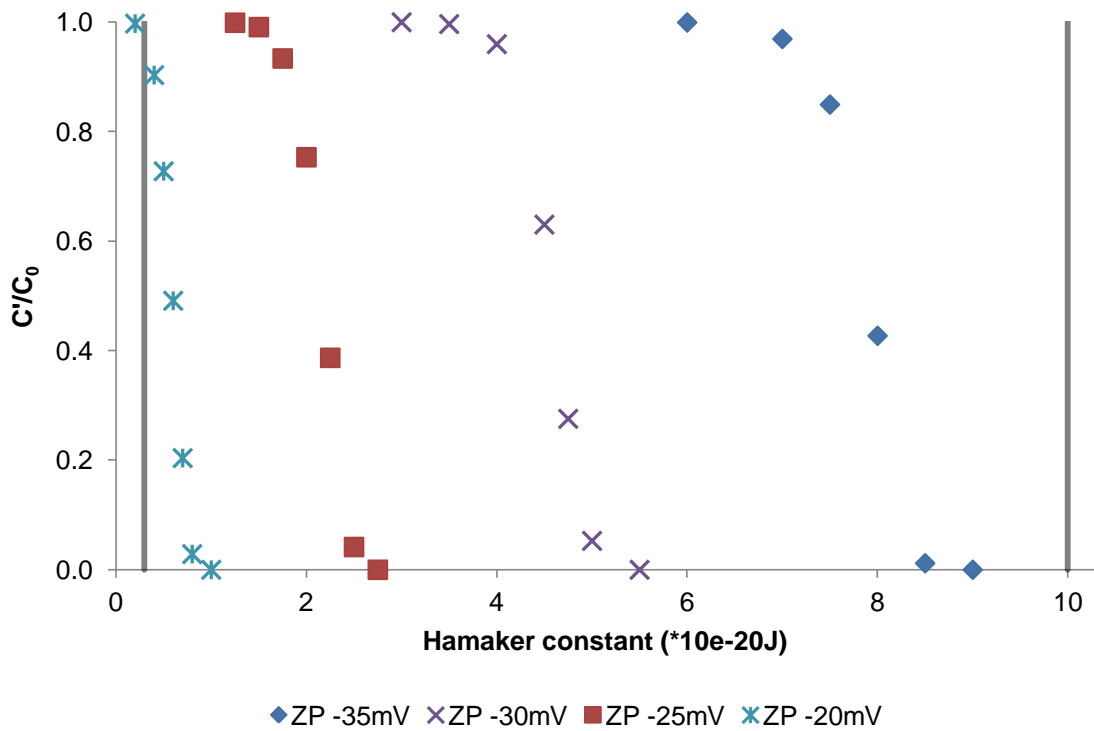
Figure 2-6 Sensitivity of C'/C₀ to changing Hamaker constant over a range of zeta potential from -20 to -35mV. Indicated on the chart are the range of Hamaker constants suggested for aqueous systems by Elimelech (1995).

The ionic strength also influences the maximum energy barrier height, due to the impact of changing ionic strength on the Debye length, the inverse of which is used in the calculation of the EDL interaction energy. The ionic strength will independently have an effect on the zeta potential, but for the purpose of these calculations a constant zeta potential is assumed with changing ionic strength.

As the ionic strength is increased there is a decrease in the double layer thickness and a decrease in the height of the energy barrier. If all other conditions remain the same, particles will be less mobile with a solution of higher ionic strength (Figure 2-7). With an increasing zeta potential, the C'/C₀ becomes less sensitive to a change in ionic strength.
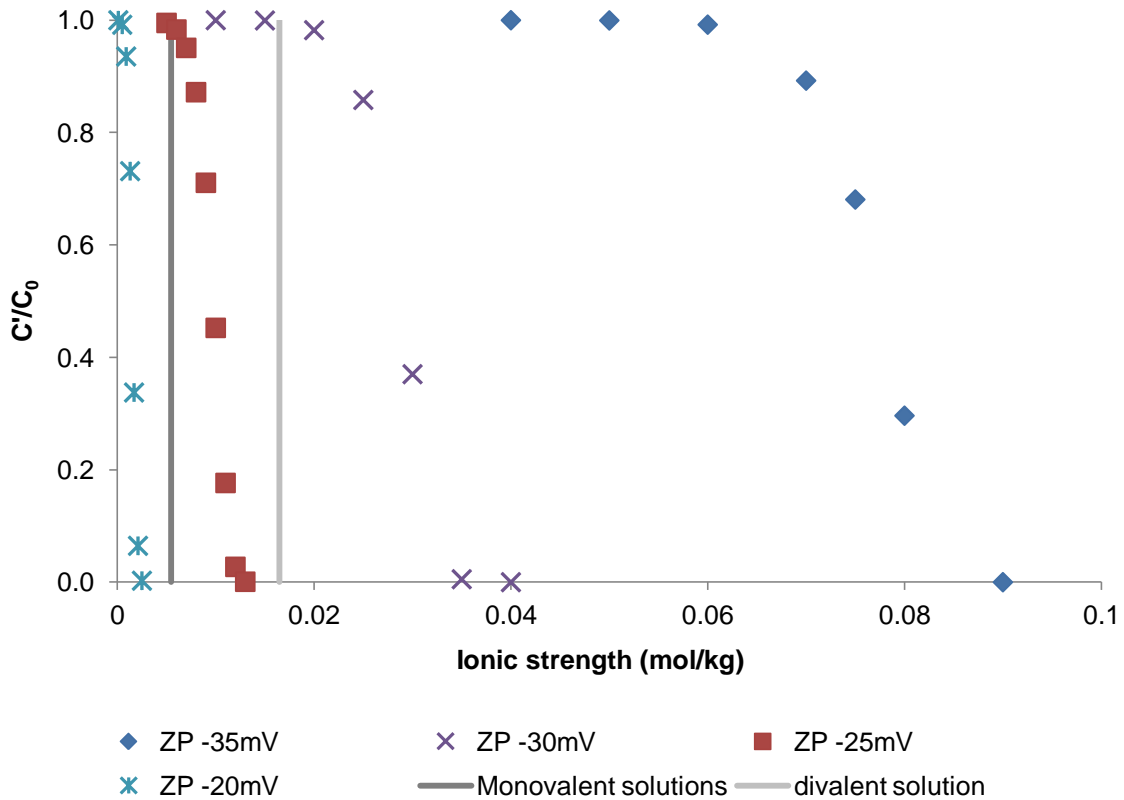
Figure 2-7 Sensitivity of C'/C$_0$ to changing ionic strength over a range of zeta potential from -20 to -35mV. Indicated on the chart are the ionic strength of the monovalent and divalent solutions used in the column experiments in Chapter 5.

2.7 Conclusions

Zeta potential is the potential at the shear surface. As it is the best description of the potential which will most directly affect interactions between two bodies in a fluid, it is often used instead of surface potential in DLVO interaction energy calculations. It can be measured by observation of electrokinetic phenomena, and used in these interaction energy calculations to inform calculations of particle transport and deposition.

There is significant sensitivity in the CFT calculations of equilibrium concentration to zeta potential, both when other model inputs are constant and changing. There is also an impact of the zeta potential on the sensitivity of the model to other parameters. When zeta potential becomes more negative there is an increased sensitivity to particle and

27

collector grain radius and a decrease in sensitivity to the Hamaker constant and ionic strength. If CFT calculations can be used to describe the transport of particles through intact rock, it will be important to carefully quantify the zeta potential of both the particle and the rock.

Another unknown value which causes significant sensitivity in the C'/C_0 value is the Hamaker constant. This will be estimated in the silica-rock system (see Section 5.5.2) in order to carry out CFT calculations. If CFT can be used as a way to predict nanoparticle mobility in intact rock, then careful attention should also be given to quantifying the Hamaker constant.

3 APPLICATION OF SINGLE-SURFACE ELECTRO-OSMOTIC FLOW MAPPING (SS-EFM) TO MINERAL SURFACES

3.1 Introduction

There are a number of techniques currently in use to measure the zeta potential of surfaces and these by their very nature all consider the movement of fluids along the solid/liquid interface. As stated in Chapter 2, there are three broad categories of approach: streaming potential, where the fluid moves along a stationary surface and the induced potential difference or current is measured; electro-osmosis, where fluid moves along a charged surface under an applied current; and electrophoresis, where the movement of charged particles within a stationary fluid under an applied current is observed (Hunter, 1981, Delgado et al., 2007). This particle observation can be made directly, using appropriate optical magnification, in microelectrophoresis or indirectly, by analysis of the light scattered by moving particles, in electrophoretic light scattering (ELS) (Delgado et al., 2007).

Streaming potential and electro-osmosis techniques both utilise a capillary flow system, where flow is created within a single capillary, between two parallel plates or in more complex systems like fibre bundles or porous plugs. Streaming potential is the most frequently used technique in investigating the zeta potential of porous material. For a streaming potential measurement there is a need for specialist equipment able to withstand the high pressures needed (e.g. Alkafeef et al., 1999 designed a high pressure, high temperature core holder device) and both streaming potential and electro-osmosis techniques require a different set up for each geometry of sample (Delgado et al., 2007).

Most importantly for the current purpose, complications are introduced to streaming potential measurements by surface conductivity in samples in contact with low ionic strength suspensions (Alkafeef et al., 1999).

Electrophoresis requires a sample of the rock to be crushed and dispersed in an electrolyte. Although this technique is convenient, without comparison with other techniques it is not possible to determine whether the measurements taken are representative of the intact rock. Size reduction will destroy natural rock fabrics and expose surfaces which would not normally be encountered by fluids (Johnson, 1999, Stephan and Chase, 2001).

In the light of these difficulties, we have used a new technique developed by Corbett et al. (2012), Single-Surface Electro-osmotic Flow Mapping (SS-EFM), based on extrapolation of apparent zeta potential measurements (of particles under influence of both electro-osmosis and electrophoresis) at different distances from the surface concerned. The technique provides measurements of surface zeta potential at the few millimetre scale; it uses intact surfaces and is conducted using a new sample cell in a standard piece of particle characterisation equipment (the Zetasizer Nano ZS, Malvern Instruments). The results of this approach have then been compared with data obtained using electrophoresis on disaggregated samples, and in combination the results have then been used to investigate the degree of zeta potential heterogeneity.

3.2 Aims

- To use a new technique to measure the surface zeta potential of sandstone;

- To assess this technique for use on complex environmental materials.

3.3 Approach

SS-EFM is a new technique, so before measurements were attempted on more physically complex surfaces, initial experiments were carried out using freshly cleaved mica and the results compared with those from the literature. Sandstone measurements were then attempted, firstly looking at repeatability of this technique on a single sandstone sample and then variability from adjacent samples from a sandstone bed. During this process, sample preparation and storage methods were finalised and the application of the technique improved with practice.

3.4 Method

3.4.1   Sandstone samples

Sandstone samples were acquired from a core of a redbed continental sandstone sequence from Preston, north-west England. The sandstone is described more fully in Chapter 4, where all lithofacies are sampled for zeta potential measurements. The samples for SS-EFM and electrophoresis measurements in this chapter are selected from lithofacies 3 (Table 3-1), and are composed of medium grain sandstone.

Lithofacies No.	Grain size	Mud clasts	Mica	Lamination	Interpreted Palaeoenvironment
1	Mudstone to siltstone	-	Yes		Abandoned channel or overbank deposits
2	Very fine sandstone	None	Yes	90% are planar and low angle	Channel fill, relatively low flow
3	Fine to medium sandstone	Very few	Yes	80% are planar and low angle	Channel fill
4	Medium to coarse sandstone	Common	Yes	90% are cross laminated	Channel fill, relatively high flow
5	Medium to coarse sandstone	Many	Yes	70% are massive	Channel lag

Table 3-1. Lithofacies definitions for the Preston core (Moran, 2008)

3.4.2 *Zeta potential measurements using electrophoresis*

Zeta potential measurements were attempted on mica and sandstone particulate samples using electrophoresis. Electrophoresis measurements were taken using a Zetasizer Nano ZS (Malvern Instruments). The induced velocity of the particles under an applied electric field (electrophoretic mobility) was measured using light scattering with a process called laser Doppler velocimetry. This velocity was then converted to zeta potential by the Zetasizer using Equation 2-4 and the Smoluchowski approximation to the Henry function.

Approximately 3g of material was disaggregated as gently as possible using a pestle and mortar; this worked well with the relatively friable sandstone samples, but the mica samples required grinding to break them up. Approximately 1g of disaggregated material was then dispersed in 25ml of the solution required and shaken for 30 minutes: the larger solids were then allowed to settle out over at least 12 hours.

3.4.3 Single-Surface Electro-osmotic Flow Mapping (SS-EFM)

The timely development of a new method for measuring surface zeta potential by Malvern Instruments has allowed the testing of mineralic surfaces at the scale of a few millimetres. The SS-EFM technique is carried out using a new surface cell in conjunction with the Malvern Instruments Zetasizer Nano ZS.

The surface cell holds a 4mm by 5mm sample of approximately 1mm thickness between two electrodes (Figure 3-1a). The cell is submerged in an electrolyte solution in which probe particles (of arbitrary material and zeta potential) are dispersed. Under an applied electric field, the probe particles have a mobility determined by the sum of the particle electrophoretic motion, which is assumed to be the same at any distance from the surface, and the electro-osmotic motion of the fluid that develops as a result of the charge at the sample surface, and reduces with distance from that surface (Figure 3-1b).
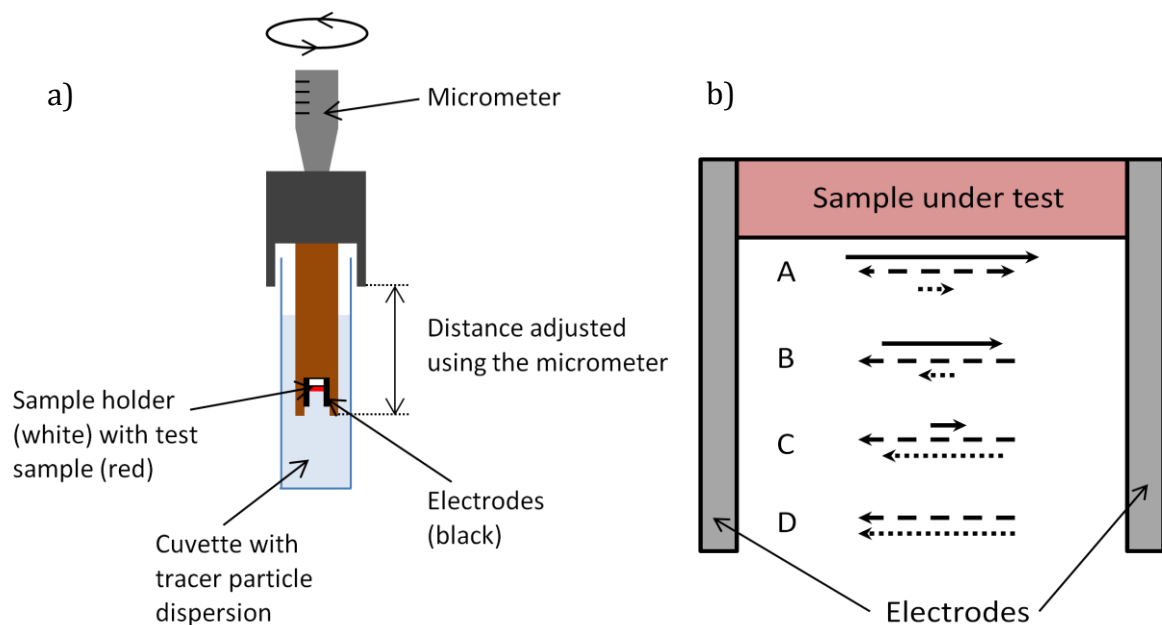
Figure 3-1 a) Schematic of the SS-EFM measurement cell. b) Diagram of the flow field near a surface sample, the letters indicate measurements at different distances. Illustrated are electro-osmosis (solid line), electrophoresis (dashed line) and the resultant apparent mobility (dotted line).

When the apparent mobility measured at a number of points within a micron of a

surface are plotted against distance from that surface, a linear relationship is observed,

an example of which is shown in Figure 3-2.

The intercept of this linear relationship can be used along with the probe particle

velocity at a distance remote from the surface (v_{ep}) in Equation 3-1 to calculate the

velocity at the test surface (v_{eo}):

$$v_{eo} = -intercept + v_{ep}$$ Equation 3-1
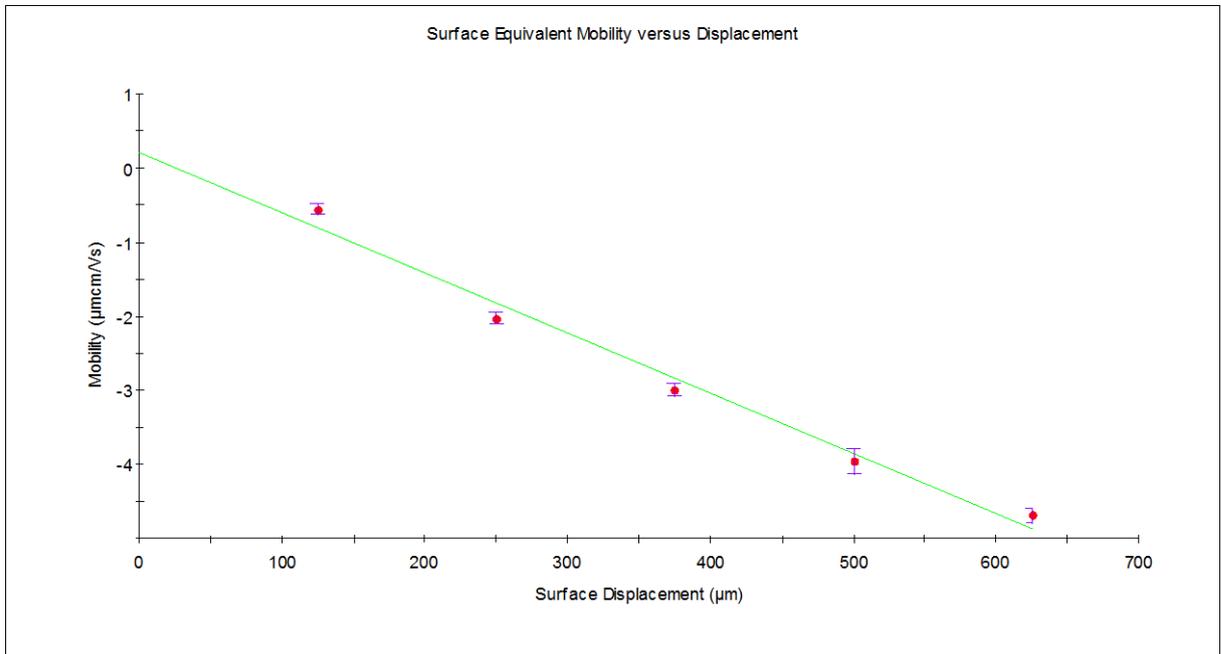
Figure 3-2 Apparent mobility (red dots) plotted with displacement from a mica surface. The error bars show the standard deviation on five measurements at each distance and the green line is the regression fit. The probe particles are latex spheres with a measured mobility of -6.4 µmcm/Vs.

The test surface is assumed to coincide with the surface shear plane, and v_{eo} is assumed

to be proportional to the surface zeta potential. v_{eo} is converted to zeta potential using

Equation 2-2. Corbett et al. (2012) provide a more detailed description of this process,

and describe derivation of the theory.

As mobility and zeta potential are proportional (Equation 2-2), for convenience in the current work, all mobility data will be reported in terms of apparent zeta potential.

3.4.4 SS-EFM sample preparation

A PEEK sample holder is glued to a representative section of sandstone, and then the sandstone grains are gradually broken away until a sample remains of 4mm wide by ≥5mm long, by ≤1mm thick.

Sides et al. (2009) described the initial aging of a mica surface from it being cleaved and immersed in an electrolyte. They found that, at least during the initial minute of surface immersion, the zeta potential was transient. This being the case, the mica surface was allowed to equilibrate with 50ml of the electrolyte used for 12 hours before a measurement was taken. Many studies, including this one, have carried out surface zeta potential measurements on mica at an ambient pH of 5.9, because this represents the pH of electrolyte solutions after equilibration with atmospheric CO_2 and aging effects are expected to be minimized at this pH (Lyons et al., 1981).

The sandstone surface samples were also equilibrated in 50ml of the particle-free electrolyte to be used for approximately 12 hours before a measurement was carried out. The pH of the equilibration solution was 6.6±0.1 after this length of time in contact with the sandstone, and at equilibrium with atmospheric CO_2. To test the equilibrium process was carried out fully; some samples were immersed in 1l of particle-free electrolyte and allowed to equilibrate for 12 hours.

To carry out an SS-EFM measurement, the equilibrated sample surface (attached to the sample holder) is inserted into the measurement cell between the two electrodes (Figure 3-1a), lowered into a cuvette containing a probe particle dispersion (see Section 3.4.5) and placed in the Zetasizer. The sample surface is found using a display of the intensity of light entering the detector from a laser light source; the intensity significantly decreases when the surface begins to block the laser. The micrometer can then be used to position the surface at an increasing distance from the laser, with a measurement of apparent zeta potential being taken at each distance (within 1μm of the surface). When these measurements are completed, a measurement of the particle electrophoresis is taken at 1μm from the surface. The apparent zeta potential values are plotted with distance and the intercept, along with the probe particle zeta potential, is used to calculate the zeta potential of the surface using Equation 3-1.

3.4.5   Probe particles

Two tracer particles were used: 300nm carboxylated latex (Invitrogen) and 100nm silica (Polysciences). These were dispersed in pH9.2 buffer (sodium tetraborate, Sigma-Aldrich) or a low ionic strength solution of KCl respectively. To record the stability of the probe particle dispersions with time, size and zeta potential measurements were taken, one set over the same period of time as one surface zeta measurement and then regular measurements during the full time over which measurements were taken. The probe solution was replaced each week, although the dispersions were observed to be stable for much longer periods than this.

3.4.6 Size measurements

Size measurements of both the probe particle and the disaggregated sandstone samples were taken, to assess for SS-EFM probe particle stability and size bias in zeta potential measurements respectively.

The particle hydrodynamic diameter was measured using the Zetasizer Nano ZS (Malvern Instruments) using Dynamic Light Scattering (DLS). DLS measures the intensity of scattered light from particles undergoing Brownian motion. The rate of light intensity fluctuation can be converted to a diffusion coefficient (D) then used to calculate particle size using the Stokes-Einstein equation:

$$D = \frac{k_B T}{6\pi\mu R} \qquad\qquad \text{Equation 3-2}$$

where k_B is the Boltzmann constant, T is absolute temperature, μ is the fluid viscosity, in this case taken to be the viscosity of water at the measurement temperature, and R is the radius of a spherical particle.

The Zetasizer Nano ZS detects backscattered light at 175°; this reduces multiple scattering from samples of higher particle concentration and the effect of large particles, which typically scatter much more light in the forward direction.

1ml of dispersion is required and the non-invasive size measurement is usually taken in a folded capillary cell before a zeta potential measurement on the same sample.

3.5 Results and discussion

3.5.1   SS-EFM test on PEEK

Before the method was applied on geological samples, it was tested on PEEK (polyether ether ketone, a thermoplastic used to make the sample holder which fits inside the cell) using latex probe particles in pH9.2 buffer (see Section 3.4.5). The results from this reported a surface zeta potential of -75mV±5mV, in close agreement with a zeta potential of -74mV±3mV found by Jacobasch et al. (1998) using a low concentration sodium phosphate electrolyte.

3.5.2   Silica probe particle characterisation

The size and zeta potential of the silica probe particles was monitored, measurements were taken on a separate aliquot of the dispersion used in SS-EFM measurements to check for stability (if the size or zeta potential changed significantly the dispersion was discarded), then electrophoresis measurements were taken as part of the SS-EFM measurement using the surface cell.

The SS-EFM measurements taken during this chapter consist of 25 individual zeta potential measurements over approximately 30 minutes. To test the stability of the silica probe particles under these conditions 25 electrophoresis measurements were taken over the same length of time. The zeta potential showed no trending and gave an average of -51.8±0.9mV.

The zeta potential of the silica probe particles taken as part of SS-EFM measurements shows a normal distribution, but an increase in the average and standard deviation compared to those of the probe particle standard (Figure 3-3). There is evidence from

SS-EFM measurements on unreactive surfaces (PEEK) to show that the use of the surface cell systematically gives lower values for the zeta potential than those measured using the folded-capillary cell normally used in electrophoresis measurements. This will have an impact on the absolute value of surface zeta potential, but comparability between measurements on different samples will remain.
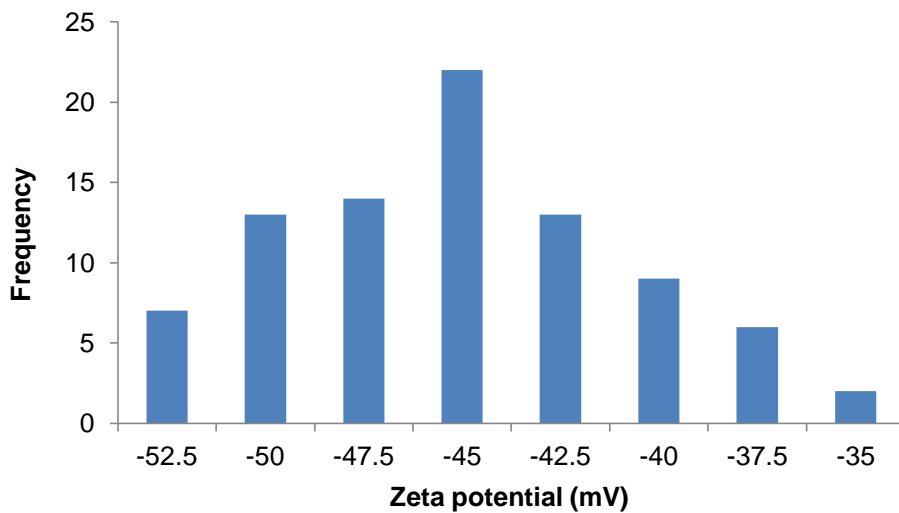
Figure 3-3 Silica particle zeta potential in 1mM KCl taken after contact with sandstone. Each of the 86 measurements here is an average of 5 measurements taken on the probe particle dispersion as part of an SS-EFM measurement; the overall average is -46.3±4.4mV.

Following a measurement there was visible evidence of indigenous particles being released into the probe solution. These particles would be measured along with the, still probably more numerous, silica particles and could contribute to the increase in range of values seen. The indigenous particles would most likely be in the fluid during the entire measurement, so would not influence the surface zeta potential value measured, as this is independent of particle type and zeta potential (as long as there is no change during a measurement).

The zeta potential and size distributions before contact with the sandstone are shown in Figure 3-4. There is a normal distribution for both, with the distribution width most likely being a result of noise in the data and the algorithms used to calculate the distributions.
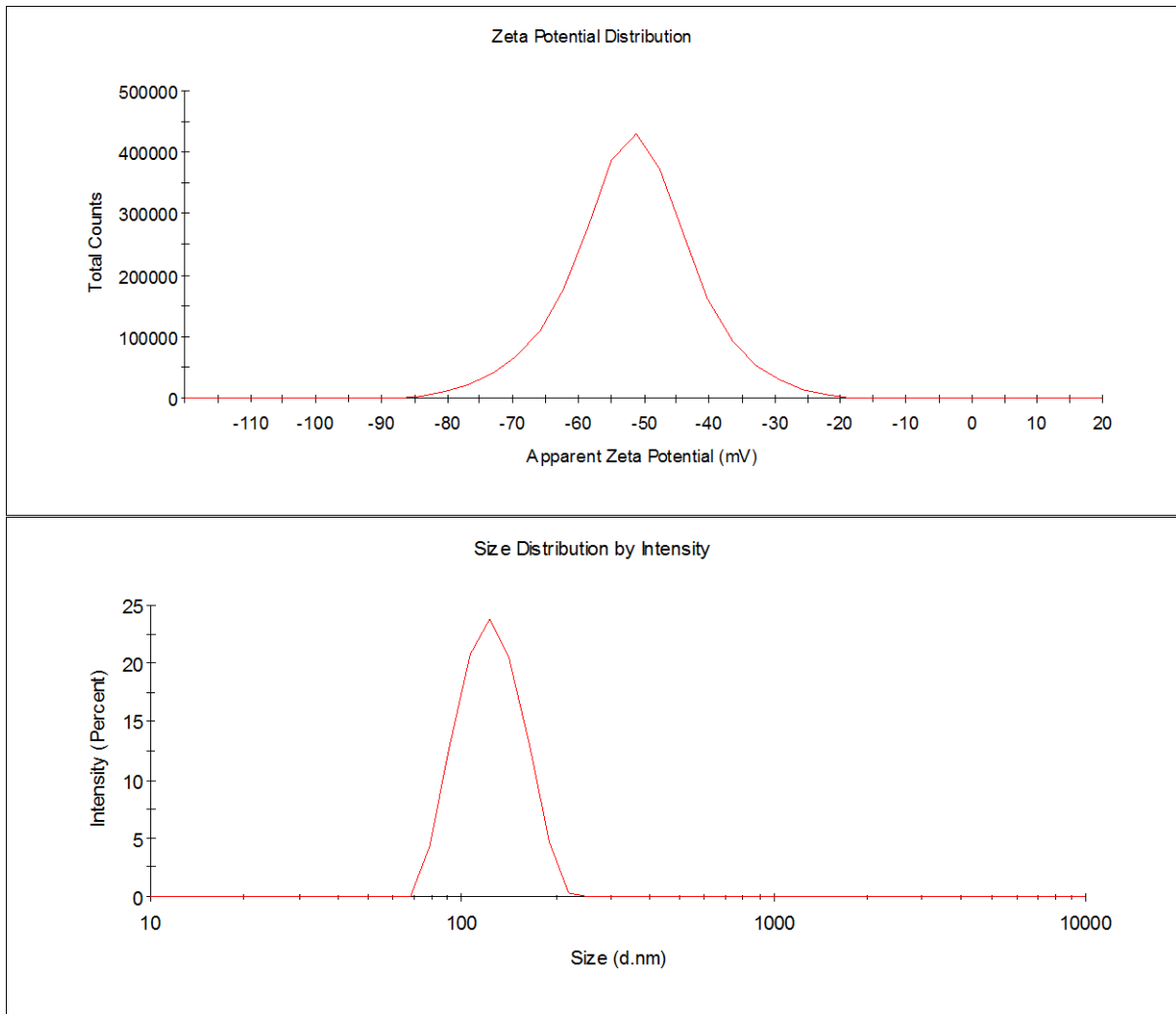
Figure 3-4 Average zeta potential and size distributions for SiO$_2$ in 1mM KCl before contact with sandstone.

3.5.3 Criteria for data quality assessment

While the calculation method of the SS-EFM measurements was relatively straightforward (Section 3.4.3), it quite quickly became clear that the practicality of taking a measurement using mineralogical samples was rather more complex. Early on

there was a significant amount of error, particularly in finding the sample surface, both

the most challenging and most important part of mastering the technique. Problems also

arose with unwanted chemical interactions between some surface samples and the

probe particle dispersion and with erroneous zeta potential measurements at some

points. Criteria for assessing the data therefore had to be developed:

1. If there was a significant change in conductivity for an apparent zeta potential value
    compared to the others in the SS-EFM measurement remove that value and
    recalculate the linear fit

2. If the apparent zeta potential at the furthest distance does not agree with the linear
    fit remove that value, as it will most likely no longer be influenced by the electro-
    osmosis due to the surface, and recalculate the linear fit

3. The apparent zeta potential at each distance and the particle zeta potential at 1µm
    are averages of five measurements, if one point is >10mV different to the others
    remove that point and recalculate the average

4. If R2 for the linear fit is still <0.95 after these changes then discard the measurement.

5. If the apparent zeta potential at the distance closest to the surface is zero or
    significantly removed from the linear fit then discard the entire measurement, as it is
    likely the surface was not correctly located.

6. If the particle zeta potential is trending over the five measurements or is very
    different from expected from initial characterisation of the probe dispersion then
    discard the measurement, as it is likely that the particles and surface are interacting.

3.5.4   Mica zeta potential measurements

High grade ruby muscovite mica (Agar Scientific) was used as a first test of geological material. Muscovite has the advantage that it is often used as an analogy for clay minerals and therefore data exist for its surface properties: it also has the advantage that it produces a atomically flat surface when cleaved (Nishimura et al., 1995), thereby avoiding any problems of surface topography interfering with the measurement. Mica did however produce problems with locating the sample surface for a SS-EFM measurement due to its transparency. This was overcome by using a combination of zeta potential and size measurements to locate the surface; measurement of these properties only being possible when the laser could pass by the sample surface into the probe particle dispersion.

Ignoring the results of Nishimura et al. (1995, 1992) previous studies based on streaming potential and electro-osmosis measurements have found the zeta potential of mica to be the range -84 to -73 mV at around pH6 and in 1mM KCl (Table 3-2). However, much lower values (-94 mV) were obtained by Sides et al. (2009) within 1 minute of cleaving the mica, and Nishimura et al. (1995, 1992) obtained the even lower values of -134 to -130 mV at a pH of 5.6 and 1mM KCl. Nishimura et al. (1992) and this study also obtained much higher values (-34mV and -45mV respectively) under similar chemical conditions using electrophoresis on crushed mica.

Measurement type	Sample	Electrolyte (pH/ionic strength)	Surface zeta potential value (mV)	Reference
Streaming potential	Ruby muscovite, freshly cleaved surface	pH5.8, 1mM KCl	-84	Lyons, 1981
Streaming potential	Ruby muscovite, freshly cleaved surface	pH5.9, 1mM KCl	-75	Scales et al., 1990
Electro-osmosis	Muscovite, stored under distilled water, freshly cleaved surface	pH5.8, 1mM KCl	-77	Debacher & Ottewill, 1991
Streaming potential	Freshly cleaved surface, cleaned with conc. HNO3 and rinsed with distilled water	pH5.6, 1mM KCl	-134	Nishimura et al., 1992
Electrophoresis	Dry grinding freshly cleaved mica, 1mg of particles ≤10μm dispersed in 100ml of electrolyte	pH6.7, 1mM KCl	-34	Nishimura et al., 1992
Streaming potential	Freshly cleaved surface, rinsed with distilled water	pH5.6, 1mM KCl	-130	Nishimura et al., 1995
Streaming potential	Freshly cleaved surface	pH6, 1mM KCl	-73	Sides et al., 2006
Streaming potential	Freshly cleaved surface, measurement 30-50s after cleaving	pH6, 1mM KCl	-94±20	Sides et al 2009
SS-EFM	Ruby muscovite, freshly cleaved surface, stored under 1mM KCl	pH5.9, 1mM KCl	-70±4	This study
Electrophoresis	Dry grinding freshly cleaved ruby muscovite, dispersed in 1mM KCl	pH 5.9, 1mM KCl	-45±3	This study

Table 3-2 Literature values of mica zeta potential

These results indicate the complexity inherent in surface zeta potential measurements of mica, reflecting the sensitivity to preparation methods, including the manner in which the sample has been cleaved, the 'conditioning' time of the sample, and the pH of the solution (Sides et al., 2009); crushing appears to have a profound effect. Lyons et al. (1981) also found that a range of values (-102 to -90mV for green mica) were obtained when applying apparently the same experimental conditions, by measuring the zeta potential of different sheets of mica from the same source.

In the present study, applying the SS-EFM technique, after equilibrating the mica with 1mM KCl at pH5.9 for the relatively long time of 12 hours, gave a value of -71±4mV. This result is much more consistent with the streaming potential and electro-osmosis methods of Scales et al. (1990), Debacher and Ottewill (1992) and Sides et al. (2006) than it is with the results of Nishimura et al. (1995, 1992). As expected it differs from the result obtained by Sides et al. (2009) within a minute of cleaving and provides further confirmation that the results of Nishimura et al. (1995, 1992) are not typical for mica.

Given the sensitivity of the results to the measurement conditions as indicated by previous studies, it is concluded that the SS-EFM method produces values not inconsistent with those obtained by other techniques, confirming the zeta potential of freshly cleaved ruby mica in 1mM KCl solution in equilibrium with the atmosphere to be in the range -85 to -71 mV: a more precise figure cannot at the moment be justified. This imprecision indicates the uncertainty associated with even a rather well-defined, mono-mineralic surface, and informs the consideration of data obtained from much more complex, intact rock surfaces.

3.5.5 Sample roughness

Previous uses of SS-EFM have been on relatively smooth surfaces, but it was important to test the impact of roughness on the surface zeta potential obtained using this technique.

A PEEK sample holder was used to assess the effects of surface roughness. An SS-EFM measurement was taken of the original surface, then that surface was scored with a Stanley knife in three directions. The scoring was approximately 1mm deep and the plastic pushed out of these score marks created a variable topography. SS-EFM measurements on these surfaces are shown in Figure 3-5.
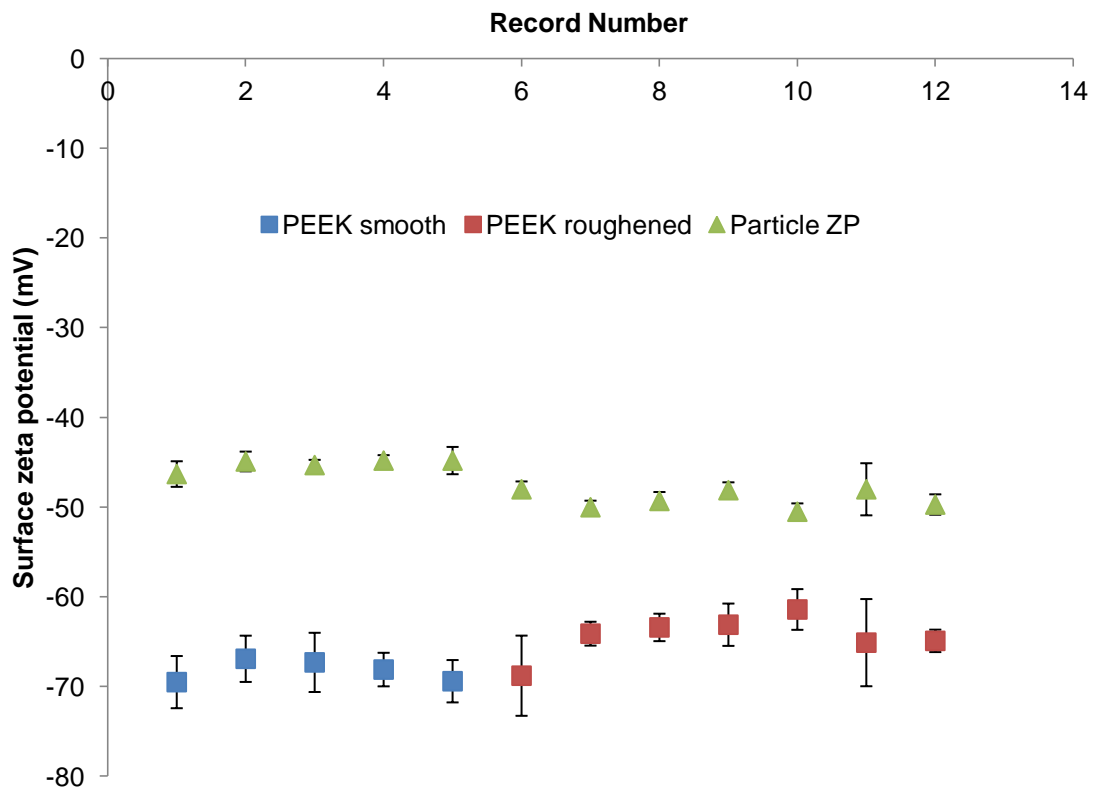
Figure 3-5 Surface zeta potential of a smooth and roughened PEEK surface measured using latex probe particles in a pH9.2 buffer.

The roughened surface gives a slightly less negative zeta potential to that of the smooth surface of the same material (averages of -64.4±2.3mV and -68.2±1.2mV respectively), although the difference is not outside of the recommended RSD of 10% of the absolute value.

The SS-EFM measurement is slightly harder to perform on the roughened surface, as locating the surface is more difficult, which would explain the increased variability on the roughened sample. However, the standard deviation in the roughened surface zeta potential measurements is not significantly higher than for the smooth surfaces, so accurate SS-EFM measurements are considered to be achievable on a rough surface.

3.5.6 *Sandstone surface zeta potential using SS-EFM – repeatability on individual samples*

Measurements on sandstone are expected to be rather more difficult than on mica, as the sandstone surfaces will have much greater topographic variation and are potentially much more heterogeneous. Consistency between measurements using SS-EMF was attempted by developing a user protocol for locating the sample surface (the zero distance position).

Early measurements undertaken in this study were rather more variable than those made later in the data collection. This is illustrated in Figure 3-6, where sample A1, on which the first measurements were attempted, showed much greater variability than the results from other samples that were measured subsequently. However, variability is still a feature of all measurements on an individual sample, and can be produced in several ways. Despite the user protocol, locating the zero position incorrectly will be the

most important. Other considerations include 1) the repeated removal of samples to clean electrodes, 2) the potential for air bubbles at the sample or electrode surface, 3) possible contamination of the testing fluid and 4) that multiple individual measurements are taken to calculate the value of one point in Figure 3-6, each producing uncertainty.

Repeated measurements on a single sample in 1mM KCl (on all the samples presented in Figure 3-6e-i) gave an average standard deviation of ±3.1 mV, corresponding to an RSD of 9% of an average value of -36.3mV. This is a similar repeatability to that of Corbett et al. (2012), who found a typical RSD for reproducibility of measurements for well-behaved systems (homogeneous and smooth surface with stable probe particles) of 10% of the absolute value.

Histograms for the samples with ≥7 measurements show that a normal distribution of values for a single sample is achieved on later measurements in 1mM KCl. Average values for a single surface are therefore presented later in this chapter and in Chapter 4.

Zeta potential (mV)

a) Sample A1a

b) Sample A1b

c) Sample A2a

d) Sample A2b

e) Sample A3

Frequency
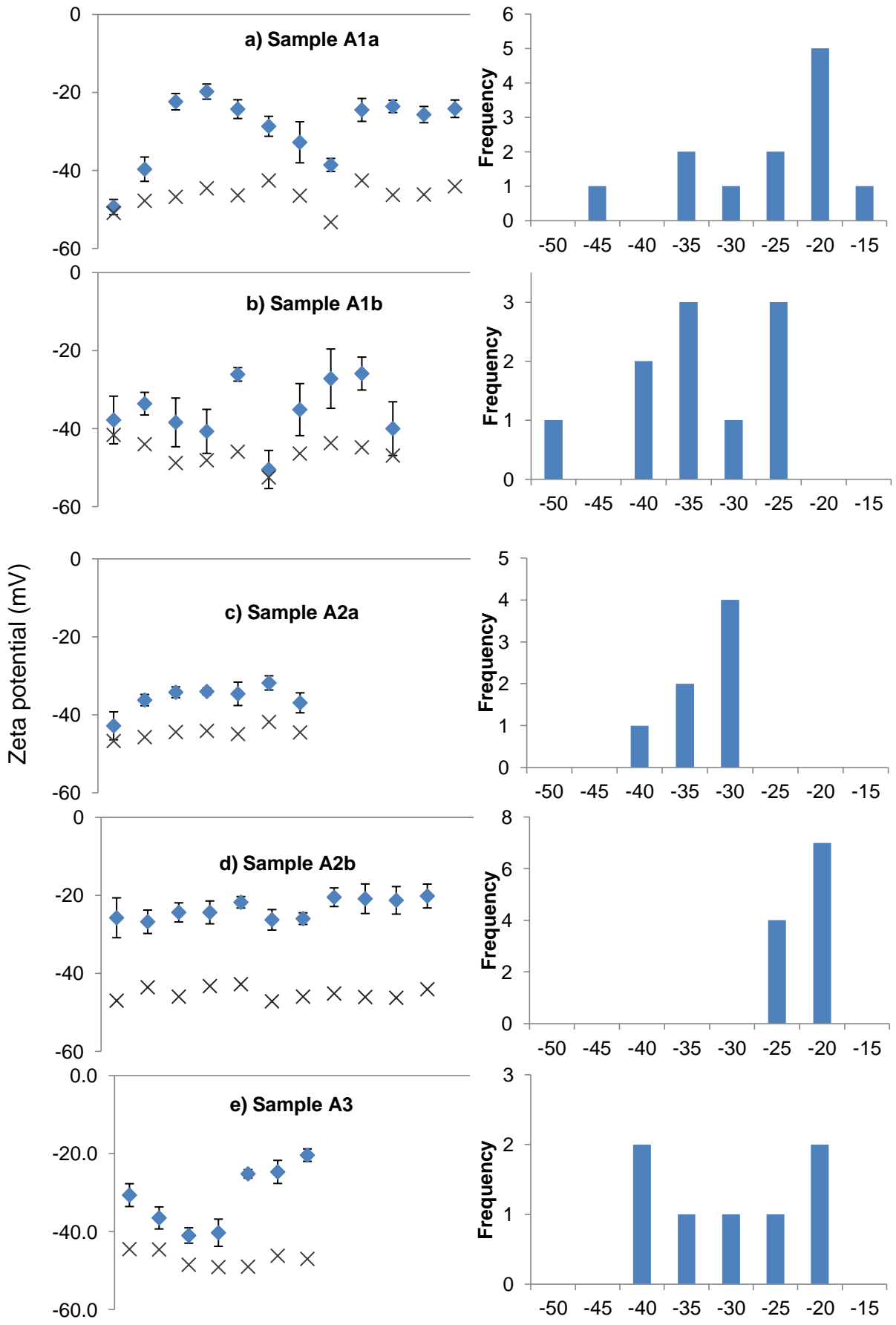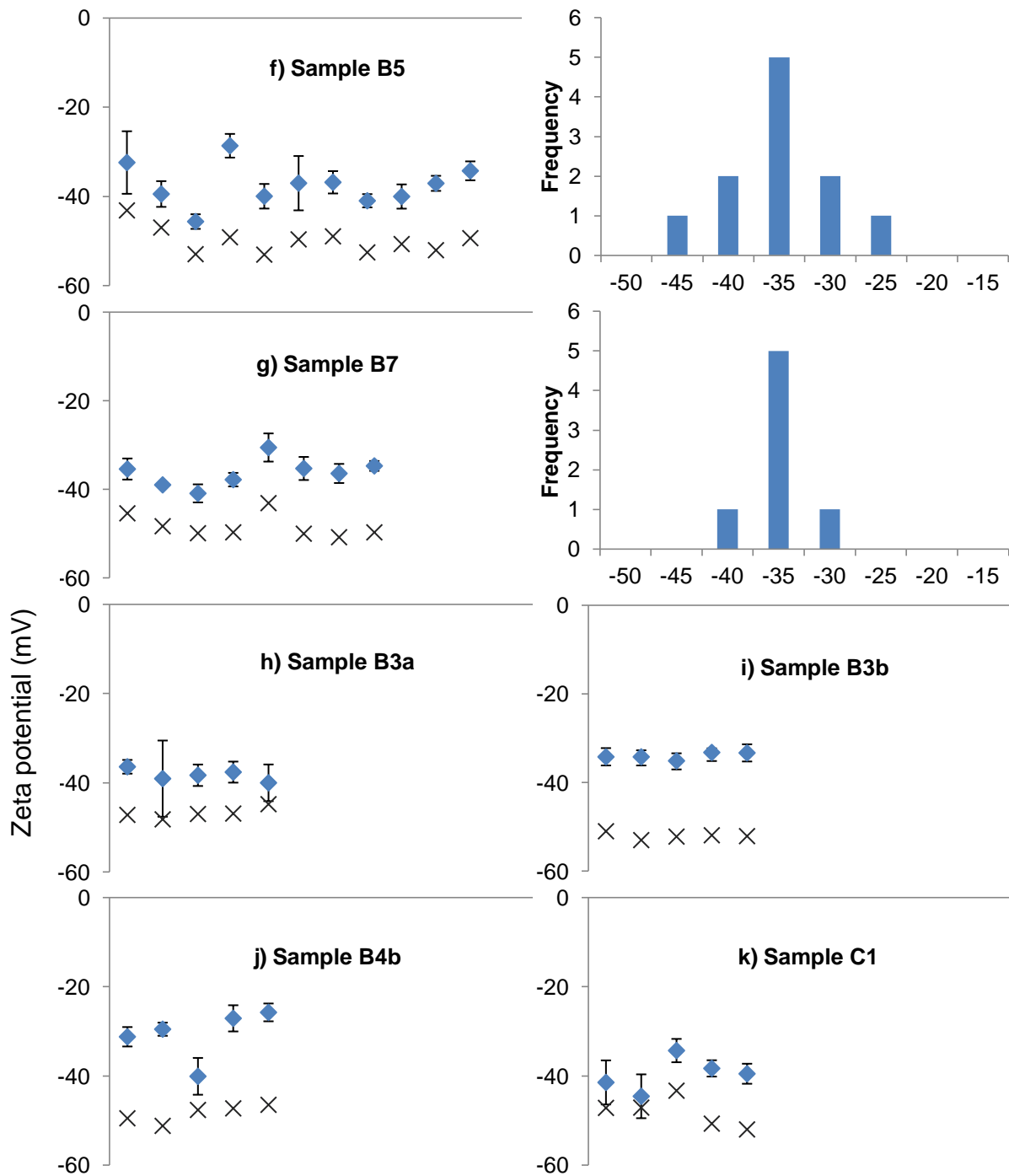
Figure 3-6. Surface zeta potential measurements on horizontally adjacent sandstone samples (blue diamonds) and corresponding probe particle zeta potential (crosses) at 69.2m depth. Measurements in a-e and h were taken in 2mM KCl and f-g and i-k in 1mM KCl, all at pH6. The error bars indicate a standard deviation on the measurement based on five repeat measurements at each distance from the sample surface. Histograms are presented for any sample with 7 or more measurements.

3.5.7   Sandstone surface zeta potential using SS-EFM –variability in a single bed

Samples were taken from 16 different locations within 10 cm of each other in the same bed, a channel unit (lithofacies 3, see Table 3-1), in order to determine local-scale zeta potential variability. This bed is made up of medium-grained sand with no mud clasts but some weak planar laminations; samples were taken from the same horizontal elevation to avoid any effects of the lamination. Ten samples were tested with a background electrolyte concentration of 2mM KCl, and seven with a background electrolyte concentration of 1mM KCl (there was one crossover sample measured in both 1 and 2mM KCl), all with a pH of 6±0.25.

Figure 3-7 illustrates the average zeta potential values for each sample, and indicates that the variability is limited. In some cases in the 2mM KCl measurements a difference between some samples may be discernible (e.g. 69.1b from c, e, and g) but, in 1mM KCl, the zeta potential values lie within ±5 mV, and little variation can be discerned in this bed at the few mm scale of the technique.

The zeta potential values at 2mM KCl are less negative than those measured at 1mM KCl (averages ± standard deviation are -30.9±7.4mV compared with -36.3±4.5mV). This would be expected simply because of the effect of ionic strength on zeta potential. However, the effect may be more complex than this, as the sandstone has a significant ion exchange capacity and the K^+ in the solution may well be sorbed, releasing Ca^{2+} into solution. This change in counter ion composition would be expected to be greater for the 2mM KCl experiments than for the 1mM KCl experiments, and is an issue which is explored further in Chapter 4.
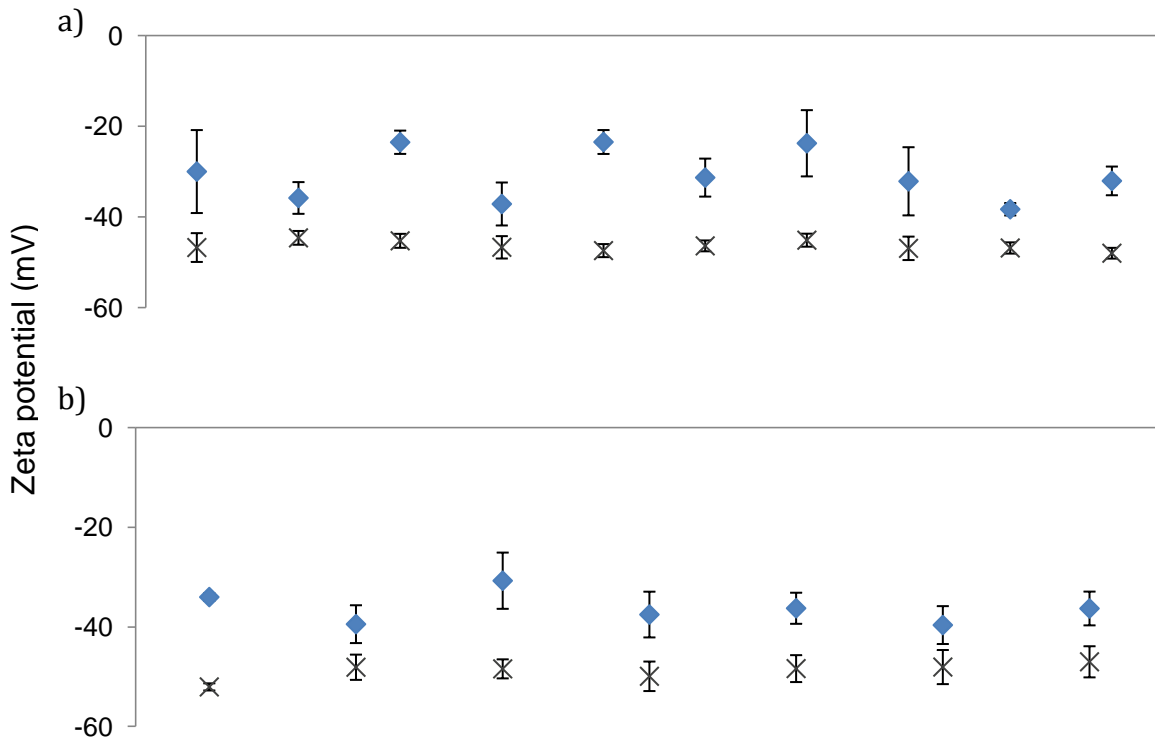
Figure 3-7 SS-EFM measurements of 16 adjacent samples at approximately pH6, a) with 2mM KCl (average zeta potential of -30.9±7.4mV) and b) with 1mM KCl (average zeta potential of -36.3±4.5mV). The crosses are probe particle zeta potential (average zeta potential of -46.4±1.1 and -48.8±1.7mV respectively). Error bars show a standard deviation on at least four measurements of the same sample.

3.5.8   Comparing the new SS-EFM technique with the established electrophoresis

technique for measuring sandstone zeta potential

Before continuing to measure the surface zeta potential of other lithofacies in the redbed

sandstone using SS-EFM, electrophoresis measurements were carried out on samples

directly adjacent to those described in Figure 3-6. Although the SS-EFM measurements

are simple and measure the zeta potential of a smaller effective area of surface, the

relative preparation and measurement time using electrophoresis is less.

Under the same ionic strength and pH conditions as the intact surface samples, the SS-

EFM and electrophoresis techniques give relatively similar results (Figure 3-8). The SS-

EFM measurements have an average of -32.6±5.6mV, while electrophoresis

measurements on adjacent samples show a much smaller range, with an average of 34.9±0.3mV. As discussed above, the SS-EFM technique offers measurements which are repeatable within 10% RSD on a single sample. The electrophoresis technique, on the other hand, is repeatable to within 1.1mV on a single sample, which represents an RSD of 3.2% of the average.
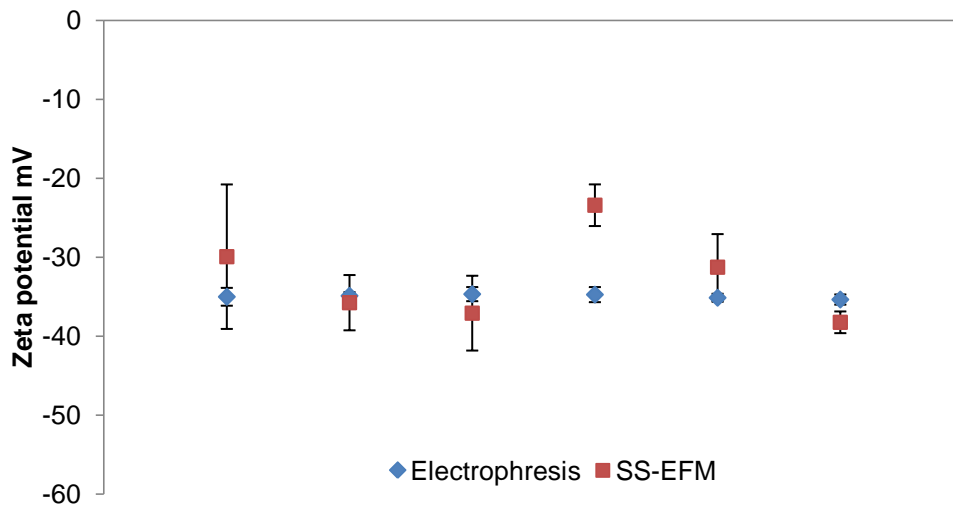
Figure 3-8. A comparison of zeta potential results from the SS-EFM and electrophoresis techniques for samples in 2mM KCl. The error bars indicate a standard deviation in the result. The error bars on the electrophoresis data are obscured by the data point marker; the standard deviation based on eight repeat measurements is not greater than 0.4mV for all results.

As the absolute values for zeta potential using these techniques were comparable, it was decided that the majority of zeta potential measurements for the length of the core (>50m) would be carried out using electrophoresis, with selected samples across the full length and range of lithofacies being measured using SS-EFM.

3.5.9   *Sample storage and equilibration solution volume*

Measurements taken after equilibration in both a 50ml and 1l equilibration volume provided comparable results. The internal integrity of the results increased with

equilibration in 1l of electrolyte, specifically, the measurements of apparent zeta potential at each distance from the sample surface showed a smaller standard deviation. The reported absolute surface zeta potential was however not reliant upon equilibration volume.

Future measurements will be taken following equilibration with 1l of the appropriate solution, due to the improvement in reported standard deviation for these measurements.

3.6 Conclusion

The SS-EFM technique was successfully applied to mineralogical material, firstly with a surface zeta potential on mica which was comparable to literature values, despite variations in sample preparation and storage between studies.

It was found that an increase in sample roughness increased the difficulty of the measurement, as the sample surface was then more difficult to locate accurately, but results in similar zeta potential values being measured. Careful sample preparation is important. There will be a point where a sample is too rough for SS-EFM to be used, but that point was not reached with these medium-coarse sandstone samples.

Repeatable measurements were achieved on intact sandstone samples. There is a certain amount of variation in repeated measurements on a single sample, but within the range of typical RSD for reproducibility of measurements on well-behaved materials found by Corbett et al., 2012.

The issue of locating the sample surface (or zero distance) accurately could potentially produce variation between different users, or a systematic error for one user. This problem increased with rougher surfaces and with reflective or transparent materials, as locating the surface became more difficult under these circumstances.

4 ZETA POTENTIAL HETEROGENEITY OF SANDSTONE

4.1 Introduction

Mobility calculations of the kind often used for manufactured nanoparticles in a porous medium require knowledge of the surface properties of the rock and the particles. Under unfavourable conditions, where both solid surfaces have like charge, nanoparticle retention is often greater in experimental studies than that predicted by theoretical calculations (Elimelech, 1991, Elimelech and O'Melia, 1990b, Elimelech and O'Melia, 1990c, Franchi and O'Melia, 2003, Hahn et al., 2004, Johnson and Tong, 2006, Li et al., 2004, Tufenkji and Elimelech, 2004b). This increased retention has been described by many as a result of heterogeneity of surface and other properties in both the porous medium and nanoparticle population.

Heterogeneity in physical and geochemical properties, at various scales, can have an impact on the transport of manufactured nanoparticles. These physical heterogeneities include differences in grain size (with associated differences in pore throat diameters) (Bradford et al., 2004, Li et al., 2008, Saiers et al., 1994, Saiers and Ryan, 2005) and surface roughness (Bhattacharjee et al., 1998, Shellenberger and Logan, 2002). Geochemical variations affecting transport arise from surface impurities and different quantities of surface coating (often ferric oxy-hydroxides) (Elimelech et al., 2000, Johnson et al., 1996, Loveland et al., 2003).

Ryan et al. (1999) have used a field study to investigate geochemical heterogeneity while Song et al. (1994) and Song and Elimelech (1994) have used numerical models to investigate the effect of patches of different surface charge on particle mobility. In

addition, well-characterised sands with varying quantities of iron oxide-coated grains (either natural or precipitated in a laboratory) have been used in transport studies to mimic heterogeneous conditions, with some investigations including the visual assessment of surface coatings and measurement of zeta potential (Elimelech et al., 2000, Johnson et al., 1996, Loveland et al., 2003, Ryan et al., 1999). However, specific studies of heterogeneity in natural systems are largely lacking.

Zeta potential has been shown (chapters 2 and 3) to be a convenient measure of surface properties, as it is a relatively simple measurement to make and the resulting value gives insight into the repulsion between charged surfaces, which is proportional to the square of the zeta potential (e.g. Hunter, 1981). Zeta potential is one of the controlling factors in particle dispersion stability, with a value closer to zero indicating a less stable dispersion: aggregated particles will be less mobile in porous media. In addition, the difference in zeta potential of the particles and the porous material has a significant effect on the attachment of the particles to the surfaces (Elimelech et al., 1995).

A small number of studies have specifically addressed the importance of characterisation of the zeta potential of the porous material for predicting particle transport in heterogeneous systems. Elimelech et al. (2000) found that the zeta potential of homogeneous porous material is useful for predicting particle transport in column studies, but the zeta potential measured over a 3cm long column of heterogeneous material (mixed aminosilane-modified and 'clean' quartz grains) could not be used to explicitly predict particle behaviour; it gave only a qualitative indication of the effect on transport behaviour with porous media surface chemistry. While zeta potential has thus far not been used successfully to predict breakthrough of nanoparticles quantitatively in

a column study, it could be used as an initial indicator of the probability of particle mobility in aquifers.

The majority of the work on manufactured nanoparticle mobility has been carried out using artificial porous media or disaggregated, cleaned and repacked materials. However, it is important to assess the transport in real intact rock, and, as such, to assess the electrokinetic heterogeneity of this material. The only studies on zeta potential distributions in intact natural media that we are aware of relate to oil recovery, and involve surfaces coated in hydrocarbons: there appears to be a lack of studies investigating the heterogeneity of zeta potential in rocks under conditions that are directly relevant to nanoparticle transport in most common, shallow aquifer systems.

This chapter follows up on the work carried out in Chapter 3, which tests a new method of attaining the zeta potential of a surface on environmental materials, by measuring the zeta potential of red bed sandstone over a variety of lithofacies (Table 4-1) to describe the electrokinetic heterogeneity. Measurements are undertaken using the new SS-EFM technique, alongside electrophoresis, for multiple samples from each sandstone lithofacies with solutions of differing chemical composition. The first section describes heterogeneity within a single sandstone lithofacies, then follows a section on heterogeneity over the full 50m of sandstone analysed, with the final section detailing the effect of solution chemistry on these values.

4.2 Aims

- To determine the zeta potential properties of an example redbed sandstone and their variation throughout a sandstone sequence.

- To determine how the zeta potential changes with chemical conditions, in particular pH and ionic composition.

- To provide explanations for the observed properties.

4.3 Method

4.3.1   Sandstone sample selection and preparation

4.3.1.1 Sandstone sequence

Samples of sandstone and mudstone were acquired from a core of a redbed continental sandstone sequence taken from a borehole in Preston, north-west England. The material is of Triassic age, and drilled into the Chester Pebble Beds Formation of the Sherwood Sandstone Group. The geological characteristics of the English Permo-Triassic sandstone sequence have been described in many studies (Allen et al., 1997, Tellam and Barker, 2006, Plant et al., 1999): the sandstones generally consist of lithic arkoses to quartz arenites. The grains are coated in haematite with small amounts of manganese oxides and an organic content of typically <0.1% (Steventon-Barnes, 2001, Shepherd, 2003).

Within the UK Permo-Triassic sandstone sequence are zones bleached by the passage of reducing fluids, probably as the result of water escaping from the underlying, organic-rich, Carboniferous sequence (Tellam, 1995). These bleached zones are grey/buff in colour rather than red, showing that the main haematite coating has been removed.

The 65m core has been split into five lithofacies; these have been defined by Moran (2008) on the basis of grain size, sedimentary structure, and presence of certain grain types (Table 4-1). Samples for this study were taken from a 50m section of this core, with each lithofacies being represented. Where mud clasts are common, these are sampled along with the bulk sandstone and are labelled 'M'. Two samples have also been taken from a bed where both red and bleached sandstone is observed; the bleached sample is labelled 'B'.

The cation exchange capacity (CEC) of 143 sandstone and mudstone samples from this core indicate a range of 1-4meq/100g dry sample for sandstone and a much higher 10-20meq/100g for mudstone (M. Jaweesh, pers. comm.).

4.3.1.2 Other samples used

While a sample was taken from a bleached zone within the core described above, there was a gradation between the red and bleached areas so directly adjacent samples could not be taken. A sandstone core sample from North Cheshire showed a sharp transition from haematite-coated to bleached sandstone which allowed samples from each <5cm apart in the same bed to be measured.

For some of the experiments where zeta potential was measured with change in pH, samples were required where the pH buffering from carbonate cement was excluded. Sandstones were sampled from a roadside outcrop in Quatt, Shropshire for this purpose, where carbonate cement had been removed by greater water circulation (J.H. Tellam, pers. comm.).

Lithofacies number	Grain size	Mud clasts	Mica	Lamination	Interpreted Palaeo-environment	Surface samples	Disaggregated samples
1	Mudstone to siltstone	-	Yes		Abandoned channel or overbank deposits	2	2[a], 3[b]
2	Very fine sandstone	None	Yes	90% are planar and low angle	Channel fill, relatively low flow	2 (+1 B)	2[a], 4[b] (+1 B)
3	Fine to medium sandstone	Very few	Yes	80% are planar and low angle	Channel fill	1	1[a], 8[b]
4	Medium to coarse sandstone	Common	Yes	90% are cross laminated	Channel fill, relatively high flow	2 (+1 M)	2[a], 7[b] (+1 M)
5	Medium to coarse sandstone	Many	Yes	70% are massive	Channel lag	2 (+1 M)	2[a], 5[b] (+1 M)

Table 4-1 Lithofacies definitions for the Preston core (Moran, 2008). The final two columns indicate the number of samples taken from each lithofacies for measurement, with B indicating a bleached sandstone sample and M a sample made up from mud clasts.
[a]this number of samples have been measured in all chemistries, [b]this number of samples have been measured in KCl.

4.3.1.3 Sandstone and mudstone preparation

The sandstone samples were prepared for SS-EFM in the same manner as described in Section 3.4.4; where the sandstone was worked to approximately 4mm by 5mm, by 1mm thick while attached to a PEEK sample holder. Mudstone samples are handled slightly differently; the mudstone is split along laminations until a piece of approximately 1mm continuous thickness is achieved. A PEEK sample holder is then attached to this and the mudstone is cut back using a craft knife to the same dimensions as the holder (4mm by 5mm). This method applies both to mudstone lithofacies (lithofacies 1) and to mud clasts incorporated in other lithofacies (samples from lithofacies 4 and 5).

Electrophoresis measurements were taken on fine material released by disaggregated sandstone and mudstone. The mudstone required more hand grinding using a pestle and mortar to disaggregate it. Approximately 3g of each sample was disaggregated and the rock mass needed for each experiment was then taken from this bulk sample. To make up the dispersion for electrophoresis, the required mass of sample was mixed with a solution of the required chemistry, left on a shaker for 30 minutes and then in a sonication bath for a further 30 minutes.

Both the SS-EFM surface samples and the disaggregated samples were left to chemically equilibrate overnight, for at least 18 hours. This equilibration time also allowed coarse material to settle out from the dispersions of disaggregated material.

4.3.2 Electrolyte solutions

Electrolyte solutions were made up using salts KCl, NaCl, $CaCl_2 \cdot 2H_2O$ and for the artificial groundwater (AGW) $MgSO_4 \cdot 7H_2O$ and $NaNO_3$. All solutions were made up at 1mM ionic strength. This value is low compared to average reported groundwater ionic strengths, but allows comparison with the greatest number of individual mineral zeta potential values in literature. The chemical analysis for the AGW is reported in Table 4-2, the cation proportions were the same as the artificial groundwater developed for Rahman (2006), but the ionic strength is much lower. The major ion concentration for KCl, NaCl and $CaCl_2$ are provided for comparison.

Ion	Artificial groundwater (mg/L)	KCl (mg/L)	NaCl (mg/L)	$CaCl_2$ (mg/L)
Na^+	1.43	-	23.0	-
Cl^-	12.05	35.5	35.5	70.9
NO_3^-	3.52	-	-	-
K^+	0.18	39.1	-	-
Ca^{2+}	6.64	-	-	40.1
Mg^{2+}	2.55	-	-	-
SO_4^{2-}	10.10	-	-	-

Table 4-2 Major ion content of the artificial groundwater solution, with comparison to KCl, NaCl and $CaCl_2$ solutions

Selected samples were pH adjusted using NaOH. Following preparation (as described above) and an initial measurement at ambient pH, 1mM NaOH was added, the sample was then sonicated for 10 minutes and a further measurement taken after an hour. This process was repeated until zeta potential values at pH values ranging from ~pH4 to pH9 were gained.

4.3.3   Zeta potential measurements

4.3.3.1 Electrophoresis

The method used for electrophoresis measurements is fully described in Section 3.4.

Measurements reported here are the mean of 10 individual measurements on the same

sample of nanoparticle dispersion each separated by a 20 second pause.

4.3.3.2 Single Surface Electroosmotic Flow Mapping (SS-EFM)

The method used for the SS-EFM measurements is fully described in Section 3.4. For the

SS-EFM measurements, 100nm silica microspheres were used as the probe particle, as

this would provide information relevant to the column experiments in Chapter 5, where

the transport of silica particles through a sandstone column was observed.

The SS-EFM measurements are calculated from zeta potentials at 4 distances, each

125µm apart, and the probe particle zeta potential at 1000µm from the surface. Each of

these five zeta potentials were the average of five individual values at that point.

4.4 Results and discussion

4.4.1   Probe particle characterisation

Before taking an SS-EFM measurement, the zeta potential of the probe particle was

measured using 25 electrophoresis measurements over 30 minutes (to reproduce as

closely as possible the conditions in SS-EFM). This gave stable results for SiO_2 in both

KCl and $CaCl_2$, with averages of -51.9±0.9mV and -25.4±0.4mV respectively. There is a

normal distribution of zeta potential values in both KCl and $CaCl_2$, with a standard

deviation of 9-9.5mV (Figure 4-1). The distribution of a latex zeta standard is also shown

in Figure 4-1 for comparison, the distribution is only slightly narrower to those found

for the probe particles.
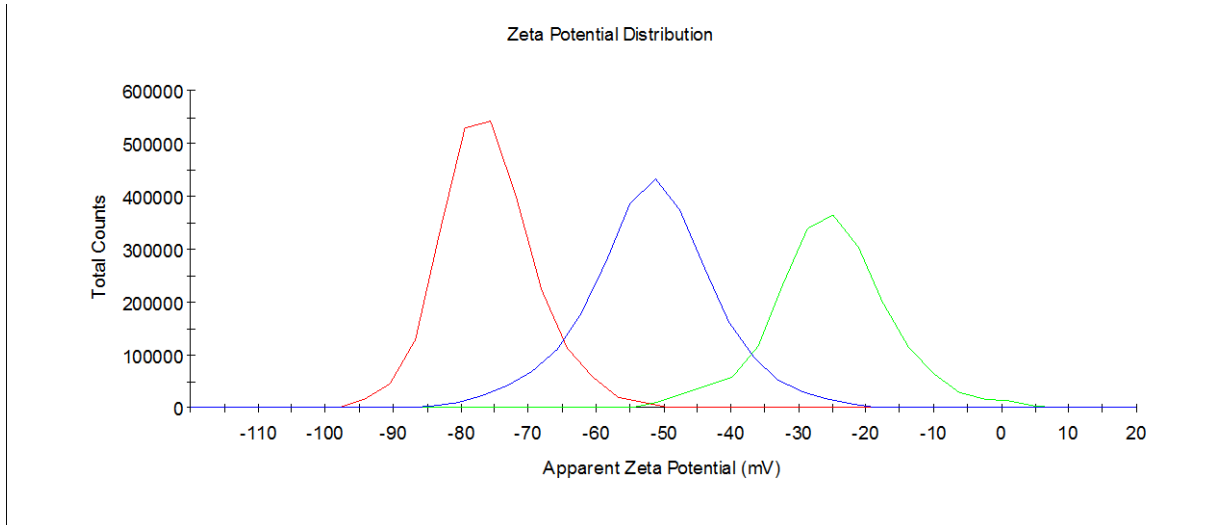
Figure 4-1 The zeta potential distribution for SiO_2 in KCl (blue, SD 9.5mV), SiO_2 in $CaCl_2$ (green, SD 9.0mV) and a latex zeta standard (red, SD 6.9mV)

The average zeta potential measured for the probe particle in KCl as part of the surface

measurement is -46.3±4.4mV and in $CaCl_2$ is -18.4±0.4mV. These values are both lower

than the initial zeta potential of SiO_2 before the SS-EFM measurement and contact with

the sandstone surface, but this is understood to be a systematic effect of the method

used to measure the particle zeta potential (see Section 3.5.2).

The size distributions for silica in KCl and $CaCl_2$ are the same, and are normal and

relatively narrow (Figure 4-2). The size is stable for more than 8 days, with a

hydrodynamic diameter, as measured using DLS, of 115-120nm.
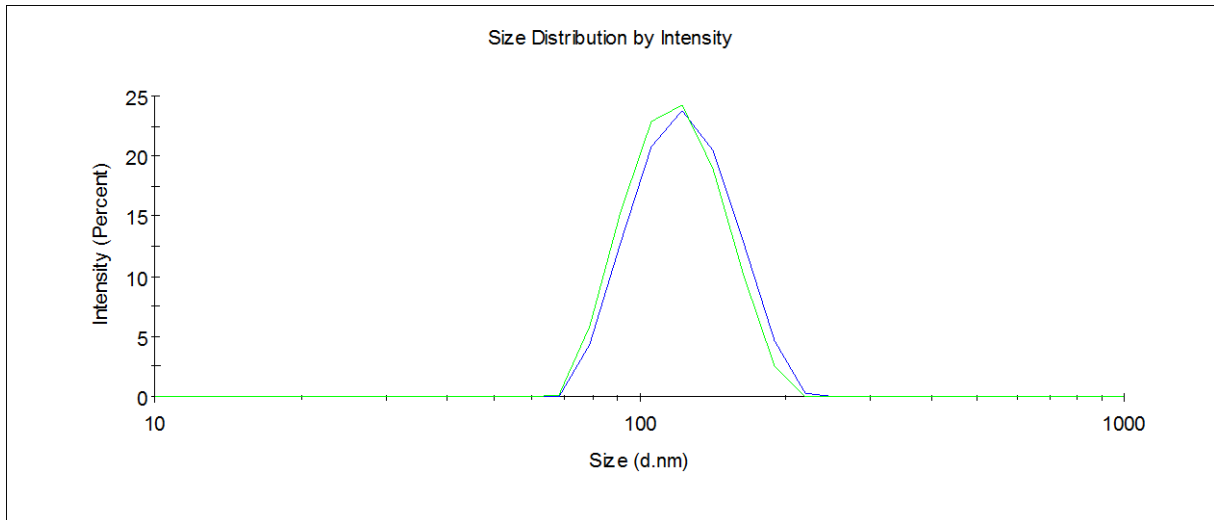
Figure 4-2 The size (hydrodynamic diameter) distribution for SiO$_2$ in KCl (blue) and CaCl$_2$ (green)

4.4.2   Variation in zeta potential through the sandstone sequence

4.4.2.1 The observed variation

Chapter 3 established that there is little variation in the average zeta potential within an individual sandstone bed. However, there may be variation between different beds of both similar and different lithofacies, and also possibly with depth (e.g. caused by different degrees of water-rock interaction in the most active part of the groundwater flow system near the ground surface). To investigate the variation of zeta potential through the sandstone sequence, SS-EFM and electrophoresis measurements were undertaken on samples from all lithofacies, as described in Table 4-1.

Figure 4-3 shows the variation in zeta potential with depth when the samples are equilibrated with 1mM KCl; measurements are taken using SS-EFM. The measurements indicate that there is little variation and no discernible systematic pattern with lithofacies for the four sandstone lithofacies, with a 1mM KCl solution.

65
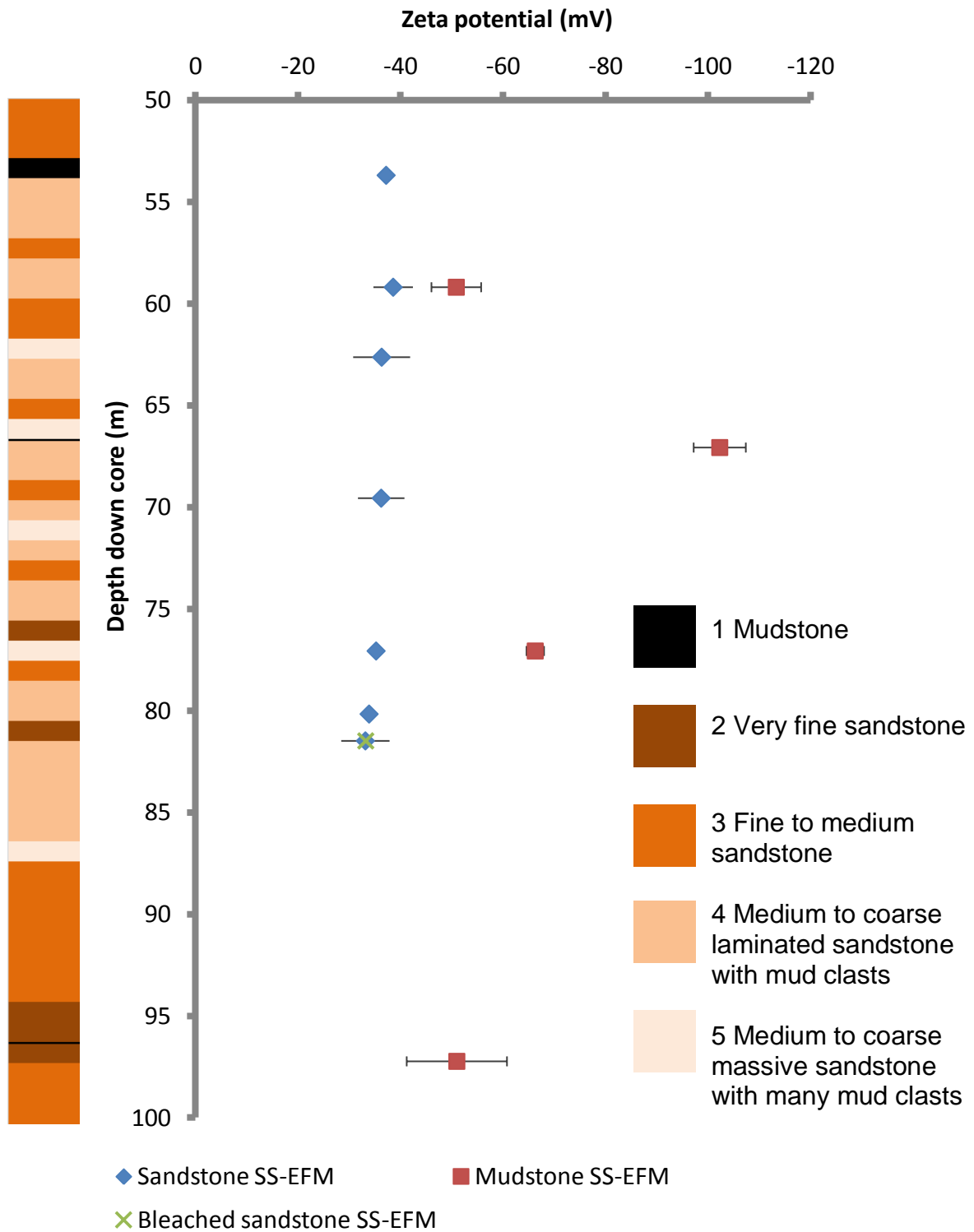
Figure 4-3 SS-EFM measurements on various samples over a 50m depth, lithofacies are indicated to the left of the data plot. The measurements were all taken after equilibration of the surface with 1mM KCl and at ambient pH (~pH6). Error bars show standard deviation for the average of a number of individual measurements on each sample.

It could be argued, however, that there is the beginning of a pattern over depth for these measurements (a linear regression gives an R^2 value of 0.78 for the zeta potential with depth). This pattern is not lithofacies-dependent and cation exchange capacity and carbonate content of the sandstone do not show any pattern with depth, the driver for the sandstone zeta potential becoming less negative with depth could not be established.

Electrophoresis measurements of sandstone and mudstone in KCl were taken on 34 samples from this 50m of core, including the samples upon which SS-EFM measurements were taken. Figure 4-4 shows that similar results were obtained for the four sandstone lithofacies using the two techniques. The electrophoresis results have a much smaller standard deviation on measurements repeated on the same sample: this is likely to be due in part to the SS-EFM measurement being a composite of many measurements (with repeated electrophoretic mobility measurements at multiple distances from the sample surface followed by further repeated measurements on the probe particle alone) with an increased opportunity for error. Electrophoresis measurements are also taken over a much shorter time period, so there is less time for changes in pH due to dissolution of atmospheric CO_2.

The sequence at Preston has only two thin mudstone units. These were sampled, but in addition samples were taken from mudstone rip-up clasts that are present within lithofacies 4 and 5. The results of SS-EFM measurements of a solid mudstone surface are included in Figure 4-3 and Figure 4-4 and indicate that the mudstone zeta potentials are significantly more negative than those for the sandstones. In contrast, the results for mudstone using electrophoresis (Figure 4-4) are indistinguishable in value from those of the sandstone lithofacies.
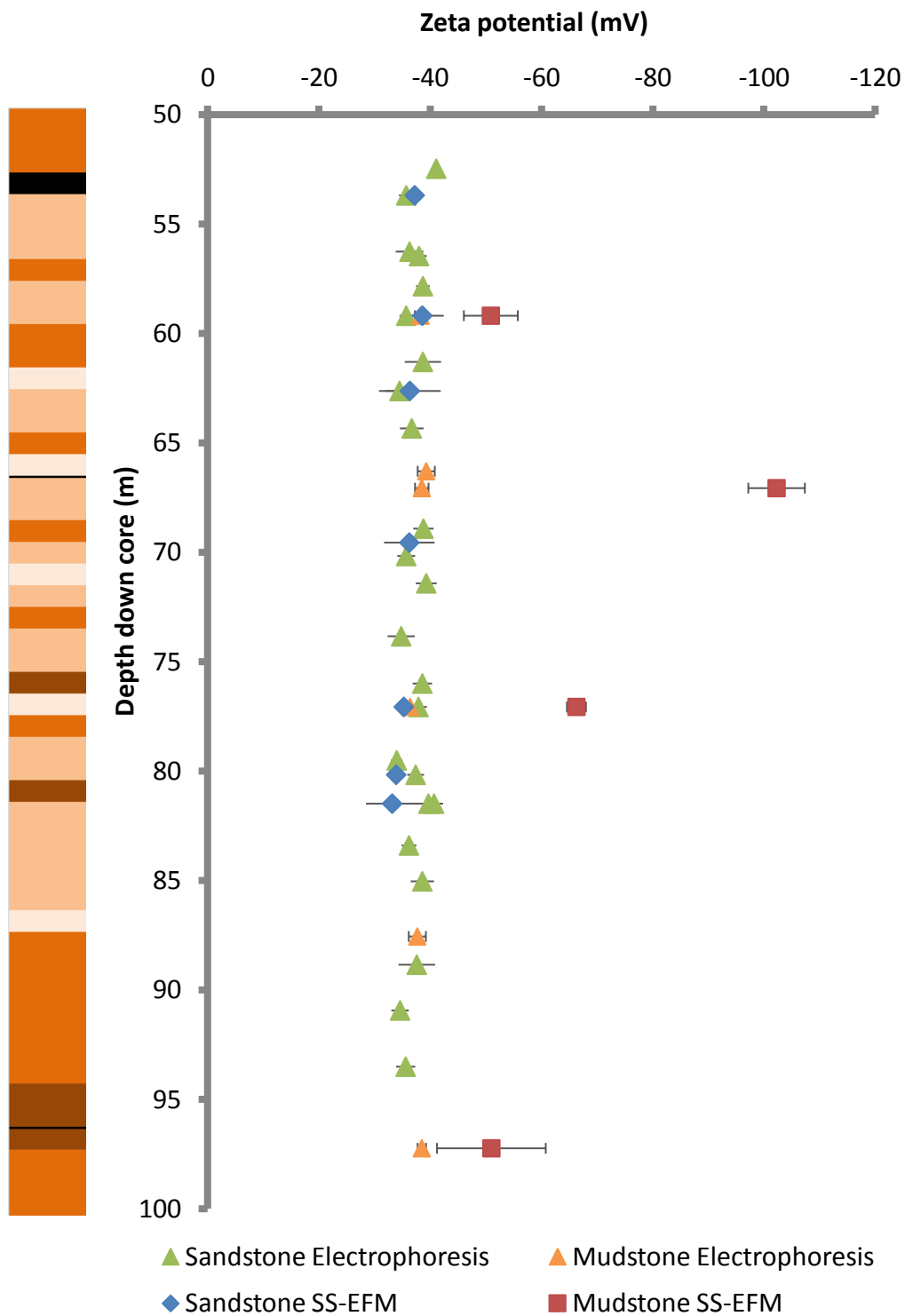
Figure 4-4 A comparison of SS-EFM and electrophoresis measurements over a 50m depth of core. The measurements were all taken after equilibration of the sample with 1mM KCl and at ambient pH (~pH6). Error bars show standard deviation, on SS-EFM for multiple independent measurements on each sample and for electrophoresis for 10 measurements on a single sample aliquot.

Three observations need explaining:

1. The similarity of zeta potentials through the sequence;

2. The difference between the zeta potentials of the sandstone and mudstone as measured by SS-EFM; and

3. The difference between the zeta potentials of the mudstones as measured using the two techniques.

These three questions are addressed in the following two sub-sections.

4.4.2.2 Controls on the zeta potential of the sandstones in the sequence

The similarity in zeta potentials within the sandstone samples was initially thought to be due to screening by the haematite coating. At a depth of 81.48m, both red sandstone and bleached, haematite-poor sandstone are present. SS-EFM measurements on nearby samples from these two colour zones are shown in Figure 4-3; the surface zeta potential was found to be the same. This result is supported by measurements on a sandstone sample from the northern end of the Cheshire Basin where red-bed and bleached samples were measured using electrophoresis as shown in Table 4-3. This similarity in zeta potential for bleached and coated samples and the difference between mudstone and sandstone measurements using SS-EFM (as mudstone is also covered in haematite) combine to form a compelling argument that the similarity in zeta potentials is not simply a direct result of the haematite coating.

Sample	Method	Zeta Potential	StDev
Preston red	SS-EFM	-33.2	4.71
	Electrophoresis	-40.7	1.63
Preston bleached	SS-EFM	-33.3	1.48
	Electrophoresis	-39.7	2.12
N Cheshire red	Electrophoresis	-41.4	1.19
N Cheshire bleached	Electrophoresis	-43.9	1.55

Table 4-3 Average zeta potential values for adjacent red and bleached sandstone samples

Johnson et al. (1996) and Elimelech et al. (2000) have carried out nanoparticle transport experiments using various mixes of clean and surface modified quartz grains, measuring the percentage breakthrough and analysing this in comparison with the overall zeta potential predicted by the mix of known surfaces. They found that mixing physically homogeneous but chemically different sand causes the overall zeta potential to follow a simple surface area-weighted linear mixing model. This would suggest that the bulk zeta potential of sandstone should be a linear mix of the zeta potential of its component parts adjusted for the volume fraction and surface area of each mineral.

The redbed sandstone contains a mix of detrital quartz (on average 50-65% of whole rock), feldspar (largely K-feldspar, 5-10%) and lithic clasts (igneous and metamorphic rock fragments and mud rip-up clasts, 10-15%) with diagenetic carbonate, mica, clay minerals (illite, smectite and chlorite) and haematite (Burley, 1984, Plant et al., 1999).

Literature values for the zeta potential of mineral constituents of redbed sandstone are shown in Table 4-6 (at the end of the chapter) along with average percentage content (from point counting on thin sections of 11 samples of the sandstone core, M. Jaweesh, pers. comm.) and estimated surface area (from literature values). From the literature

values it would be expected that the overall zeta potential for the sandstone would be negative, with mica rich regions promoting the transport of negatively charged nanoparticles, with dolomite, and potentially calcite and haematite, providing more attractive patches for nanoparticle retention.

Surface area for a particular mineral has been estimated from literature and reported in Table 4-6 (Dubois et al., 2010, Macht et al., 2011, Dogan et al., 2006). The value is difficult to evaluate due to its dependence upon grain size, which could be very different for individual minerals in the sandstone used here compared to the materials measured in literature. However, the surface area for clay minerals compared to other sandstone components is invariably high, so the calculations will have limited sensitivity to small changes in the surface area of other components. These average mineral surface area values are used, along with the percentage proportion by volume of each mineral within the redbed sandstone (Table 4-6), to give a mineral surface area for each mineral specific to the sandstone used.

The mixing model will be sensitive to the values of zeta potential attributed to individual minerals, and particularly to clay minerals. There is a large range in reported zeta potential values for individual minerals even under similar chemical conditions; there are a number of potential reasons for this observation. Selection of the sample itself is important to the zeta potential as naturally occurring minerals can give different values to synthesised material, and the conditions of deposition or synthesis can also alter surface properties. In Table 4-6 haematite zeta potentials at the same pH and ionic strength range between strongly positive in synthetic samples and negative in natural mineral samples. This is understood to be due to silica impurities in the natural samples

masking the haematite zeta potential (Carlson and Kawatra, 2013, Hunter, 1981). The effect of impurities has also been observed measurements of clay zeta potential, where silica and alumina from the clay edges is deposited on the crystal face and can cause variability in the measured zeta potential (Hunter, 1981, Lyons et al., 1981).

Sample preparation and equilibration can also significantly affect the zeta potential of a surface. A number of the samples have been chemically and physically cleaned to remove impurities and have been equilibrated with various solutions before the zeta potential is measured. The electrolyte solution the sample is exposed to before the measurement could affect the surface species due to ion exchange reactions; the aging time in this solution will also have an effect depending on the rate of this exchange reaction. For calcite, the concentration of solids (rock/water ratio) is important, and has even been observed to change the sign of the particle zeta potential (Siffert and Fimbel, 1984). To a certain extent, the measurement technique and, in electrophoresis measurements, the equation used to convert electrophoretic mobility to zeta potential has an effect on the final value. This measurement technique may be particularly important if there is heterogeneity of charge on the particle, so clay minerals, where different zeta potentials are found on the crystal face and edge (e.g. Zhao et al. 2008), may be misrepresented using some measures of zeta potential.

The approximate percentages, surface area and range of zeta potential values for each mineral do not allow an exact calculation of the sandstone zeta potential. However, using the percentage content, surface area and average zeta potential information available, a surface area-modified linear mixing model is used to estimate a zeta potential range.

Table 4-4 provides a worked example of the calculation carried out to estimate the sandstone zeta potential using a surface area-modified linear mixing model. Further calculations within the percentage content and zeta potential ranges described in Table 4-6 provide an estimate of -30 to -35 mV for a sandstone sample with 1mM KCl.

The estimate above is only slightly lower than the average value for a sandstone surface measured using SS-EFM of -36.2mV, which indicates the success of the mixing model. The clay minerals provide the dominant control on average sandstone zeta potential using this method, due to their large surface area relative to the other minerals. An estimate of the surface zeta potential made using charge density gave the same bulk value to that of the mixing model above.

Mineral	Density	Volume proportion of mineral in sandstone (Table 4-6)	Mineral surface area (Table 4-6)	Average zeta potential (Table 4-6)	Surface area per unit volume (x)	x adjusted for zeta potential (y)	Surface area weighted zeta potential Sum(y)/Sum(x)
	kg/m^3	%	m^2/g	mV	m^2/m^3	-	mV
Quartz	2650	59	0.1	-50.5	157338	-7945555	-33.5
K-Feldspar	2560	5	0.1	-68.0	13894	-944780	
Clay minerals	2600	18	30	-33.7	14004545	-472491818	
Haematite	4000	3	5	-13.5	640000	-8640000	
Calcite	2710	1	0.1	-14.7	3006	-44083	
Biotite	3000	1	5	-78.0	150000	-11700000	
Lithic clasts		12					
Sum		100			14968783	-501766236	

Table 4-4 A worked example of the calculation carried out to produce a value for sandstone zeta potential using a surface area weighted linear mixing model

4.4.2.3 Controls on the measured zeta potential values of the mudstones in the sequence

The surface zeta potential measurements for mudstone using SS-EFM were distinctly more negative than the sandstone results. In line with the mixing model, these more negative values could be due to an increased proportion of oriented clay minerals and mica. The more negative zeta potential values were not observed when measuring crushed mudstone samples using electrophoresis.

As mentioned above, clay minerals are observed to have different surface properties and zeta potential on the crystal face compared to the crystal edges, with the crystal face being much more negative (Zhao et al., 2008). The intact mudstone used in SS-EFM is measured along a cleavage plane, with the exposure of clay crystal faces being more likely. Nishimura et al. (1992) observed a zeta potential of -34mV for crushed mica in 1mM KCl at pH 6.7, compared to -134mV for a surface measurement on an intact piece of cleaved mica. These observations could explain the differences between measurements using disaggregated and intact mudstone. The similarities between sandstone and mudstone zeta potential when measured using electrophoresis are also explained, especially for a mica-rich sample.

A mica sheet was used to investigate the impact of the different preparation methods used for SS-EFM and electrophoresis on the mudstone samples. An intact surface sample and particle dispersion were prepared from a single sheet of mica and measured using the SS-EFM and electrophoresis. The results (Table 3-2) show a significant difference between the two techniques (although still not as large a difference as that found by Nishimura et al. 1992) with a zeta potential of -45±3mV for the ground sample compared with -70±3mV for the intact sample. This result is in keeping with the findings

in Figure 4-4, where electrophoresis gives a lower magnitude zeta potential for disaggregated mudstone than the SS-EFM measurements on intact samples.

Increased amount of clay in a sandstone unit would reduce the permeability, however with zeta potentials which are significantly more negative greater nanoparticle mobility would be expected (for a negatively charged particle). Mudstone pellets are a feature of these sandstone units, and the different permeabilities and particle transport behaviours between these and the surrounding sandstone could create a dual-porosity type effect.

4.4.3   Sandstone under changing chemical conditions

All the measurements in section 4.4.2 were taken with a monovalent ion (KCl) at a concentration of 1mM and at the ambient pH of the electrolyte-sandstone system (pH6-6.5). Typical groundwater usually contains a combination of ions, both mono and polyvalent. To investigate the response of the sandstone zeta potential to changing chemistry the counter-ion valence and the pH were varied and zeta potential results recorded. Figure 4-4 indicates that equivalent data can be gained for sandstone with both SS-EFM and electrophoresis; therefore, while some measurements were undertaken using SS-EFM; the majority were undertaken using the more convenient electrophoresis technique.

Zeta potential values, from electrophoresis, for disaggregated sandstone and mudstone samples with solutions of different chemical composition with the same ionic strength are shown in Figure 4-5, with Table 4-5 containing the average zeta potential values for both disaggregated and intact samples, measured using electrophoresis and SS-EFM

respectively. The zeta potential values for all chemical compositions tested are negative. Solutions containing monovalent cations (KCl and NaCl) give the most negative zeta potential values, while the solution containing divalent cations ($CaCl_2$) gave the values closest to zero. Less negative zeta potential values with divalent ions are expected as there is a greater decrease in potential with distance from the particle or surface as the valency increases. Artificial groundwater contains a mixture of mono- and divalent ions (although divalent ions are dominant, see section 4.3.2 for details). All samples with AGW, excluding the carbonate-free sandstone, exhibit a zeta potential range slightly more negative than the sandstone in $CaCl_2$ solution.

A dispersion is often considered stable if the absolute sum of the zeta potential of the interacting surfaces is greater than 60mV (Hunter, 1981), so the silica particles in $CaCl_2$ and AGW may not be considered to be stable. In terms of particle transport through this sandstone, systems containing divalent cations would be expected to be more favourable for particle attachment than ones with the availability of only monovalent cations.
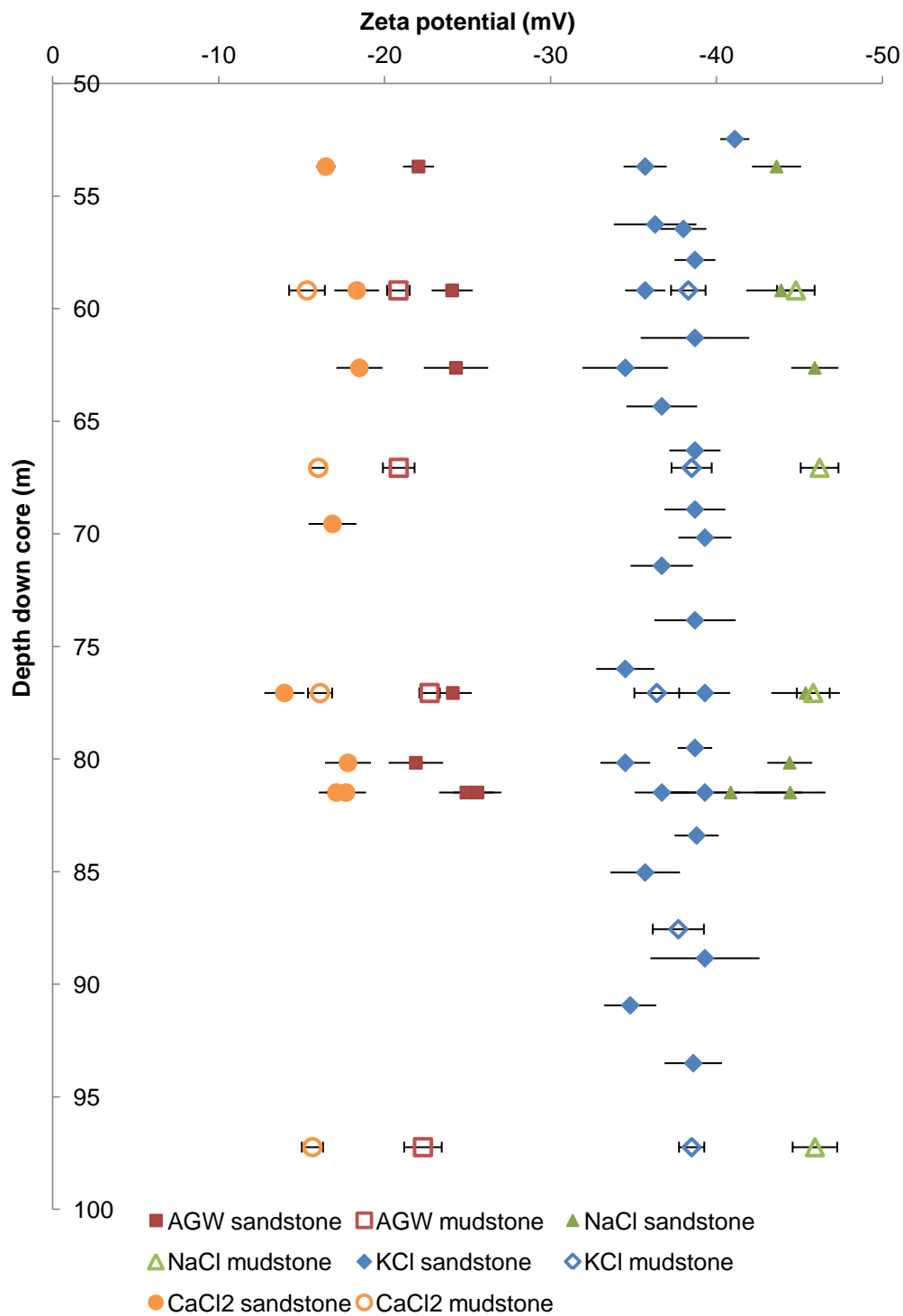
Figure 4-5 Electrophoresis measurements of sandstone and mudstone zeta potential taken with solutions of different chemistry at an ionic strength of 1mM, error bars indicate the standard deviation for 10 measurements on the same sample.

	Ionic strength	Type	SS-EFM				Electrophoresis		
	M	-	Number of samples	Number of Measurements	ZP mV	SD	Number of samples/ measurements	ZP mV	SD
KCl	0.001	Sandstone	16	69	-36.2	2.76	28	-37.9	2.36
		CaCO$_3$-free sandstone	0	0	--	--	3	-37.5	1.88
		Mudstone	4	11	-67.6	24.21	6	-37.9	0.80
NaCl	0.001	Sandstone	1	4	-39.3	2.20	8	-44.4	1.79
		CaCO$_3$-free sandstone	1	5	-41.1	3.23	3	-42.6	1.64
		Mudstone	1	2	-124.0	1.41	4	-45.7	0.63
CaCl$_2$	0.001	Sandstone	0	0	--	--	8	-17.1	1.44
		CaCO$_3$-free sandstone	0	0	--	--	3	-19.1	0.68
		Mudstone	0	0	--	--	4	-15.8	0.36
AGW	0.001	Sandstone	0	0	--	--	8	-24.0	1.33
		CaCO$_3$-free sandstone	0	0	--	--	3	-16.7	0.62
		Mudstone	0	0	--	--	4	-21.7	0.98

Table 4-5 Average zeta potential values for sandstone and mudstone measured under different chemistries using SS-EFM and electrophoresis. The standard deviation stated is for the average of the number of zeta potential measurements per material type.

Carbonate-free sandstone was initially used to measure the response of the sandstone zeta potential to changing pH, to avoid the problem of pH buffering of the solution due to calcite dissolution. Carbonate-free sandstone samples with solutions of differing chemistry all become more negative with increasing pH (Figure 4-6). The monovalent solutions show a larger change in zeta potential with pH than solutions containing divalent ions (between pH 5 and 9 the NaCl zeta potential range is 21.1mV and the AGW range is 13.2mV). The conductivity change is also indicated here; the amount of NaOH required to adjust the pH between pH 5 and 7 is such that the conductivity was relatively unaffected (Figure 4-6). To adjust the pH up to pH 9 a larger volume of NaOH was necessary, which caused a jump in conductivity, perhaps indicating a increase in ionic strength. However, the zeta potential at pH 9 is consistent with the pattern of earlier results, so any change in ionic strength was not enough to affect the bulk surface properties.

The effect of changing pH was also investigated using a number of sandstone samples from the core itself, both in KCl and $CaCl_2$. These results (Figure 4-7) also show 1) a general pattern of zeta potential becoming more negative as the pH increases, and 2) that sandstone in KCl has a greater change in zeta potential with pH than in $CaCl_2$. Sandstone 36 in KCl is an exception to this, and shows very little change in zeta potential over a pH range of pH 6.75 to 9.5. This could be due to the presence of carbonate, substantiated by the initial pH being higher than for other samples.
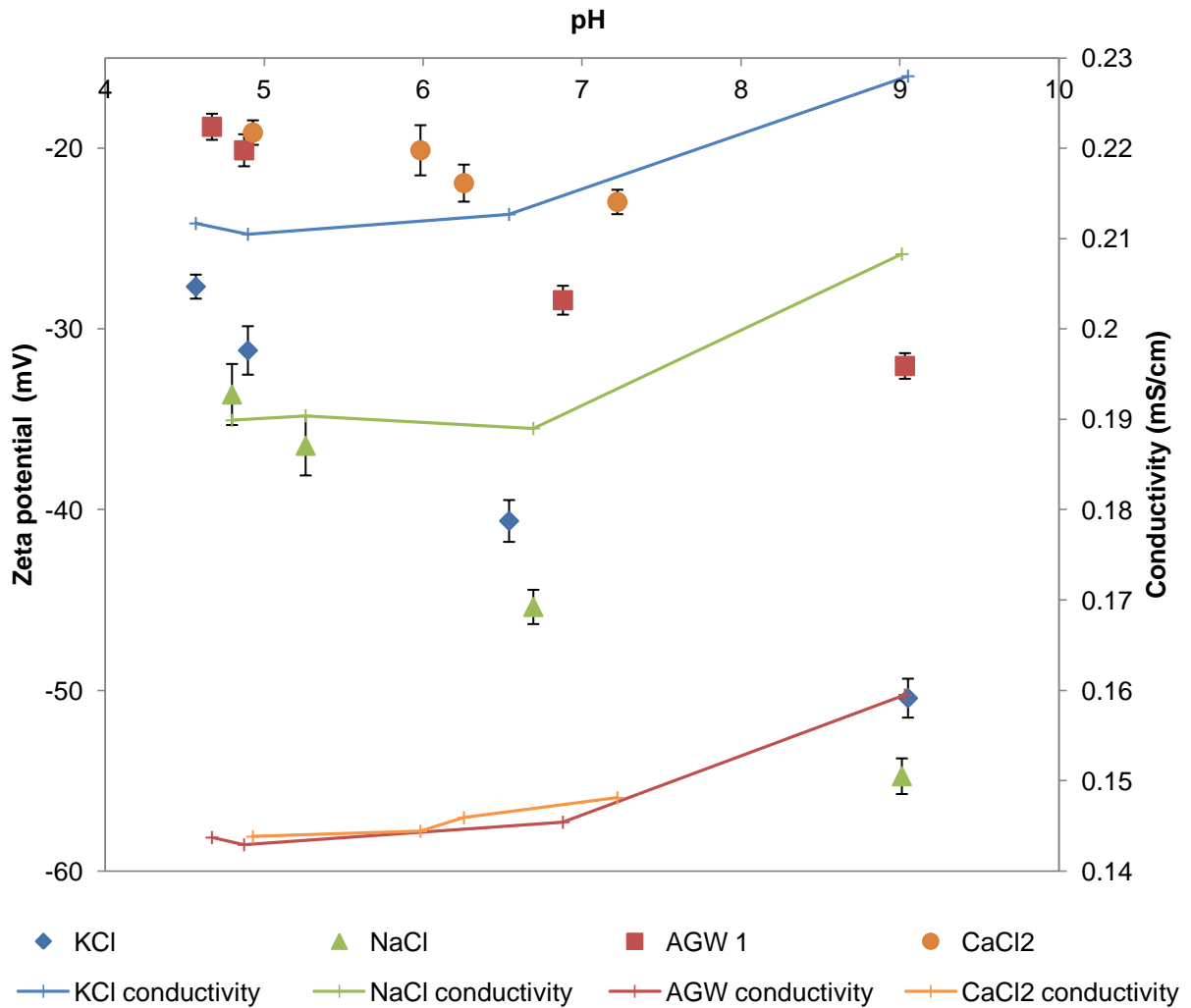
Figure 4-6 Zeta potential and measurements on carbonate-free sandstone with increasing pH. The pH is adjusted using 1mM NaOH.

The pH and zeta potential of these sandstone and mudstone samples is sensitive to changing rock/water ratio. It is observed in Figure 4-8 that different solution chemistries give rise to different responses when the rock/water ratio is increased from 0.02g to 0.5g in 25ml.

There are a wide range of pH values observed for each rock/water ratio (e.g. between 5.5 and 7.2 for 0.02g samples in AGW and KCl), which is likely to be a result of different volumes of carbonate in each sample. A general pattern of increasing pH with increasing

rock volume is observed. This is likely to be largely a result of increased carbonate dissolution; the amount of carbonate available for dissolution is likely to increase with sample size.

Samples in $CaCl_2$ and AGW follow the behaviour expected with an increase in pH, with the zeta potential becoming more negative at the same rate as it did with the carbonate-free samples in Figure 4-6. The samples in monovalent ion solutions deviate from the pattern observed with carbonate-free samples where the pH was controlled using OH^-. The zeta potential becomes less negative with increasing rock volume and pH, particularly markedly in KCl. In these samples there will be ion exchange with more favourable Na^+ and K^+, releasing Ca^{2+} from surface sites and into solution. This mechanism will increase with increasing rock volume. The addition of divalent ions to the solution causes the zeta potential of the particles to become less negative, with (in KCl) surface properties much closer to those in $CaCl_2$. In KCl solutions, greater ion exchange may be observed as K^+ is more favoured by the exchange sites than Na^+, Ca^{2+} and Mg^{2+} ions.

The data presented here shows the sensitivity of the system to changes in pH and available ion species, particularly Ca^{2+}.
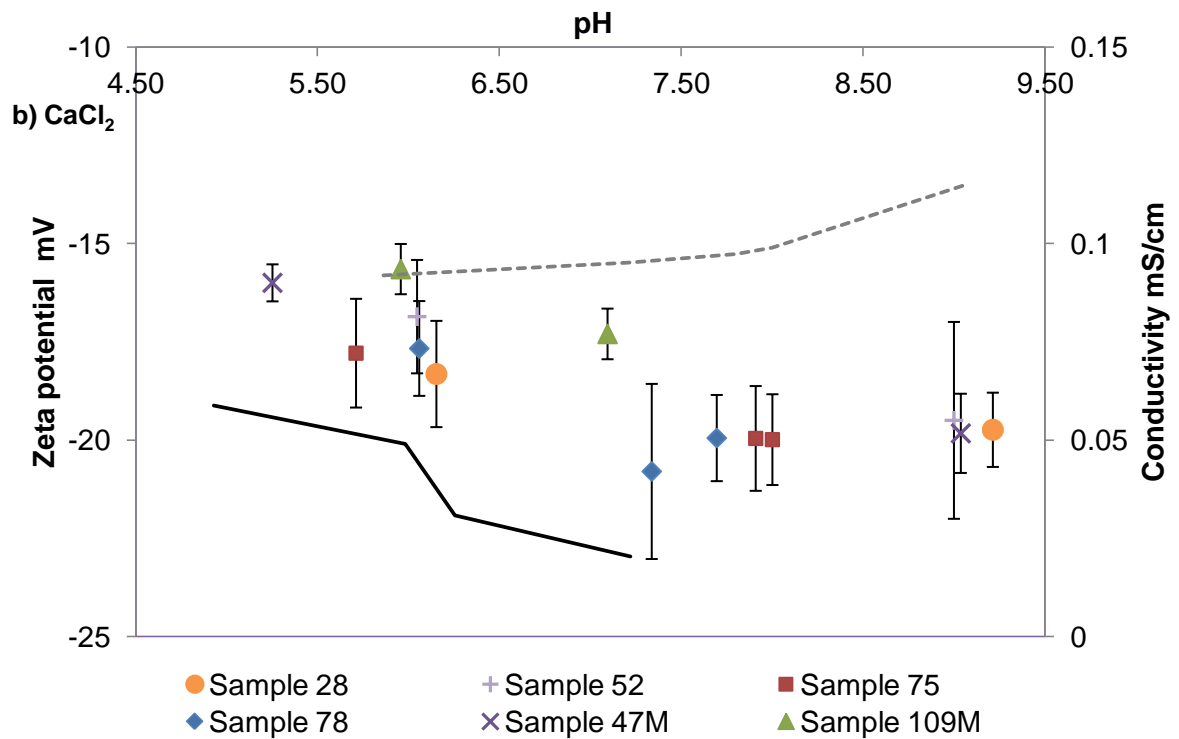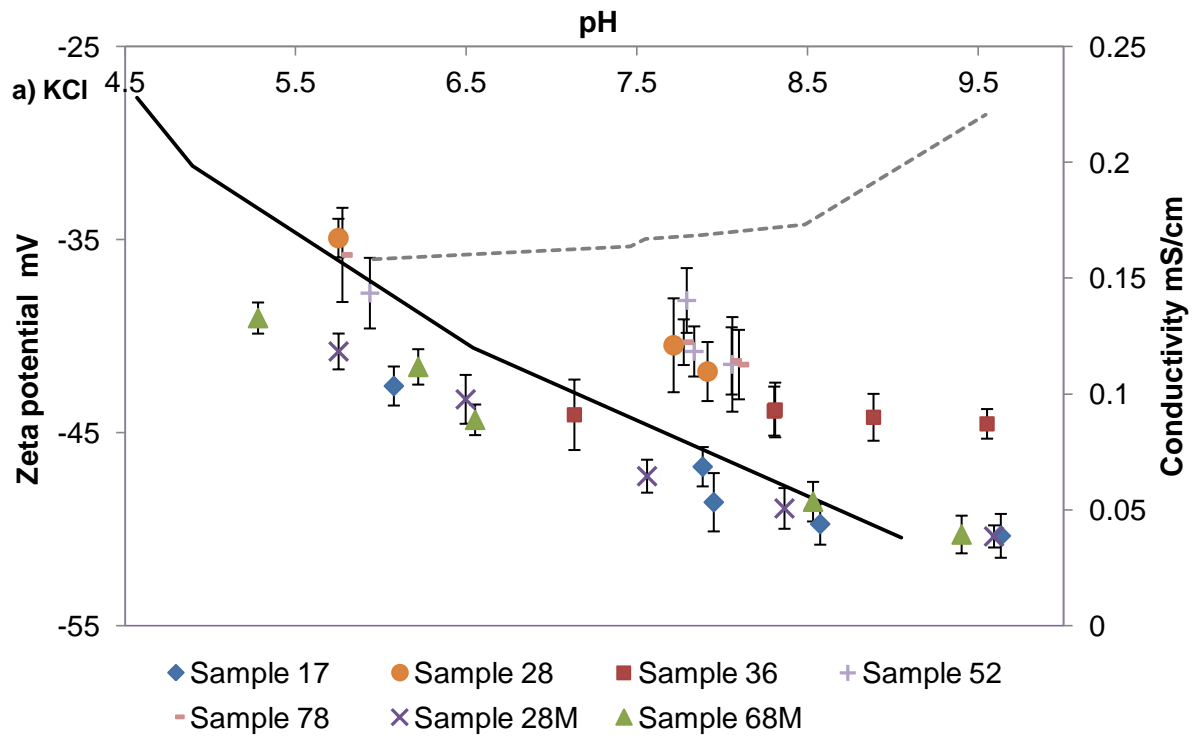
Figure 4-7 Sandstone and mudstone samples with a) KCl and b) CaCl$_2$ solutions (0.02g in 25ml) over a range of pH values. NaOH was used to adjust the pH, the average sample conductivity is shown as a grey dashed line. The black line indicates the zeta potential with pH for a carbonate-free sandstone sample with the same background chemistry. The suffix 'M' indicates the sample is a mudstone.
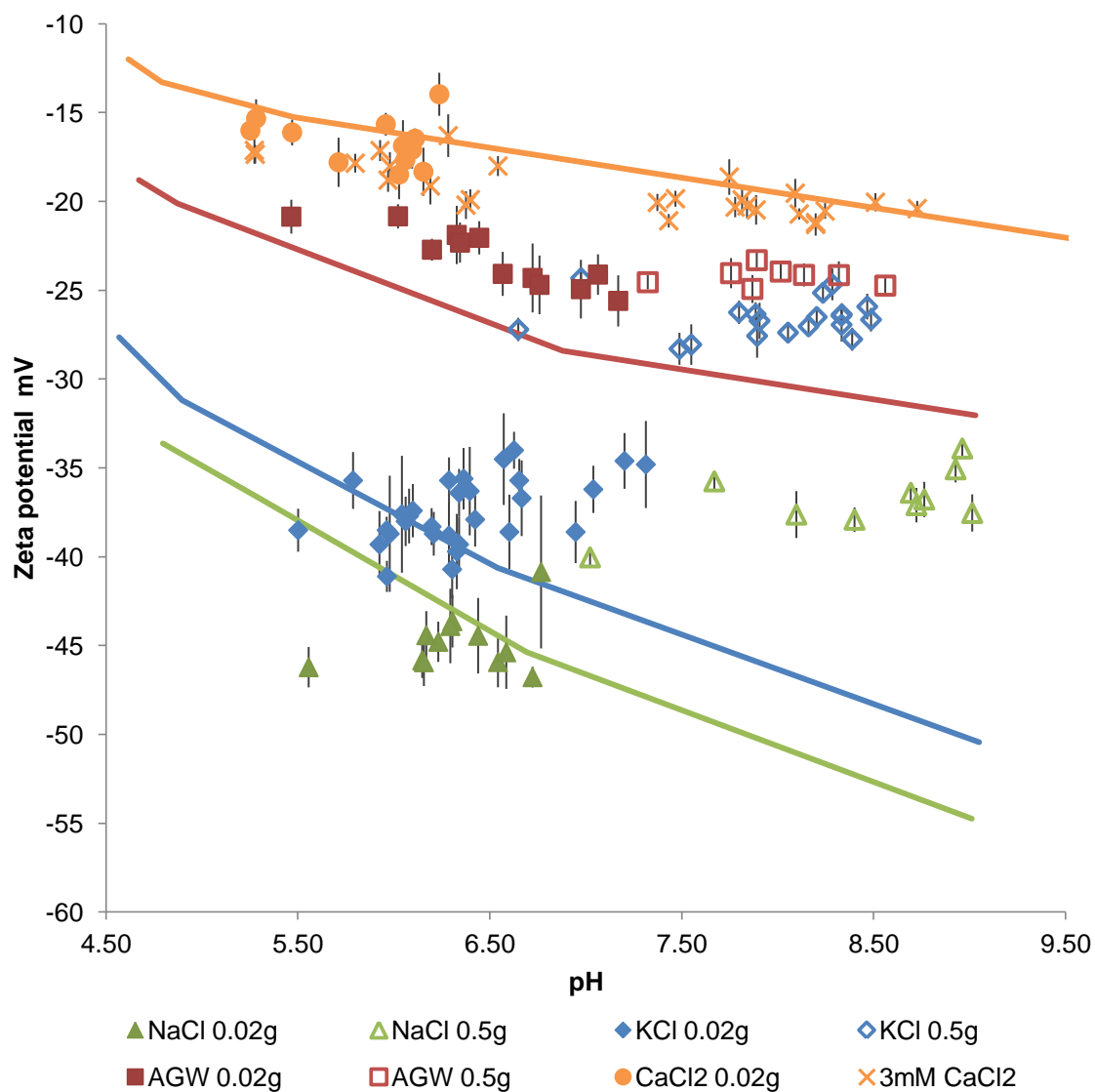
Figure 4-8 The effect of changing rock/water ratio on both pH and zeta potential. The amount of sample in grams which is mixed with 25ml of solution is shown in the legend. The solid lines are the trends for carbonate-free sandstone with pH (changed using NaOH). All solutions are 1mM ionic strength, except where indicated. The error bars show standard deviation for ten measurements on the same sample aliquot.

4.5 Conclusions

Extensive zeta potential measurements using both SS-EFM (a new technique from

Malvern Instruments) and electrophoresis have been used to characterise the zeta

potential of samples from a 50m long redbed sandstone core interbedded with

mudstones. These measurements have shown that there is little zeta potential variation

within a single sandstone bed and in samples from various sandstone lithofacies. It has been demonstrated that the similarities in sandstone zeta potential are not due simply to the haematite coating of the sandstone, as red and bleached samples give the same values. Rather, it is likely that the zeta potential values are a surface-area modified linear mix of the zeta potential of the samples component parts. It appears that clays are the dominant minerals in this sandstone, due to their large surface area.

More extreme heterogeneity than that encountered in the sandstone sampled here (for example, mica-rich beds) and changes in chemistry (and therefore sorbed species) could have a considerable effect on the zeta potential.

When measured using SS-EFM, mudstones offer a much more negative zeta potential to sandstone samples measured with the same technique. However, the same mudstones when disaggregated and measured using electrophoresis give the same zeta potential as the sandstone. The mudstone zeta potential is more negative than the sandstone due to a higher proportion of platy clay minerals and mica in the mudstone. It has been shown that platy minerals behave differently in intact and disaggregated samples, due to a difference in zeta potential between the crystal face and edge. The mineral edge zeta potential must be similar to that of the bulk sandstone samples, as the zeta potential of mudstone in electrophoresis measurements is the same as that of the sandstone.

It has been shown that the chemical composition of the solution is important to the zeta potential value. Less negative zeta potentials are measured on samples as the proportion of divalent ions in solution increases compared to monovalent ions. Zeta potential in this

sandstone is also influenced by the addition of divalent ions via ion exchange with more favourable ion species.

The mineralogical composition of the rock and the chemical composition of the solution will both control the potential mobility of manufactured nanoparticles in red-bed aquifers. A mica-rich bed would promote greater mobility for negatively charged nanoparticles, as it has such a negative zeta potential which would cause increased repulsion. Carbonates would have the opposite effect, with a combination of low zeta potential values and the ability to adjust the groundwater composition in such a way as to make the nanoparticle and bulk surface zeta potential much less negative, making attachment more likely.

Mineral	Average % and surface area	Method	Equation*	Sample preparation	Solution	Zeta potential ~pH6 (mV)	Zeta potential ~pH9 (mV)	Reference
Quartz	55-65% 0.1m²/g	EP		Qtz ground, washed with hot HCl, >24 hrs equil., 0.3-0.5μm, 4.8m²/g	1mM NaCl	-65	-70	Michael & Williams (1984)
					10mM NaCl	-50	-60	
		SP	N/A	Qtz ground, sieved, washed in distilled water & hot 1M HCl, 5-20μm, 0.7m²/g	1mM NaCl	-60 (pH 5.6)	-96	Li & de Bruyn (1966)
					10mM NaCl	-41	-68	
		EP		Berea sandstone sonicated and centrifuged to remove clays, ground to 2-5μm, 30.8m²/g	1mM NaCl	-28	-32	Schramm et al. (1991)
		EP & EA		Qtz powder washed with HCl, overnight pH equil, ave 2μm, 6m²/g	10mM NaCl	-45 to -29	-79 to -57	Kosmulski et al. (2002)
		SP & EP		Qtz sand washed with 0.1M HCl, ground to <1μm for electrophoresis	1mM KCl	-50 to -48±2	-58 to -55±1	Johnson (1999)
					10mM KCl	-39 to -34±5		
		EP		Qtz ground, <55μm, 2.17m²/g	10mM KCl	-42	-65 (pH 10.6)	Besra et al. (2000)
		EP		Crushed Ottawa sand, washed with ammonium acetate	10mM KCl	-30	-35	Yukselen-A & Kaya (2011); Kaya & Yukselen (2005)
					10mM CaCl₂	-21 (pH7)	-15 (pH8.2)	
K-feldspar	5-6% 0.1m²/g	EP		Ground microcline, 15 min equil, <38μm	1mM NaCl	-68		Demir et al. (2003, 2001)
					1mM KCl	-68		
					1mM CaCl₂	-29		

Mineral	Average % and surface area	Method	Equation*	Sample preparation	Solution	Zeta potential ~pH6 (mV)	Zeta potential ~pH9 (mV)	Reference
Calcite	1-2% 0.1m²/g	EP		Ground calcite, natural 6.6m²/g, synthetic 17m²/g	1mM NaCl	Natural calcite -16 Synthetic +11	Natural -20 Synthetic +19	Vdovic & Biscan (1998)
		EP		Ground, few hours pH equil, 2-10μm, natural 1-5.2m²/g, synthetic 2.2-17m²/g	1mM NaCl	Natural -14 Synthetic -2	Natural -29 to -15 Synthetic +12	Vdovic (2001)
		EP	Henry	Precipitated calcium carbonate, average 5μm	1mM NaCl	-14	-29	Sondi et al. (2009)
		EP		Ground calcite, 2.5-3μm, 2-4m²/g	1mM NaCl		-25 to +15	Siffert & Fimbel (1984)
		EP		Limestone ground to <5μm, 10.4m²/g	1mM NaCl		-7	Schramm et al. (1991)
		SP	N/A	Ground synthetic calcite, 106-150μm	5mM NaCl		-19	Thompson & Pownall (1989)
		EP		Ground, <25μm, 2.46m²/g	10mM KCl	+33	-30	Besra et al. (2000)
		EA	N/A	Ground calcium carbonate, 0.9μm, 8.3m²/g	10mM NaCl		+22	Nyström et al. (2001)
					10mM CaCl₂		+28	
		EP		Ground calcite, <10μm, ionic strength kept at 0.03M using KCl	1mM CaCl₂		-6	Cicerone et al. (1992)
					10mM CaCl₂		+18	
Dolomite	1%	EP		Dolomite ground to <5μm, 11m²/g	1mM NaCl		-15	Schramm et al. (1991)
		SP	N/A	Crushed dolomite, 0.125-0.25 mm	1mM NaCl/KCl		-18	Marouf et al. (2009)

Mineral	Average % and surface area	Method	Equation*	Sample preparation	Solution	Zeta potential ~pH6 (mV)	Zeta potential ~pH9 (mV)	Reference
					10mM NaCl/KCl		-2	
		SP	N/A	Crushed then ground dolomite	1mM KCl		-26	Predali & Cases (1973)
					10mM KCl		-19	
		EP		Ground, washed with distilled water, settled to <10μm	10mM NaCl	-5	-21 (pH9.6)	Gence & Ozbay (2006)
					10mM CaCl$_2$	-16	-44	
Mica	1% 5m^2/g	SP	N/A	Freshly cleaved surface, no pre-treatment	1mM NaCl	-86±4 to -83±6	-109±2	Adamczyk et al. (2010b, 2010a)
					10mM NaCl	-78±8 to -64±4	-73±5	
		SP	N/A	Freshly cleaved surface, cleaned with conc. HNO$_3$, rinsed with distilled water	1mM KCl	-133 to -131	-141	Nishimura et al. (1995, 1992)
		SP	N/A	Freshly cleaved surface, immersed 20s after cleaving	1mM KCl	-94±20	-108±20	Sides et al. (2009)
		SP	N/A	Freshly cleaved surface	1mM KCl	-85		Lyons et al. (1981)
					10mM KCl	-39		
		SP	N/A	Freshly cleaved surface	1mM KCl	-80 to -77	-83	Scales et al. (1990)
					10mM KCl	-45		
					1mM NaCl	-93		
					10mM NaCl	-75		
					1mM CaCl$_2$	-69		
					10mM CaCl$_2$	-38		
		EO	N/A	Freshly cleaved surface	1mM KCl	-76		Debacher &

Mineral	Average % and surface area	Method	Equation*	Sample preparation	Solution	Zeta potential ~pH6 (mV)	Zeta potential ~pH9 (mV)	Reference
					10mM KCl	-41		Ottewill (1992)
		SP	N/A	Freshly cleaved surface	1mM KCl	-73	-83	Sides et al. (2006)
		SS-EFM	N/A	Freshly cleaved surface, 18 hr equil time in electrolyte	1mM KCl	-66±8		This study
		EP		Dry grinding freshly cleaved mica				
		EP		Dry grinding freshly cleaved mica	1mM KCl	-36		Pashley (1985)
					10mM KCl	-14		
		EP		Dry grinding freshly cleaved mica, ≤10µm	1mM KCl	-34 (pH6.7)	-43	Nishimura et al. (1992)
Clay minerals: Kaolinite	15-25% 30m²/g	EP		Kaolinite, <75µm, 13meq/100g	1mM NaCl	-41±1.5		Alkan et al. (2005)
					10mM NaCl	-51±1.5		
					1mM KCl	-32±1.5		
					10mM KCl	-42±1		
					1mM CaCl$_2$	-10±3		
					10mM CaCl$_2$	-8±1.5		
		EP	Henry	Removed org. matter and surface oxides, <2µm	1mM NaCl	-38	-47	Sondi et al. (1997)
		EP		Kaolin, minimum equil time, 0.9µm	1mM KCl	-34 to -32	-36 to -29	Greenwood et al. (2007)
		EP		Kaolinite, pre-treated with 1M KCl	1mM KCl	-31 to -22	-49	Vane & Zang (1997)
					10mM KCl	-25 to -17	-51 to -44	
		EP		Kaolinite, washed with	10mM KCl	-26 (pH6.7)	-33 (pH 8.4)	Yukselen-A & Kaya

Mineral	Average % and surface area	Method	Equation*	Sample preparation	Solution	Zeta potential ~pH6 (mV)	Zeta potential ~pH9 (mV)	Reference
				ammonium acetate	10mM NaCl	-37 (pH6.7)	-42	(2011, 2003); Kaya & Yukselen (2005)
					10mM CaCl$_2$	-12 (pH6.9)	-12	
		EP		Kaolinite, <20μm, 8.62m^2/g	10mM KCl	-25	-28 (pH10.6)	Besra et al. (2000)
Clay minerals: Smectite		EP	Smoluch-owski, O'Brien & White	Montmorillonite & bentonite, washed with 1M NaCl & HCl then with cation solution used in expt, then methanol 750m^2/g, 81C/g	1mM NaCl	-63 to -40		Horikawa et al. (1988)
					10mM NaCl	-42 to -33		
					1mM CaCl$_2$	-12 to -10		
					10mM CaCl$_2$	-13 to -12		
		EP	Henry	Montmorillonite, removed org. matter and surface oxides, <2μm, 78m^2/g, 124meq/100g	1mM NaCl	-40 to -36	-40	Sondi et al. (1996)
					10mM NaCl	-32 to -28	-35	
					1mM CaCl$_2$	-10		
					10mM CaCl$_2$	-9		
		EP	Henry	Montmorillonite, removed org. matter and surface oxides, <2μm	1mM NaCl	-33	-36	Sondi et al. (1997)
		EP	Smoluch-owski, O'Brien & White	Montmorillonite, 48hr pH equil, two different ZP calculations	1mM NaCl	-31 to -25	-33 to -26	Delgado et al. (1986)
		EP		Bentonite, pre-treated with 1M KCl	1mM KCl	-27		Vane & Zang (1997)
					10mM KCl	-31	-36	
		EP		Montmorillonite, washed with ammonium acetate	10mM NaCl	-31 (pH6.5)	-32	Kaya & Yukselen (2005)
					10mM CaCl$_2$	-12 (pH6.9)	-15	
		EP		Montmorillonite, pre-treated	10mM NaCl	-36	-40	Duran et al. (2000)

Mineral	Average % and surface area	Method	Equation*	Sample preparation	Solution	Zeta potential ~pH6 (mV)	Zeta potential ~pH9 (mV)	Reference
				with 1M NaCl, 54.1m²/g				
		EP		Montmorillonite, pre-treated with 1M NaCl, <2μm, 800m²/g	10mM NaCl	~ -31	~ -31	Avena & Pauli (1998)
Clay minerals: Illite		EP	Smoluch-owski, O'Brien & White	Illite, washed with 1M NaCl & HCl then with cation solution used in expt, the methanol 140-190m²/g, 19-36C/g	1mM NaCl	-47 to -31		Horikawa et al. (1988)
					10mM NaCl	-34 to -24		
					1mM CaCl₂	-11 to -9		
					10mM CaCl₂	-7 to -6		
		EP		Removed org. matter and surface oxides, <2μm, 37m²/g, 25meq/100g	1mM NaCl	-44 to -26	-59	Sondi et al. (1996)
					10mM NaCl	-40 to -27	-46 (pH9.6)	
					1mM CaCl₂	-10		
					10mM CaCl₂	-7		
Clay minerals: Chlorite		EP	Henry	Ripidolite ultrasonication, removed org. matter and surface oxides, <2μm	1mM NaCl	-53	-53	Sondi et al. (1997)
		EP		Chlorite, crushed and sieved to <25μm	1mM KCl	-31±4	-44±2	Alvarez-Silva et al. (2010)
					10mM KCl	-34±2	-47±2	
		EP	Henry	Removed org. matter and surface oxides, <2μm, 4.8m²/g, 12meq/100g	1mM NaCl	-13 to -5	-25 (pH9.6)	Sondi et al. (1996)
					10mM NaCl	-9 to -6	-15	
					1mM CaCl₂	+2		
					10mM CaCl₂	+1		
Haematite	2-5%	EP		Washed natural haematite,	1mM NaCl	-2	-29 (pH8.4)	Das et al. (2005)

Mineral	Average % and surface area	Method	Equation*	Sample preparation	Solution	Zeta potential ~pH6 (mV)	Zeta potential ~pH9 (mV)	Reference
	5m^2/g			baked at 700°C, 1.67m^2/g				
		EP		Ground haematite test chips, 2hrs equil	1mM KCl	-25	-28	Carlson & Kawatra (2011), 2011
		SP	N/A	Iron oxide-coated quartz sand	1mM KCl	+15		Johnson (1999)
		EP		Colloidal iron oxyhydroxide	1mM KCl	+34 (pH5.6)	-33	Johnson et al. (1996)
		EP		Synthesised haematite particles, average 49nm	1mM KCl	+35	+7	Zhang & Buffle (1995)
		EP	O'Brien & White	Synthesised haematite particles, average 60nm	10mM NaCl	+10	-16	Plaza et al. (2001)
		EA	N/A	Pure haematite, Average 2.7μm, 8.8m^2/g	10mM NaCl	+28	0	Nanthakumar et al. (2010)

Table 4-6 Mineral content of redbed sandstone, from point counting of stained thin-sections of samples used for surface zeta potential measurements (M. Jaweesh, pers. comm.), along with the estimated surface area and the zeta potential range found in the literature. EP=Electrophoresis, SP=Streaming potential, EA=Electroacoustics, EO=Electroosmosis
* where not stated, the Smoluchowski Equation is used for conversion from electrophoretic mobility to zeta potential

5 TRANSPORT OF MANUFACTURED NANOPARTICLES IN SANDSTONE

5.1 Introduction

Chapter 4 has demonstrated that, at the scale of the new SS-EFM technique, the zeta potential of redbed sandstone material varies very little with depth through a sequence and with changing lithofacies. A constant value can therefore be assumed for sandstone at this millimetre scale. Heterogeneity, however, is introduced by mudstone layers and mud pellet beds, due to the higher zeta potential of the clay mineral crystal face.

Haematite does not control the surface properties of this sandstone, despite providing a covering and red colouration on most grain surfaces. This is observed in the similarity of zeta potential measurements of red and bleached sandstone and in the difference between sandstone and mudstone zeta potential when measured using SS-EFM. Surface-area weighted calculations of zeta potential from the individual mineral component zeta potentials provide a good match to measured values. The bulk minerals are considered to be of lesser importance, due to their small surface area to volume ratio. The most significant mineral group for zeta potential in this rock system are clay minerals, as they have at once large surface areas and extremely negative zeta potentials on the crystal face (Zhao et al., 2008).

Fluid chemistry has a dominant influence on the zeta potential of the sandstone surface; measurements in Chapter 4 focussed on the effect of chemical composition. The surface zeta potential changes significantly with increasing quantities of divalent rather than monovalent ions in solution. Changes in pH also have a significant effect and Chapter 4

has highlighted the interrelationship between pH and chemical composition in this sandstone as a result of calcite dissolution and ion exchange at grain surfaces.

Zeta potential is an important property for indicating the likely mobility of nanoparticles, either using CFT-based calculations or by offering a traffic-light style assessment directly from the zeta potential values. As changes in chemical conditions significantly affect the zeta potential of the sandstone surfaces, it is important to test whether these conditions will have an equivalent effect on nanoparticle mobility. The effect of interactions between nanoparticles and a porous medium on that nanoparticle population is important in understanding their onward transport. The permanence of the attachment between a particle and surface is also critical when the assessing long-term behaviour.

5.2 Aims

The main aims of this chapter are:

- To assess whether zeta potential measurements can be used in estimating nanoparticle mobility in intact sandstone under different chemical compositions
- To find out if size and zeta potential measurements will provide insight into processes within the column

More specifically, there are four questions to be answered:

1. Do the changes in zeta potential with different chemical conditions seen in Chapter 4 significantly affect breakthrough of particles in intact sandstone?

2. Do the interactions between nanoparticles and surfaces result in significant particle fractionation by zeta potential during passage through these columns?

3. Can breakthrough be estimated using a DLVO/CFT approach using zeta potential as measured here and in Chapter 4?

4. Are the attachments permanent?

This chapter addresses these questions, by describing the results of column experiments, with the ultimate aim of determining the relevance and utility of surface and particle zeta potential measurements in indicating nanoparticle mobility and fate in the environment.

5.3 Approach

The majority of studies on the transport of manufactured nanoparticles are carried out in artificial model systems; however there is a need to test the mobility of nanoparticles in systems closer to real-world aquifers, not only in the sense of using natural mineral assemblages as has been done in earlier chapters, but also in terms of using natural pore architectures. Intact sandstone columns have therefore been selected for use in this study. Laboratory column experiments on this sandstone were undertaken, as field experiments using nanoparticles are not allowed in the UK. Column experiments have been performed under three chemistries, to investigate nanoparticle behaviour with monovalent, divalent and mixed mono- and divalent ion solutions.

Colloid Filtration Theory (CFT) calculations have been carried out using measurements of the zeta potential of the silica particles obtained during these column experiments and the zeta potential of the sandstone surface measurements described in Chapter 4.

Size and zeta potential measurements have been taken during all three column studies, and are analysed for information about particle aggregation and fractionation due to

zeta potential. Mass balance calculations were carried out in order to quantify attachment.

5.4 Method

5.4.1 Column studies

5.4.1.1 Sandstone sample

Four sandstone column samples were drilled from a core of redbed continental sandstone from Preston, north-west England. This sequence has been previously described in Chapter 4 as being of largely haematite-coated quartz dominated sandstones with small amounts of potassium feldspar and calcite cement, with some beds rich in mica and mudclasts. The porosity and hydraulic conductivity of the Chester Pebble Beds are understood to be 12-22% and 0.0008-1.1m/day respectively (from core plug samples, Ban To, pers. comm.), in good agreement with previous work by Allen et al. (1997).

The pore throat size might directly affect the physical straining of colloids and nanoparticles within an aquifer. Using mercury injection capillary pressure measurements, Bloomfield et al. (2001) found that pore throat sizes in 153 samples of Permo-Triassic sandstone from the UK range from 0.01-427µm, with the most frequent median pore throat sizes in the range 10-60µm, and perhaps a few % of pore diameters less than 0.1 µm. Thus 100nm silica microspheres are unlikely to be physically strained through the majority of the pores, unless aggregation is a dominant process, though the standard constrictivity equation suggests effects become apparent even when pores are an order of magnitude larger than 'particles', at least in the case of molecules (e.g. as summarised by Bashar & Tellam, 2011).

5.4.1.2 Sandstone column preparation

Four columns of 35mm diameter were drilled horizontally from a relatively homogeneous bed free of mud clasts and visible laminations and trimmed to an average length of 60mm. The columns were vertically adjacent and taken from the depth range 67.98-68.16m.

The pore volumes of the samples were measured using the saturation method, and the porosity determined by dividing this by the bulk volume of the column (obtained from diameter and length measurements). The columns were dried at a constant temperature of 110°C for 24 hours and then saturated with deionised water (DIW) using a vacuum pump. Column properties are given in Table 5-1. The mean hydraulic conductivity for sandstone at this depth is 0.023m/day.

The column samples were prepared for use in a flow-through experiment by sealing them, first with a layer of PTFE tape and then PVC bungs all held in place with heat-shrink sleeve. The PVC bungs were slightly concave where they met the rock to allow water to infiltrate across the entire sample face and the sleeve was flush with the sample surface to prevent water from bypassing the column (Figure 5-1).

Chemistry applied	Length	Diameter	Dry mass	Saturated mass	Pore volume	Porosity
	mm	mm	g	g	ml	%
AGW	60.5	35.0	139.96	151.43	11.47	19.7
KCl	60.0	35.0	136.21	148.37	12.16	21.1
CaCl2	59.0	35.0	124.23	135.27	11.04	19.4

Table 5-1 Details of the three sandstone columns used for laboratory column experiments.
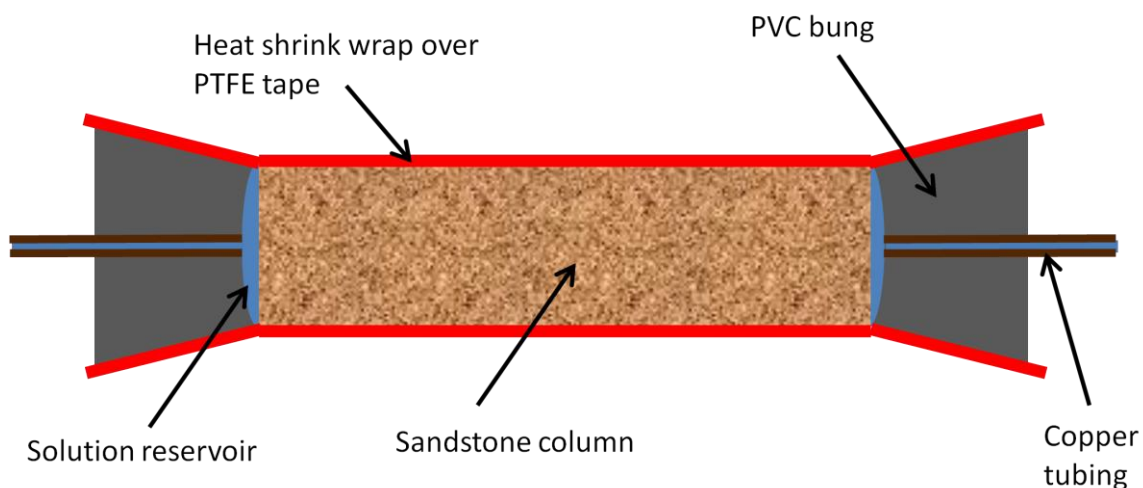
Figure 5-1 Preparation of the sandstone columns

When the preparation was complete the samples were re-saturated using the vacuum pump and stored under DIW in a refrigerator at 10°C to maintain saturation and reduce bacterial growth, which could alter the hydraulic properties. During an experimental run the prepared samples were connected into the experimental kit with a short piece of copper piping.

5.4.1.3 Electrolyte solutions

All solutions were made using Milli Q Gradient A10 deionised water (DIW, 18.2MΩcm, TOC 2-3ppb). Solutions of NaCl, KCl and artificial groundwater (AGW, chemical composition as described in Chapter 4) of 5.5mM ionic strength were used, along with a 16.5mM ionic strength $CaCl_2$ solution. The ionic strengths of NaCl and KCl were chosen to allow breakthrough to occur at an appropriately measureable concentration; though it had been intended that the same ionic strength would be used for the $CaCl_2$ solution, a higher concentration, but one nevertheless that is still appropriate for fresh groundwaters, was inadvertently used. All solutions were left open to air in the refrigerator to allow them to equilibrate thermally and with atmospheric CO_2 before use.

5.4.1.4 Nanoparticle dispersions

The nanoparticles used in the experiments are monodisperse silica microspheres (Polysciences Inc.) with a reported diameter of 0.1µm±0.03µm. Rahman (2006) used a combination of Transmission Electron Microscopy (TEM), Environmental Scanning Electron Microscopy (ESEM) and Atomic Force Microscopy (AFM) to confirm this size, finding the microspheres were spherical in shape and a size of 0.1µm±0.007µm (Figure 5-2).
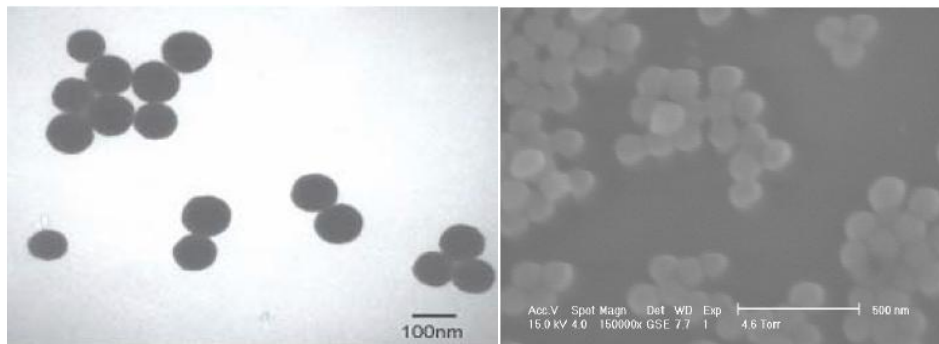
Figure 5-2 TEM and ESEM images of silica microspheres (Rahman, 2006)

The silica microspheres were provided in a 5.59% aqueous dispersion and were diluted with DIW to produce a 100mg/l stock solution, which was later diluted to 10mg/l for experimental runs using a solution with the chemistry of choice. The purchased particles were provided with NaOH as a stabilising agent, the concentrated dispersion is diluted to such an extent that the NaOH concentrations are assumed to have no significant effect on the particle behaviour during experiments. The pH of 100mg/l silica solution was 6.0±0.25, which supported this assumption. The higher concentration silica dispersions were sonicated for 15 minutes prior to dilution to disaggregate and disperse the particles. The behaviour of the particles with pH in DIW and 10mM AGW was assessed in Pattenden (2007) and Anderson (2008) and the results are shown in Figure 5-3.
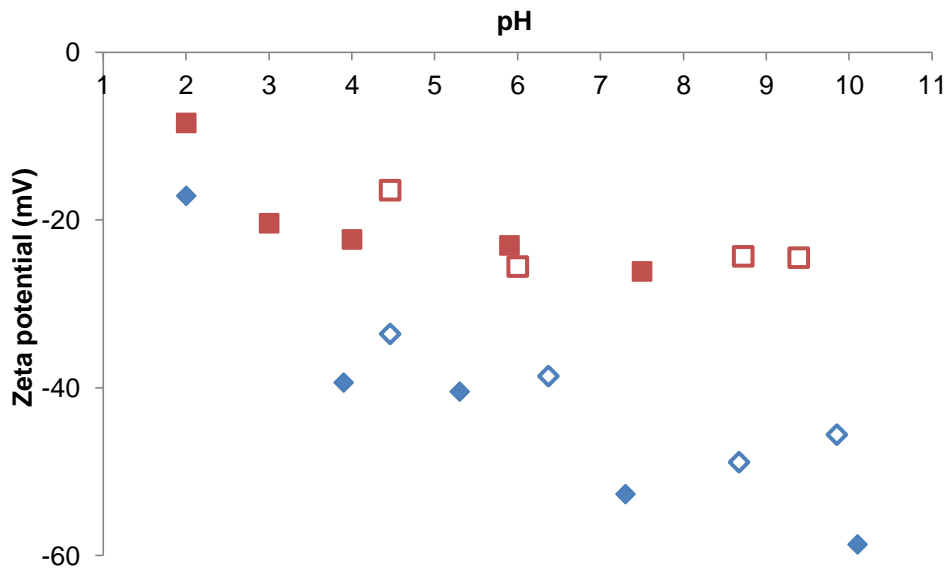
Figure 5-3 The behaviour of silica nanoparticles with pH in DIW (blue) and 10mM AGW (red). Filled symbols are data from Pattenden (2007) and open symbols from Anderson (2008). The pH was changed using NaOH and HNO$_3$.

5.4.1.5 Nephelometer

A nephelometer was developed at Birmingham University (Greswell et al., 2010) to take a continuous record of particle effluent concentration from a laboratory column experiment. The nephelometer detects the intensity of light scattered by particles at 90° to a light source and converts this to a voltage output. By calibrating the detection unit using particle concentration standards (for the particle type to be used, as particle size will affect scattered light intensity) concentration can be directly reported. A low volume flow-through cell of 200µl is used to reduce the impact of dispersion in this reservoir on the breakthrough curve.

This instrument was updated for the current work by replacing the laser light source with a more powerful version to increase the sensitivity and adding an adjustable output to the laser to allow a larger range of particle concentrations to be detected.

A 5-point calibration under pumping conditions was carried out before each experiment, with a 10ppm standard being run at the start and end of each run to allow adjustments for experimental drift, if any (see Section 5.4.1.7 for details of experimental stages). An example calibration is shown in Figure 5-4; the R^2 value for these calibrations did not fall below 0.99.
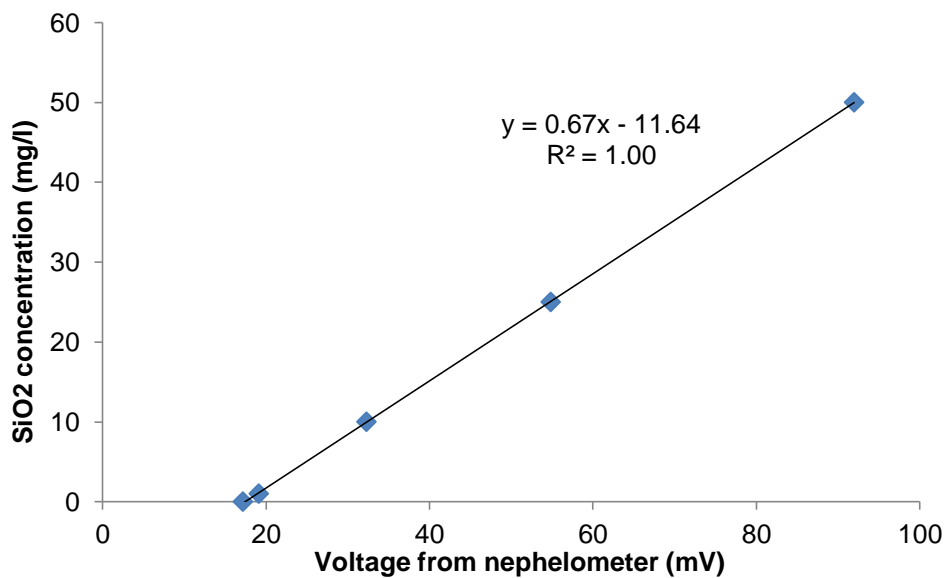
Figure 5-4 An example 5-point calibration to convert the voltage recorded by the nephelometer to concentration

The concentration detected by the nephelometer is dependent upon the particle size, as larger particles scatter more light, so would influence concentration by recording higher values. To use the nephelometer an assumption of constant particle size is made. This will not be strictly correct for the poly-disperse particle populations observed here, however this assumption has not proven to affect experimental results to a great degree (see below).

A further assumption has been made that differences between C_0 and the effluent concentration are a result of material being retained by the sandstone column. A small

proportion of material will be removed due to interactions between particles and the experimental equipment, primarily the peristaltic pump tubing and the low diameter tubing. This error in particle concentration will be consistent throughout all experimental runs and is factored into the nephelometer calibration.

The results will also be influenced to a certain degree by dispersion in the measurement cell of the nephelometer. This could lead to enhanced tailing.

5.4.1.6 Column equipment

The fluid is pushed from a reservoir and around the system (Figure 5-5) by a peristaltic pump (Ismatec IPC 4-Channel) which was calibrated before starting any experiments using four speed settings. Two bubble traps are incorporated into the system; the first is positioned before the column to prevent air from entering the column and altering the flow behaviour by reducing the saturation with water. The second is before the nephelometer stopping air bubbles from entering and becoming subsequently trapped in, the flow cell. Air bubbles refract significant amounts of light producing a false concentration peak. If the bubble becomes trapped in the flow-through cell, these errors can be continuous over a long period of time.

A pH electrode (Metrohm Aquatrode Plus) is placed in series after the nephelometer and was calibrated using three pH calibration standards (pH 4, 7 and 9.2). A temperature probe is placed in the refrigerator and was calibrated using a mercury thermometer and three different temperature environments; air temperature, refrigerator temperature and a water bath set to 35°C.
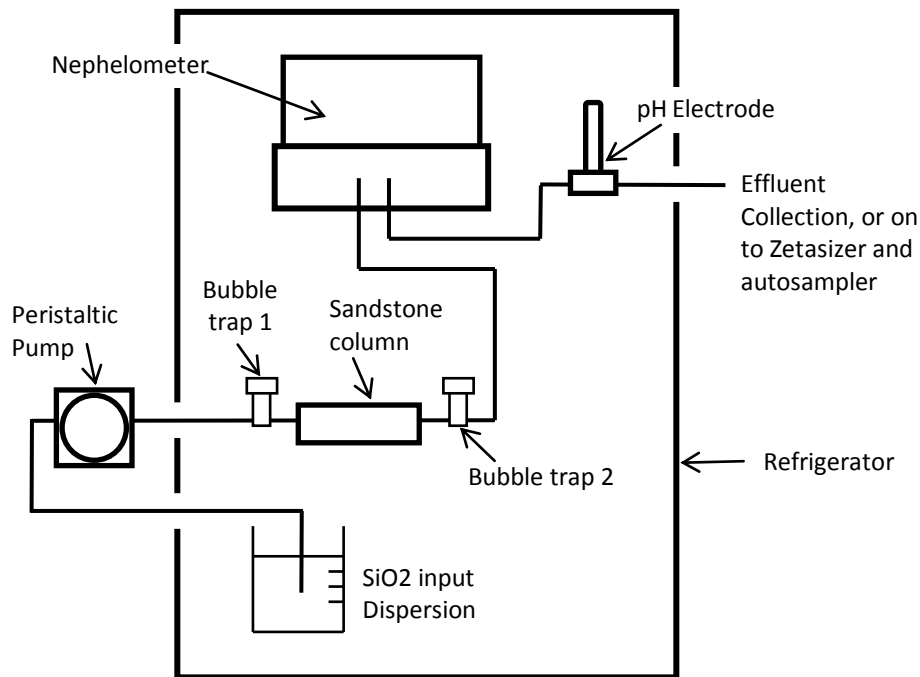
Figure 5-5 Diagram of the column experiment equipment

A data logger (DataTaker DT80) is used to collect voltage data from all the devices described above at an assigned time interval of one minute. The data logger uses a relay to turn the nephelometer laser on then a voltage measurement is recorded after a one second warming period. After this the laser is turned off using the relay, and measurements of temperature and pH are recorded. Electrical noise in the data was reduced by taking an average of multiple individual voltage readings over a short space of time. Measurements from the nephelometer were an average of 100 readings and from the other detection devices, an average of 50 readings.

The experiment (including test solution reservoirs) was carried out almost entirely within a refrigerator to maintain a relatively constant temperature of 10°C, a value chosen as an approximation of UK groundwater temperature. This also allowed some stability for the temperature dependent nephelometer. Only the peristaltic pump

remained outside the refrigerator, as space inside was at a premium and the vibrations from the pump would disturb the sensitive equipment within.

Prior to loading in a column sample and starting any experiments, the tubing and measurement cells were cleaned. This cleaning consisted of flushing through with 5% Decon followed with copious DIW, a process which removed visible deposits from previous experimental work.

5.4.1.7 Experiment stages

The column experiments were split into seven sections which are described below. All solutions were refrigerated for at least 12 hours before being used to allow for equilibrium with test temperature and atmospheric CO_2.

1. Standard solution of silica microspheres in DIW at 10ppm injected through the system, bypassing the column.
2. DIW flush to clean out system, then the column is attached and a DIW flush to remove loose natural material; flush being continued until C/C_0 returns to zero.
3. Flush column with a solution of the same chemistry as that used in the experiment to allow chemical equilibrium to be gained, this step was carried out over 10 or more pore volumes; Andrews (2007) found that chemical equilibrium was gained after 5 pore volumes.
4. Main experiment stage where silica microspheres are flushed through the column in a solution of the chosen chemistry. The output here is assumed to be the silica microspheres which have not attached to the sandstone surface; size and zeta potential measurements are undertaken to explore this assumption.

5. Flush through with a particle-free solution of the same chemistry to remove any particles in the column pore water, flush being continued until C/C_0 returns to zero.

6. Flush with DIW to test the reversibility of the particle attachment to the sandstone surface, flush being continued until C/C_0 returns to zero.

7. Repeat standard to check for instrumental drift, bypassing the column.

Some experiments had an additional step between steps 5 and 6 where the ionic strength of the solution was halved before being reduced to effectively zero with DIW.

5.4.2 *Particle characterisation measurements*

5.4.2.1 Particle size measurements

Particle size measurements of the input silica microspheres and the column effluent were carried out using a Zetasizer ZS Nano (Malvern Instruments Ltd). The measurement process has been described previously in Chapters 3 and 4 so will not be described in detail here.

Initially sampling from column effluent was undertaken to collect aliquots for size measurements. 3ml samples were taken and 1ml removed from this for size measurements, which were carried out in a folded capillary cell. Later a 40μl flow-through sizing cell was obtained for the Zetasizer ZS and was added to the experimental kit in series after the pH probe. The instrument was outside the refrigerator, but placed close by with the internal temperature kept at 10°C.

The Zetasizer was then used to take size measurements at time intervals throughout the duration of the column experiment. Two types of size measurement were taken during

this phase; the first was a single 120 second measurement run, where all the data collected are included in the measurement. The other was made up of 12 ten second measurement runs, where the data from the most consistent 6 runs is used to find the average hydrodynamic diameter and the distribution of size values. The latter measurement approach is the one used as standard, with the former being used to check for uncommon instances of very large particles (which would probably be in the runs discarded by the standard approach). There was little difference between the two datasets, so when size measurements are referred to it is the more standard measurement approach which has been used.

As part of the data used to calculate particle size the Zetasizer collects a count rate of photons hitting the detector, which is an indicator of particle concentration if a constant particle size is assumed. The count rate was calibrated using silica standards (the same as those used to calibrate the nephelometer) and used to produce a second breakthrough curve for comparison. The Zetasizer detects backscattered light (at 127°) so will be less sensitive than the nephelometer to bias introduced by large particles. As the cell volume is smaller here than in the nephelometer, the Zetasizer data will also give rise to less dispersion in the measurement cell. The time over which the measurement is carried out is longer for the Zetasizer (120 seconds rather than 2 seconds in the nephelometer), so the results will be smoothed. These continuous measurements were only interrupted for the Zetasizer to be used to make zeta potential measurements, see below.

5.4.2.2 Zeta potential measurements

The zeta potential measurement process is also fully described in Chapter 3 and 4, so these details will not be repeated.

The batch sampled aliquots collected for size measurements were also measured for particle zeta potential; the same 1ml sample was measured in the folded capillary cell once the non-invasive size measurement had been carried out. Later, an autosampler was added to the experimental equipment in series after the Zetasizer. This allowed 3ml samples to be collected at regular time intervals, which varied between 5 and 7 minutes, depending on the coverage of data required. During points of the experiment where the concentration was too low to allow for size measurements, these aliquots were measured for particle zeta potential.

Continuous zeta potential measurements were not possible for this system as the minimum concentration threshold for reliable measurements under flow conditions, even at flow rates less than 1ml/min, was higher than the input SiO_2 concentration.

5.5 Results and discussion

5.5.1 Overview of nanoparticle column experiments

In this section the discussion will focus on the results of three column experiments, all run under very similar conditions:

1. Silica nanoparticles with 5.5mM ionic strength KCl;

2. Silica nanoparticles with 5.5mM ionic strength artificial groundwater; and

3. Silica nanoparticles with 16.5mM ionic strength $CaCl_2$.

In these sandstone columns, silica particles in a single monovalent ion solution more quickly reach a higher steady-state normalised concentration (C'/C_0) than particles in mixed valence or divalent solutions (Figure 5-6). KCl has a C'/C_0 of 0.89, and takes 53 pore volumes from the introduction of particles to reach 0.95 of this value (V_E or equilibrium volume). When the system is equilibrated with AGW (a mix of monovalent and divalent ions) there is a slower breakthrough over 150 pore volumes to 0.95 of a lower C'/C_0 of 0.42. There is no breakthrough of particles in the single divalent ion solution; the ionic strength was, however, three times higher in this experiment than any of the other runs. Exploratory CFT calculations indicate that similar results would have been obtained using 5.5mM solution.

Zeta potential values from Chapter 4 indicate a qualitative relationship with these C'/C_0 data (Table 5-2). Sandstone and silica particles equilibrated with KCl give the most negative zeta potential values, suggesting they would be the least likely to form attachments and silica would be most mobile in a KCl dominated system. Sandstone and silica in $CaCl_2$ have the least negative zeta potentials, so this would be the least stable system with less mobile silica particles. The particles in AGW have a zeta potential between these values, and the silica mobility would be expected to be between these two extremes.

	C'/C_0	Sandstone mV	Silica mV
KCl	0.89	-37.9 ±2.36	-39.9 ±0.85
AGW	0.42	-24.0 ±1.33	-24.3 ±1.06
$CaCl_2$	0	-17.1 ±1.44	-21.5 ±0.32

Table 5-2 C'/C_0 for three solution chemistries compared with the sandstone and silica zeta potential measured using electrophoresis. The measurements were taken with a 1mM solution and at pH6.4±0.4.

When there is a significant change in effluent particle concentration, particularly from high to low, the concentration change is not fast, there being a significant tailing during most experiments. Some of this will be due to particle retention in various parts of the experimental equipment, including the tubing, solution reservoirs next to the face of the sandstone (see Figure 5-1) and the detection cells.

For two of the column experiments, concentration data were collected not only by the nephelometer but also by the Zetasizer during a size measurement. The Zetasizer finds significantly less tailing during stages where the concentration is changing, suggesting that some of the tailing in the nephelometer data is directly a result of the detection equipment. As the Zetasizer is placed after the nephelometer, the difference in size of the detection cells (200µl in the nephelometer compared with 40µl for the Zetasizer) is unlikely to be the cause as the tailing would be observed in both traces. The instruments have different detection angles (90° and 127° respectively), with the 90° angle being more sensitive to bias from large particles. This could mean a slightly higher concentration is measured be the nephelometer when large particles are present.

Other factors to take into account during these periods of particle concentration change are the length of time over which the measurement is carried out, which for the nephelometer is 2 seconds but a size measurement on the Zetasizer takes 120 seconds. This will increase the lag time for the Zetasizer measurements. Finally, physical properties of the sandstone columns will have an impact. The sandstone is a multi-region material; the distribution of pore sizes and pore water velocities will cause a certain amount of dispersion.

There is a favourable comparison between nephelometer and Zetasizer data for steady state values of C/C_0 (Figure 5-6). The C/C_0 values found during the DIW flushes, both as the column is attached into the equipment and after the main experimental introduction of silica particles, where the concentration is changing very quickly, are different for the two pieces of equipment. The nephelometer gives a higher C/C_0 value for the initial flush, with the Zetasizer giving a higher value for the post-particle DIW flush. This could, once again, be linked to the different length of time over which these measurements are taken and the size bias in the nephelometer.

The pH and conductivity values collected show a significant increase when the sandstone columns come into contact with DIW, both during the initial and the post-experimental flush (Figure 5-6). This indicates that the sandstone is changing the solution properties, probably through calcite dissolution which would both add Ca^{2+} to the solution and cause the pH to rise.

During the electrolyte input the fluid pH drops to 9-9.5, there is still calcite dissolution, but the pH-controlling carbonate equilibria are affected by other factors, particularly the presence of Ca^{2+} in the fluid phase. During the KCl experiments ion exchange reactions will release Ca^{2+} into solution, thus reducing calcite dissolution. The direct addition of Ca^{2+} would limit the ion exchange and also calcite dissolution in the $CaCl_2$ experiment, thereby limiting the change in pH. Both of these processes will be occurring in the AGW experiment. The fluid pH increases again when the solution is returned to DIW.
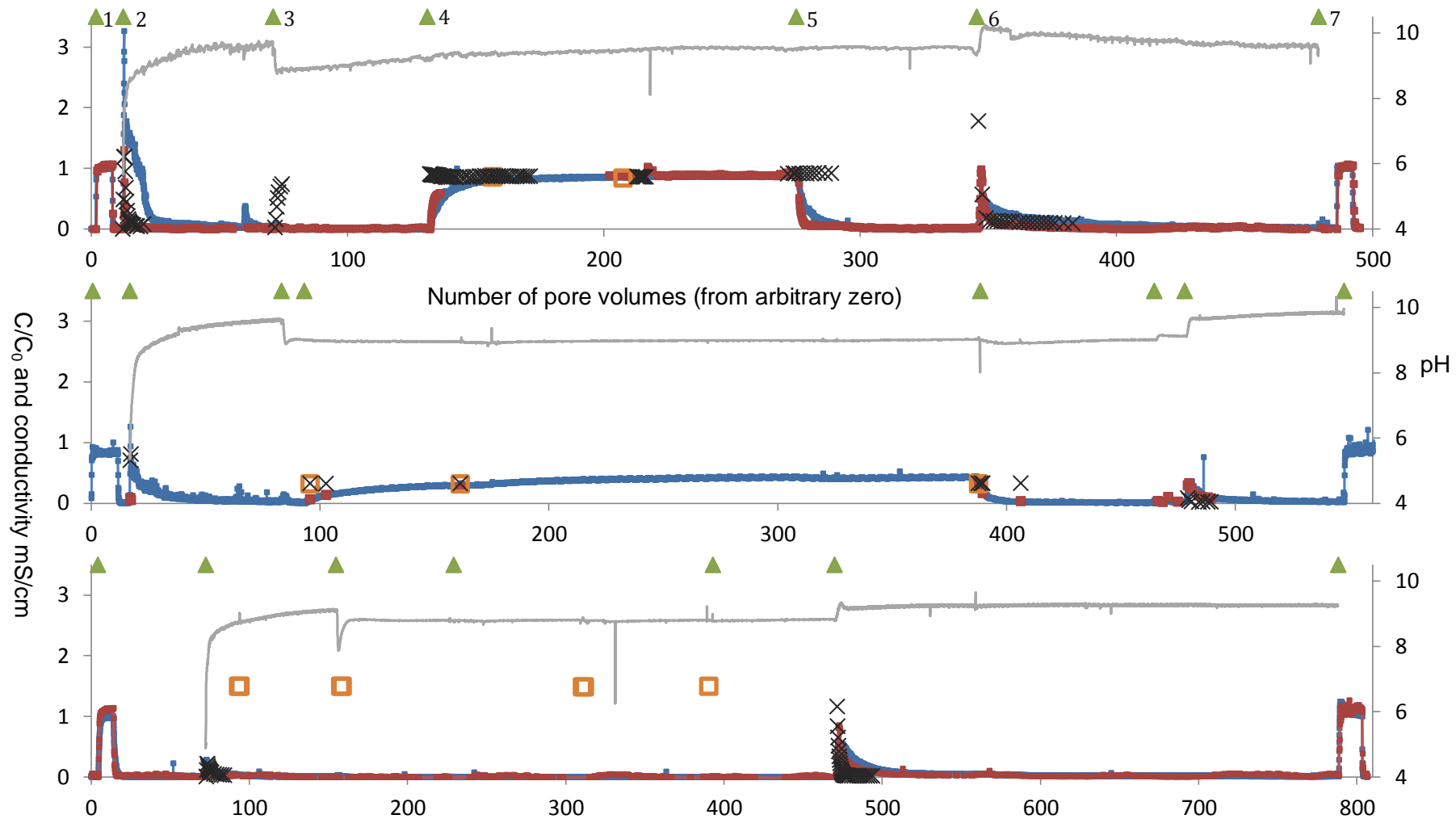
Figure 5-6 Full experimental pH, effluent conductivity and C/C_0 results for a) KCl, b) AGW and c) CaCl$_2$, using both the nephelometer and Zetasizer ZS to measure particle concentration (note the difference in scales on the x-axis). The numbers in a) indicate the stage change as described in section 5.4.1.7

The conductivity during the experiment is largely controlled by the concentration of salts added to the fluid. The KCl reaches a higher conductivity than AGW as higher concentrations of salts are required to produce the same ionic strength in a monovalent solution. During both the KCl and AGW runs the conductivity remains stable throughout the period of electrolyte introduction. The conductivity was not measured during the $CaCl_2$ experiment as it is generated as part of a zeta potential measurement and there was no particle breakthrough while $CaCl_2$ was being added.

5.5.2 *Calculations of particle breakthrough using CFT*

5.5.2.1 Sandstone grain size

A rough average grain size was estimated using the intercept method (Friel, 2000). A quick estimation of size, rather than an in depth study, is believed to be justifiable for the purpose of these calculations, especially as micrographs indicate that there is significant variability in grain size in all of the sandstone samples.

The intercept method is a quick and simple estimation of grain size. Several randomly oriented straight lines are superimposed onto thin section micrographs, where this line intercepts a grain; a grain boundary intersection is counted. These intersections are counted across the length of all the lines applied to the micrograph. The total line length on the micrograph is scaled using the magnification applied in viewing the thin section. The average grain diameter (d) is calculated using:

$$d = \frac{L}{P}$$
<div style="text-align: right">Equation 5-1</div>

where L is the summed length of the lines and P is the number of grain boundary intersections.

In this study, five micrographs were taken at various points from a single sandstone thin section. 470 grain boundary intersections were counted over a line length of 50mm, which gives an estimated average grain diameter of 0.11mm.

5.5.2.2 Hamaker constant

CFT is sensitive to the Hamaker constant value so, while some studies use it as a calibration variable (Elimelech et al., 1995), a value will be estimated here from the literature. The Hamaker constant will be calculated using the geometric mean of the three interacting phases (as in Equation 2-9b, Chapter 2), inputting individual Hamaker constant values for the particle material (A_{11}), separating medium (A_{33}) and surface mineral (A_{22}), each with a vacuum.

Water is used as the separating medium, although there would be some screening effects of the added electrolyte in the solutions (Israelachvili, 2011). Literature values for A_{11} and A_{33} can be found in Table 5-3.

Literature values for the Hamaker constant of sandstone have not been found, presumably because it is a complex and heterogeneous material which will not be easily described with a single value. To attempt to calculate the system Hamaker constant without this value, Hamaker constants for individual minerals present in sandstone for which literature values are available have been used (Table 5-3). Another source of data is the literature values for A_{132} for silica interacting with the surface of a mineral relevant to the sandstone across water (see Table 5-4).

	Material	Hamaker Constant E-20 J	Method	Reference
A_{11}	Silica	6.5	Lifshitz calculation	(Bergstrom et al., 1996)
		6.35 - 6.5	Lifshitz calculation	(Bergstrom, 1997)
		6.1	Calculated from immersion enthalpy	(Medout-Marere, 2000)
		6.6	Lifshitz calculation	(Ackler et al., 1996)
		6.6	Full spectral calculation	(French et al., 1995)
		5.45 - 7.72	Experimental - FFF	(Farmakis et al., 2006)
		6.55	Unknown	(Hunter, 2001)
		8.6 / 50	Microscopic/Lifshitz methods	(Shaw, 1992)
		6.3 - 6.5	Lifshitz calculation	(Israelachvili, 2011)
A_{33}	Water	4.38	Unknown	(Visser, 1972)
		3 - 6.4	Unknown	(Bernhardt, 1988)
		3.7	Unknown	(Hunter, 2001)
		3 - 6.4	Microscopic/Lifshitz methods	(Shaw, 1992)
		2.43 - 4.35	Calculated	(Hiemenz and Rajagopalan, 1997)
		3.7 - 5.5	Lifshitz calculation	(Israelachvili, 2011)
A_{22}	Quartz	8.7	Calculated from immersion enthalpy	(Medout-Marere, 2000)
		8.86	Lifshitz calculation	(Bergstrom, 1997)
		8.83	Unknown	(Hunter, 2001)
		11-18.6	Microscopic/Lifshitz methods	(Shaw, 1992)
	Mica	9.86	Lifshitz calculation	(Bergstrom, 1997)
		6.96	Lifshitz calculation	(Ackler et al., 1996)
		7 - 10	Lifshitz calculation	(Israelachvili, 2011)
	Haematite	9.2	Lifshitz calculation	(Faure et al., 2011)
	Chlorite	23.3	Calculated from immersion enthalpy	(Medout-Marere, 2000)
	Talc / chlorite	19.3	As above	
	Illite	8.6	As above	
	Mont-morillonite	7.8	As above	
	Kaolinite	6.8	As above	
	Calcite	24	Calculated from immersion enthalpy	(Medout-Marere, 2000)
		10.1	Lifshitz calculation	(Bergstrom, 1997)
		10.1	Unknown	(Hunter, 2001)

Table 5-3 Hamaker constants from literature for silica (A_{11}), water (A_{33}) and minerals used as A_{22}

The average values (leaving out the highest values reported by Shaw (1992) which do not correspond well with other estimations) for A_{11} and A_{33} are $6.71\pm0.73\times10^{-20}$J and $4.25\pm0.56\times10^{-20}$J respectively. The effective Hamaker constant (A_{132}) for silica-water-quartz is calculated using Equation 5-1. Using A_{22} for quartz of $9.35\pm1.1\times10^{-20}$J, a range of 0.47×10^{-20}J to 1.06×10^{-20}J is calculated. A range of $0.67-2.35\times10^{-20}$J is achieved if the value for chlorite (the clay mineral with the greatest reported Hamaker constant, or indeed the higher value for calcite) is used as A_{22}. In general the values match relatively well with literature values found for these systems (Table 5-4).

Material 1 / 2	Across 3: Vacuum / Water E-20 J	Reference
Silica / Quartz	7.59 / 0.63	(Bergstrom, 1997)
	- /0.47-1.06	This study
Silica / Mica	8.01 / 0.69	(Bergstrom, 1997)
Silica / Calcite	8.07 / 0.69	As above
Silica / Haematite	- / 2.1	(Wang et al., 1992)
Silica / Chlorite	-/1.46-2.35	This study

Table 5-4 Literature values for A_{132} for silica approaching other mineral surfaces across a vacuum or water

A surface area approach was used in Chapter 4 in order to quantitatively describe the zeta potential of the sandstone surface. This approach suggests that clay minerals are the most important when characterising surface properties. Therefore, the Hamaker constant range used in the following CFT calculations is that estimated for silica-water-chlorite above.

5.5.2.3 Comparing calculated and experimental breakthrough

To check the applicability of calculations developed for interactions under unfavourable conditions, the systems were assessed using DLVO theory (Figure 5-7). It is assumed

that the surface potential of the silica nanoparticles and sandstone can be substituted by

the relevant zeta potentials, as described in Chapter 2.

From the size of the energy barrier predicted for KCl and AGW (38.1kT and 15.5kT

respectively), interactions between particles and surfaces in these systems are

considered to be unfavourable so Equations 2-13 and 2-17 can be used. In $CaCl_2$

however, the energy barrier to attachment is predicted to be 3.6kT. With such a low

energy barrier the $CaCl_2$ system could be considered to be favourable to particle

attachment, and so the aforementioned equations are not valid for this system, the

collision efficiency (*a)* is equal to 1 and the attachment is described by the collector

efficiency (η).
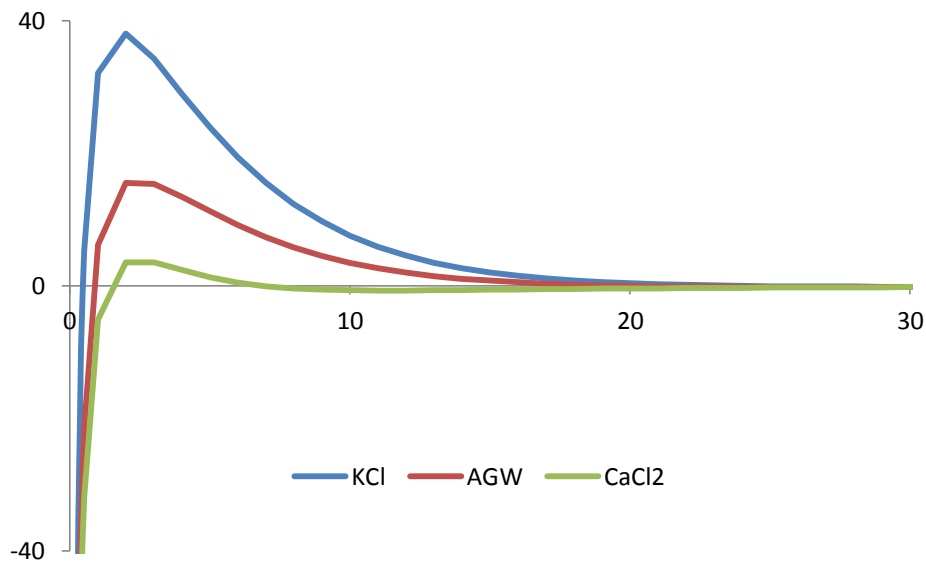
Figure 5-7 The total interaction energy for 5.5mM KCl and AGW and 16.5mM $CaCl_2$. The particle radius is 50nm; The Hamaker constant is the average of that for the silica-water-chlorite system of 1.51×10^{-20}J and the zeta potentials for the particles and surfaces are reported in Table 5-5 below.

The values used as CFT model inputs are reported in Table 5-5. The particle zeta

potential for KCl and AGW is that of the column output particles, as these are at the

correct pH. A zeta potential of the effluent fluid particles was taken when the effluent concentration had stabilised, it is assumed here that the effluent particles are silica (see Figure 5-10 and Section 5.5.5). As there was no breakthrough in the $CaCl_2$ experiment, the input particle zeta potential was used.

The sandstone zeta potential for KCl and AGW is measured in Chapter 4, although under 1mM ionic strength conditions. The zeta potential for $CaCl_2$ was measured at 3mM ionic strength. The ionic strength has an effect on the zeta potential, as described in Chapter 2; however the difference is less than an order of magnitude so it will be assumed here that the difference will be small. All the zeta potential values were taken using electrophoresis with a high rock/electrolyte solution ratio (as in Figure 4-10) as this was considered to most closely match the sandstone conditions in the column experiments, in particular the pH.

A low dispersivity of 0.0025m was thought appropriate, due to the small size of the column and the lack of dispersion observed in previous column experiments under similar conditions.

Parameter	Unit	KCl	AGW	CaCl$_2$
Porosity	-	0.21	0.2	0.19
Particle radius	nm	50	50	50
Collector radius	mm	0.055	0.055	0.055
Particle potential	mV	-38	-22	-20.5
Surface potential	mV	-26.5	-24.5	-20
Ionic strength	mol/kg	0.0055	0.0055	0.0165
Velocity	m/s	5.07E-05	5.32E-05	5.60E-05
Column length	m	0.06	0.0605	0.059
Dispersivity	m	0.0025	0.0025	0.0025
Collector efficiency η	-	0.45	0.47	0.49

Table 5-5 The parameter values used in CFT calculations for the three chemistry conditions.

The collector efficiency was calculated using Equation 2-17; the values for each sample are slightly different due to the differences in porosity.

Colloid Filtration Theory (CFT, see Chapter 2) with first order decay was used to calculate predicted breakthrough curves for KCl and AGW. An approximation to the Fuchs equation (Equation 2-16) is used to estimate the theoretical collision efficiency from the height of the energy barrier to attachment, evaluated using DLVO theory. As described earlier, the collision efficiency for the $CaCl_2$ system is equal to 1. With such a high collector efficiency, no breakthrough is predicted by CFT for this system, a prediction which is confirmed by the experimental results.

The α_T value for the KCl system is many orders of magnitude smaller than the α value found experimentally (Table 5-6). High particle stability and no attachment are predicted in this system using α_T in CFT calculations. While this predicts that silica nanoparticle mobility is very likely, it does not completely describe the behaviour seen, with a C'/C_0 of 0.89 for KCl (Figure 5-8).

The α_T is predicted well for a system in equilibrium with AGW, although with a strong dependence on the Hamaker constant, A_{132} (Table 5-6). Using the zeta potential values in Table 5-5 and the average A_{132} for a silica-water-chlorite system, the C'/C_0 is almost exactly predicted (Figure 5-8). If a lower A_{132} is used (see Table 5-4), then a higher or complete breakthrough is predicted, which may not replicate experimental results but still gives an indication that some mobility should be expected.

Chemistry	KCl			AGW		
Hamaker constant $A_{132} \times 10^{-20}$J	0.67	1.51	2.35	0.67	1.51	2.35
Experimental C'/C$_0$	0.89			0.42		
Experimental α_{ex}	3.4E-04			2.4E-03		
Theoretical α_T	3.8E-17	4.0E-13	3.5E-10	2.8E-6	2.4E-3	0.16
Stability ratio $W=1/\alpha_T$	2.6E+16	2.5E+12	2.9E+9	3.6E+5	4.1E+2	6.17
C'/C$_0$ from CFT calculations	1	1	1	1	0.43	0

Table 5-6 A comparison of results from CFT/DLVO calculations and column experiments
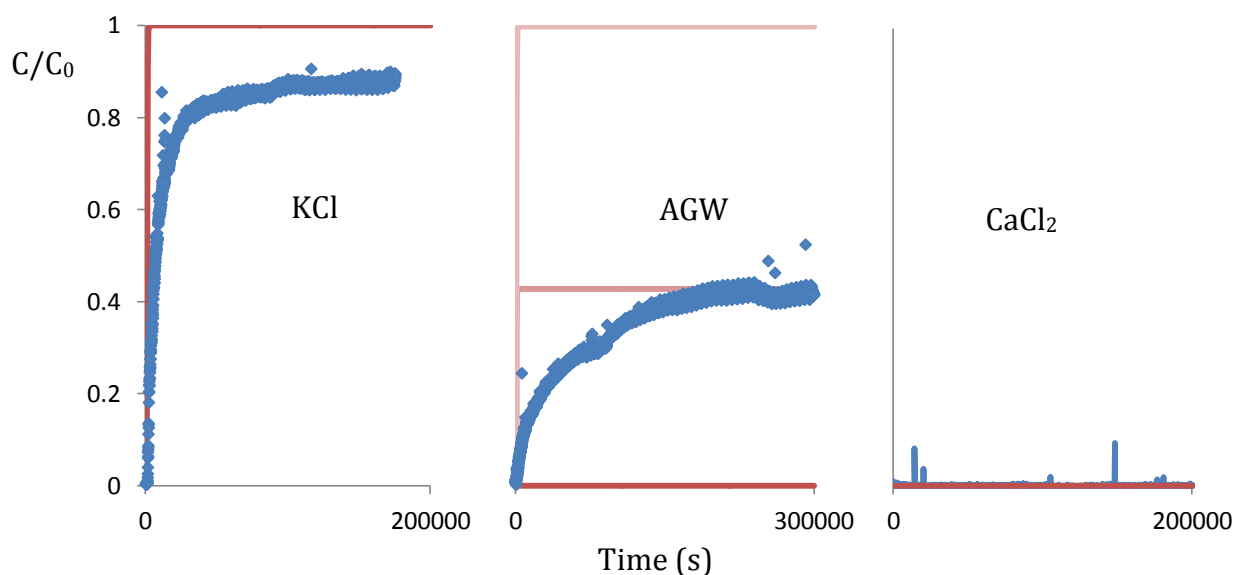
Figure 5-8 A comparison of predicted (red) and experimental (blue) breakthrough for the three chemical compositions. For AGW the three lines represent the three results using different A_{132}, with a darker red for a higher value. 200000 seconds is equivalent to approximately 165 pore volumes in this system. The predicted breakthrough reaches equilibrium concentration (C'/C$_0$) after approximately 2500 seconds, or 1.6 pore volumes.

The two parameters which have the greatest impact on the collision efficiency estimations are the Hamaker constant and zeta potential, as these control the van der Waals and electrical double layer interactions respectively. The Hamaker constant has been carefully constrained using available literature; however the range estimated is still large enough to significantly affect the model output. Further work is necessary on Hamaker constants, particularly of interactions of specific nanoparticles with rock material under a variety of ionic strength and chemical composition fluid conditions.

A small change in zeta potential of just 1 or 2mV for the AGW system would result in the correlation of experimental and theoretical C'/C_0 being lost. The KCl system could see an improved correlation with an increase in zeta potential of the silica and sandstone of 5mV. Lower zeta potential values could be observed if there was heterogeneity in surface properties below the scale of the SS-EFM measurement. This kind of variability has already been observed in the zeta potential of mica and other platy clay minerals in Chapter 3, and also in clay mineral basal and edge specific surface areas by Macht et al. (2011).

While C'/C_0 can be predicted to some extent, the predicted shape of the breakthrough curve does not match that found experimentally. Significantly more tailing is observed in the experimental data than in that predicted by CFT (the predicted data reached C'/C_0 after 1.6 pore volumes, while in the experimental data it took more than 100 pore volumes). The nephelometer data has been used as it is the most complete; the Zetasizer data for KCl shows less tailing, but still notably more than the CFT prediction. This tailing could indicate dispersion in the equipment used to carry out the experiment (dispersion in the sandstone is accounted for), a non-equilibrium process in the sandstone (either physical, through immobile zones or dead-end pores, or chemical non-equilibrium in reactions) or some other process which is not accounted for in CFT calculations. A slow increase in concentration is also observed when there is blocking (limited sorption sites for attachment), however, the increase would be expected to increase to a C'/C_0 of 1, which is not seen here. It is not possible otherwise, without further investigation, to identify the specific process causing this phenomenon.

5.5.3   *Overview of particle characterisation data*

In this section, the zeta potential reported alongside C/C_0 data is an average value based on the full distribution, so some values may be biased by tailing. Distribution curves are also presented so this effect can be assessed. The average data is not reported for size as the distribution is often bimodal; instead the values for peaks in the measured light intensity distribution are presented.

Throughout the three experiments the particle hydrodynamic diameter remains at or just above the size of the input silica microspheres (Figure 5-9). This indicates that the silica particles are stable in all three of the chemistry conditions applied, at least over the length of the experiments performed (up to 8 days). The input silica particle zeta potential is less negative in AGW and $CaCl_2$ than in KCl, as might be expected from the zeta potential measurements on sandstone under these chemistries in Chapter 4 (Figure 5-10, Table 5-7). The effluent particle zeta potential during the silica input stage in KCl and AGW is approximately the same, within error margins, as the injected particles. The pH of the effluent solutions (8.8-9.4) is considerably higher than the input solutions (5.5-6.4) so a more negative zeta potential might be expected. The zeta potential could, however, be influenced by Ca^{2+} or impurities released from the sandstone which work counter to the effect of pH.

These particle size and zeta potential results will be discussed in more detail in the following sections. In these sections, the data will discussed by comparing the results for the same experimental stage for each chemistry
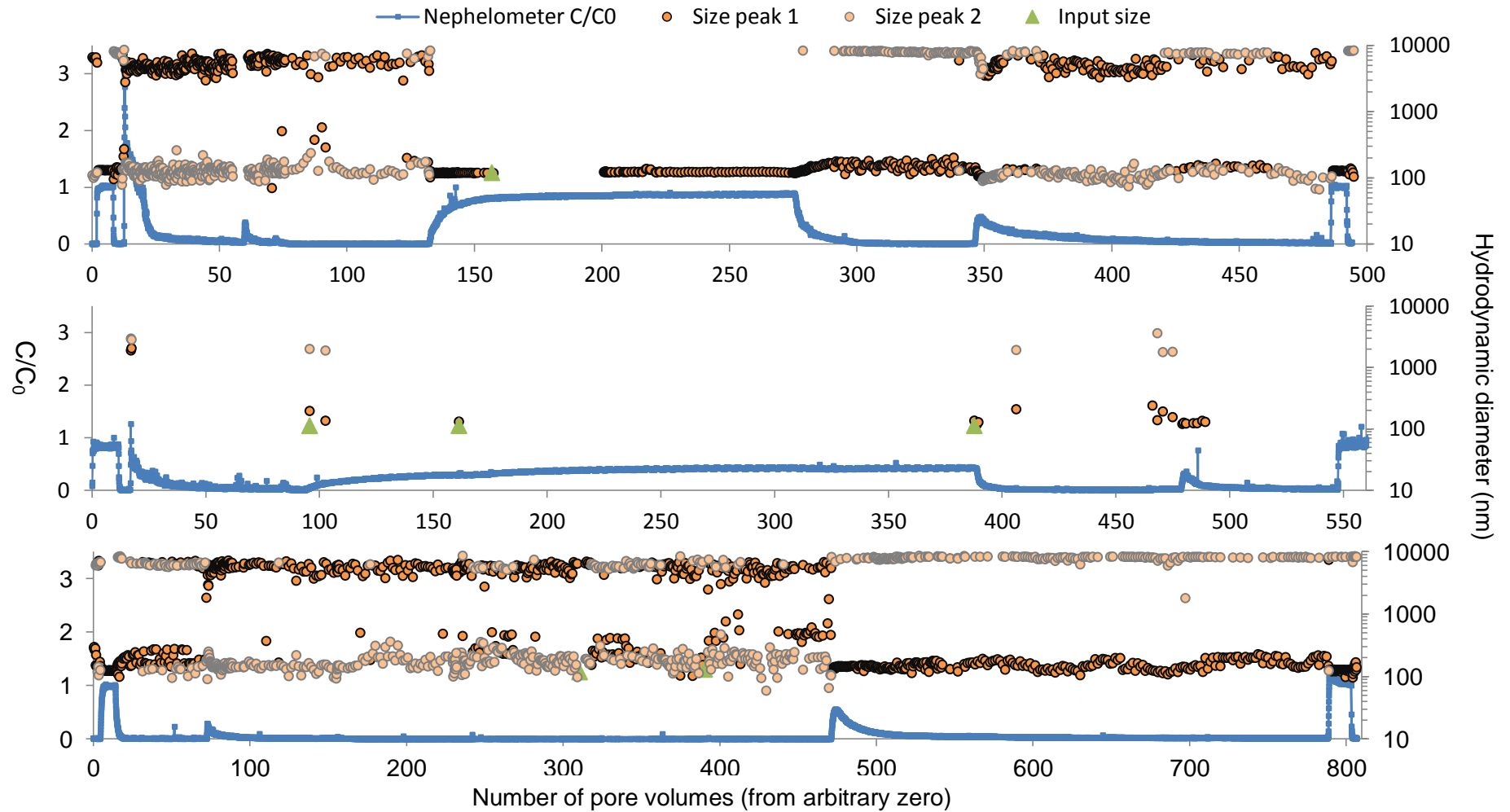
Figure 5-9 Hydrodynamic diameter measurements for full a) KCl, b) AGW and c) CaCl$_2$ experiments. The particles are often polydisperse, so the major peak (by percentage intensity) is shown with a dark orange circle, while the secondary peak is in pale orange.
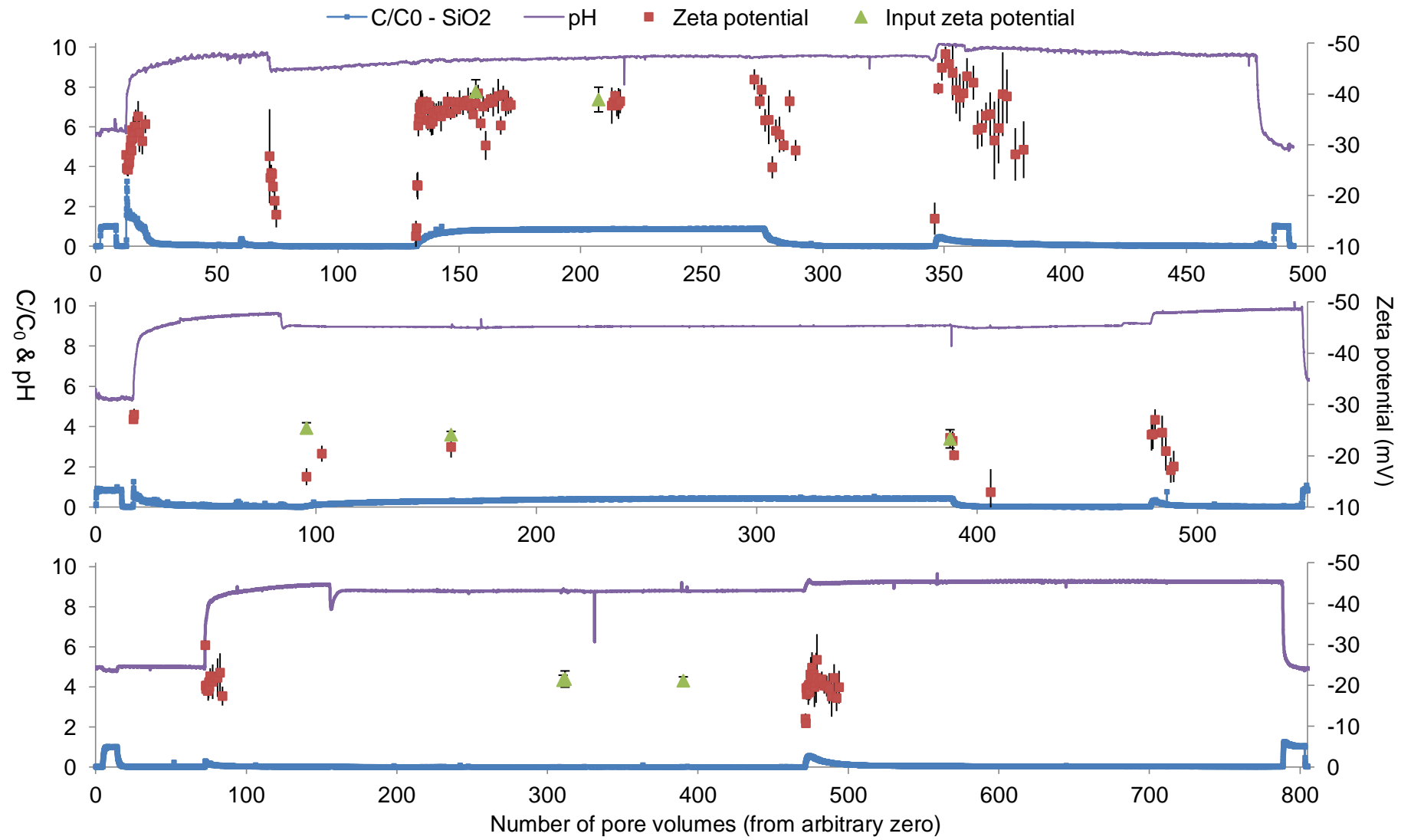
Figure 5-10 Zeta potential measurements for full a) KCl, b) AGW and c) CaCl$_2$ experiments

Chemistry	5.5mM solution	1mM solution	Column effluent from main input stage
	This chapter	Chapter 4	This chapter
KCl	-39.9±0.9	-45.8±4.5	-37.2±1.9
AGW	-24.3±1.1	-	-21.9±1.6
CaCl$_2$	-21.5±1.0	-25.4±0.8	-

Table 5-7 Comparison of silica zeta potential under different chemistries; the 5.5mM solution is the silica input solution for the column studies and the 1mM solution the probe particle for sandstone surface measurements. These solutions are freshly made and measured before contact with the sandstone.

5.5.4 Initial DIW flush of sandstone column

The initial flush of the sandstone column with DIW gives output of natural material, most likely from hydraulic flushing of pore debris (Figure 5-6). The maximum C/C_0 is observed to be different for each column used which is presumably due to different availability of material in each column. The natural materials from each of the columns have slightly different size signatures, and while the columns used in the KCl and CaCl$_2$ experiments have the same overall pattern of two groups of particle sizes, with the most significant in number being those at 100-300nm (Figure 5-11a and b). The column used in the AGW experiment is very polydisperse with a further size class at <100nm.

All columns indicate a zeta potential distribution peak at between -23 and -26mV with this distribution tailing towards less negative values (Figure 5-11c).

After a very brief time of becoming more positive, the average zeta potential values become more negative over time during the DIW flush (Figure 5-12), an observation which is most evident in Figure 5-12a, before the KCl experiment (from approximately -25 to -35mV).
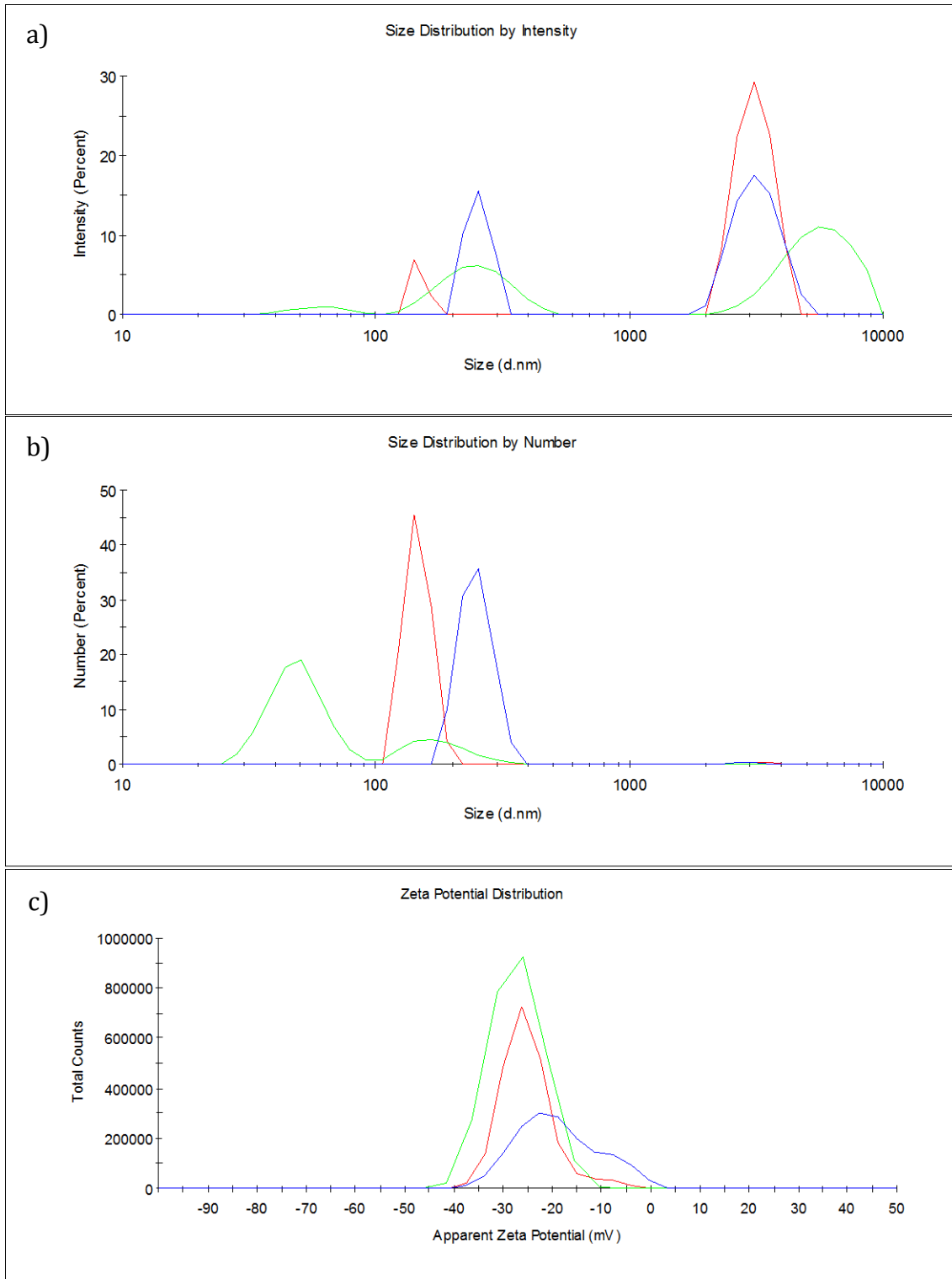
Figure 5-11 Comparison of a) size by intensity and b) size by number of particles, and c) zeta potential distributions of natural sandstone particles released during the initial DIW flush from the three columns used in the experiments. Red is column 1 (used in the KCl experiment) at 13 pore volumes (pv); green is column 2 (AGW experiment) at 17pv and blue is column 3 (CaCl₂ experiment) at 73pv.

This is a period of flux as the sandstone column is initially introduced to the experimental system and begins to influence the water chemistry. In Figure 5-12a, the initial zeta potential measurement is -30mV and could represent indigenous particles washed from the end of the column where the bulk solution chemistry has not yet been significantly altered by the sandstone. The columns will be prepared with a DIW solution where there will be low or no CO_2 due to the saturation taking place under a vacuum. This means there will be less carbonate dissolution, and the pH will be lower.

As the DIW breaks through there is a temporary peak in conductivity which could be due to the way the columns were prepared for the experiment. When the columns were oven dried there may have been precipitation of salts which then dissolved into the fluid phase when the DIW flush began. This momentary increase in ionic strength causes zeta potential values to become less negative. As the ionic strength reduces (indicated by conductivity) and the pH increases, due to carbonate dissolution, the zeta potential of the effluent particles becomes more negative.

The plots of hydrodynamic diameter show there is polydispersity in the form of a distinct bimodal distribution (Figure 5-13). The measurements in Figure 5-13 are from an intensity distribution as this gives the most accurate indication of size. The number distributions for these measurements, like in Figure 5-11c, indicate that the smaller size class forms the vast majority of the particle population with just a small number of particles being larger than 1000nm.
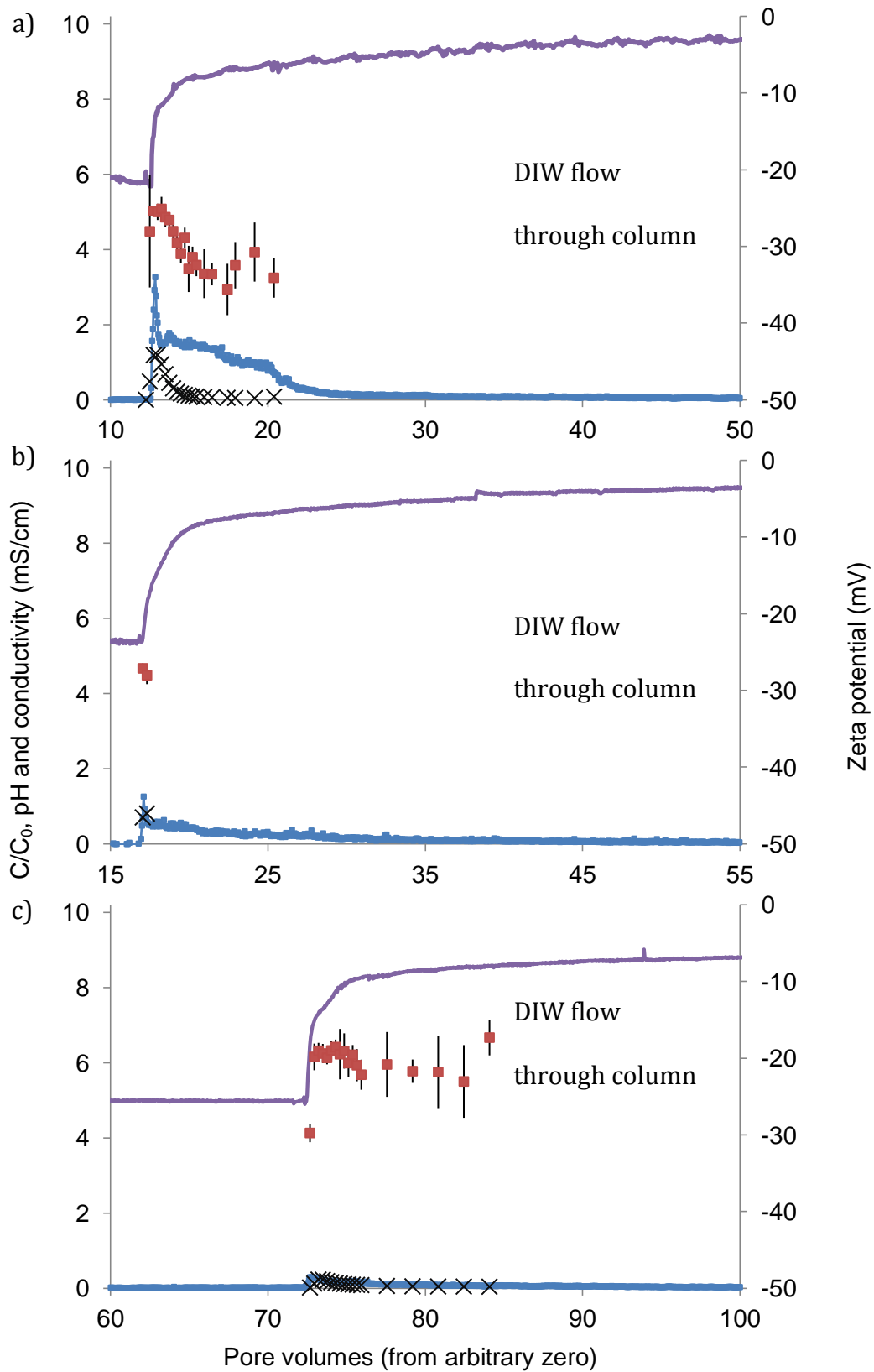
Figure 5-12 Average zeta potential of effluent particles during intial DIW flush for the columns used in the a) KCl, b) AGW and c) CaCl$_2$ experiments, error bars show standard deviation for five measurements. The traces are C/C$_0$ (blue) and pH (purple) and the crosses are conductivity.
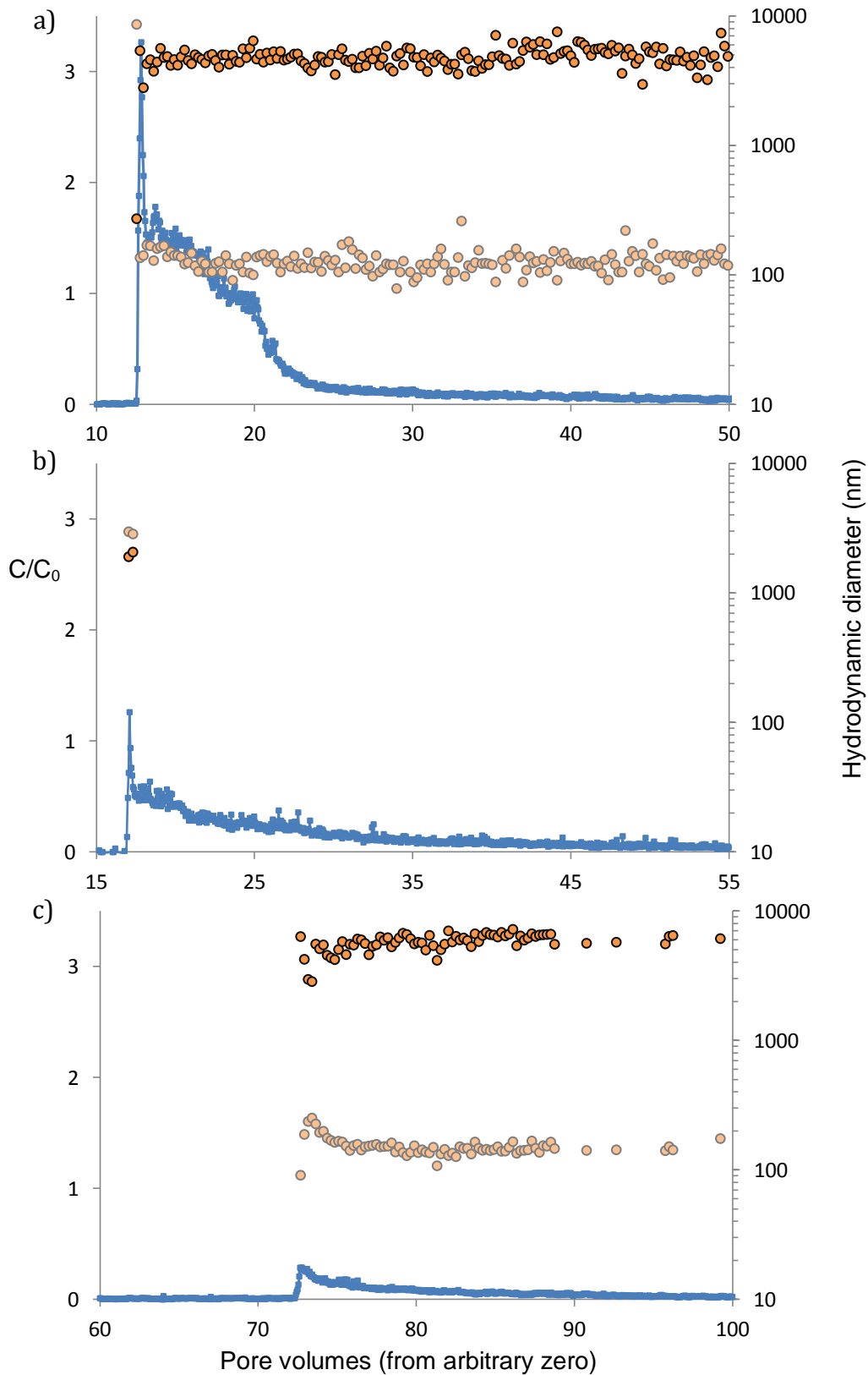
Figure 5-13 Size measurements of effluent particles during intial DIW flush for the columns used in the a) KCl, b) AGW and c) $CaCl_2$ experiments. The particles are normally polydisperse, so the major peak (by percentage intensity) is shown with a dark orange circle, while the secondary peak is in pale orange. The blue trace is C/C_0.

5.5.5 *SiO₂ particles introduced with electrolyte solution*

When silica particle breakthrough occurs with KCl and AGW, particle size quickly becomes very similar to the size of the input particles. In the KCl breakthrough, within one pore volume the size is reported as 120nm, which is the same as the input particles (Figure 5-14 and Figure 5-15). Size distribution curves comparing input silica particles and particles in the effluent show the similarity of the input and effluent populations (Figure 5-15). This suggests that the particles in the effluent are silica and that little aggregation is occurring. Input and output particle sizes remain stable during the full period of silica input.

The initial zeta potential measurements for effluent particles from the KCl column experiment (from 132-133 pore volumes, Figure 5-14) are taken before the breakthrough of silica nanoparticles occurs, as shown by the size data. The initial values of -12 to -22mV must therefore relate to indigenous particles which are washed out before the silica. The zeta potential then becomes more negative, reaching a similar value (-38 to -39mV) to the input particles (-40mV) (Figure 5-16a).
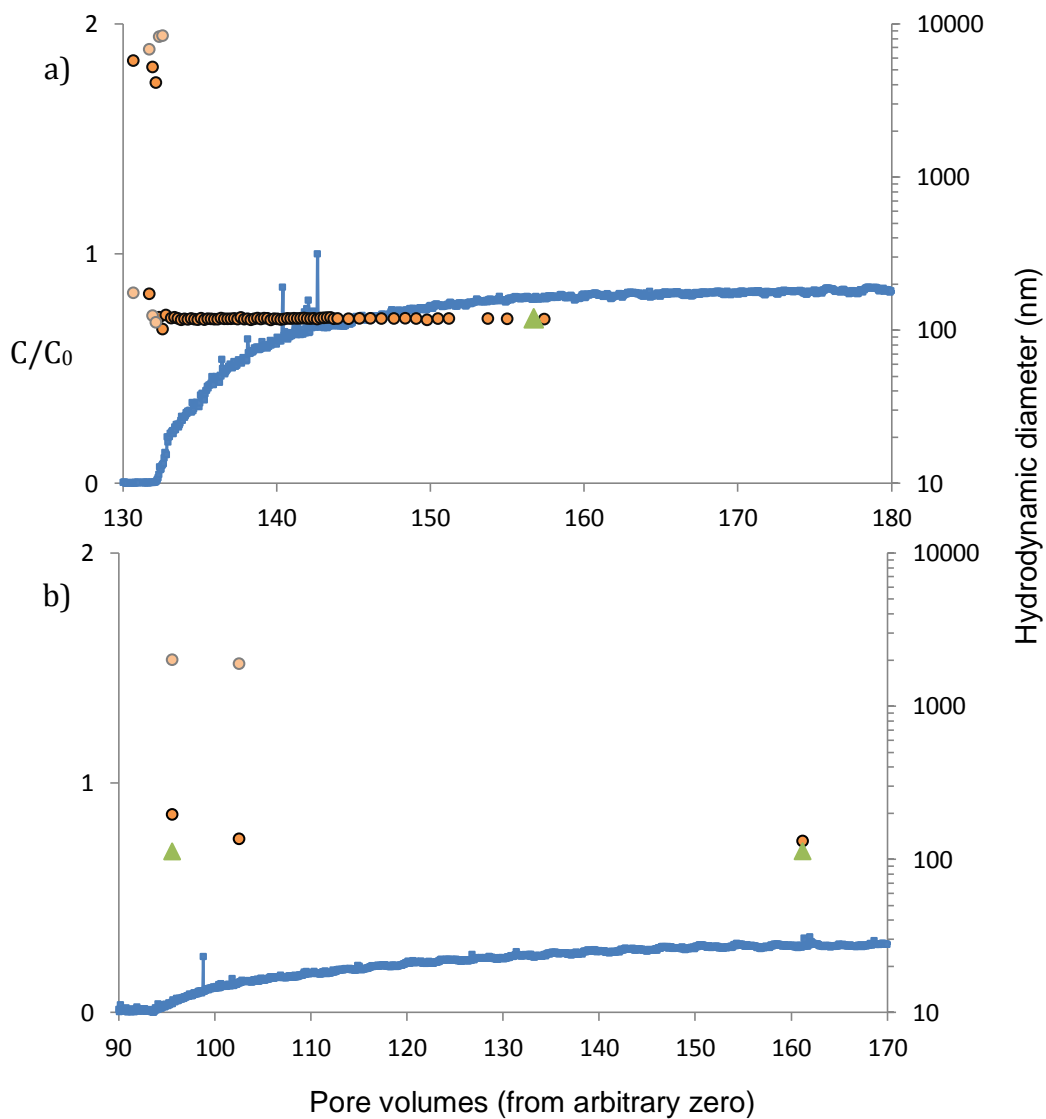
Figure 5-14 Size measurements of effluent particles during main silica nanoparticle input stage for a) KCl and b) AGW. The major peak (by percentage intensity) is shown with a dark orange circle, the secondary peak is in pale orange and green triangle points are input particle size. The blue trace is C/C_0.
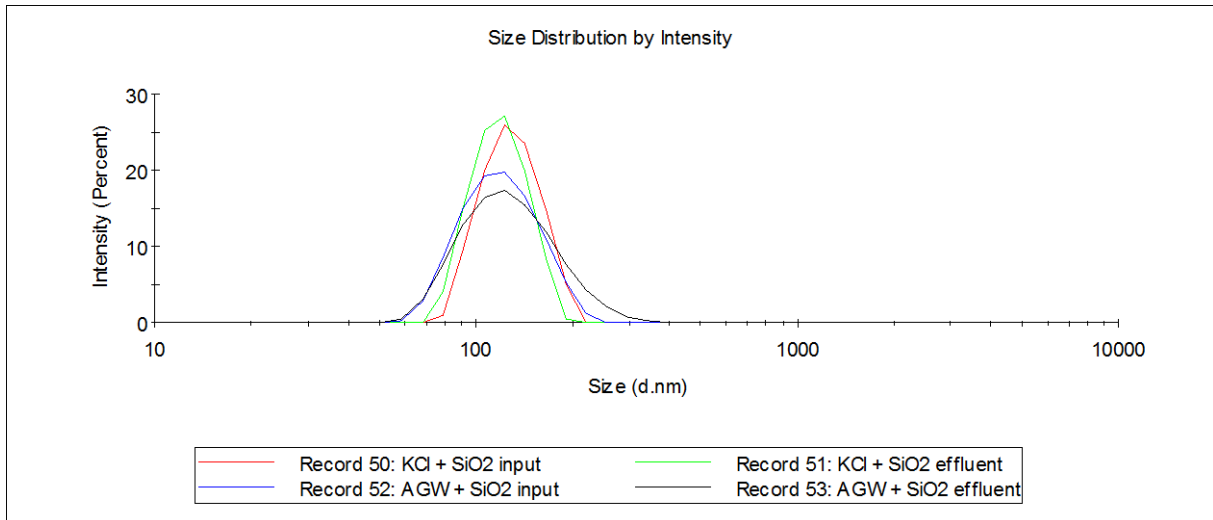
Figure 5-15 Size distribution curve for input silica and effluent particles in both KCl and AGW

In the AGW column experiment, the zeta potential also changes from a less negative (-15mV) to more negative value (-24mV), suggesting indigenous particles are released first followed by silica (Figure 5-16b). By the point at which the concentration begins to stabilise, the zeta potential for the input and output match in value.

In Figure 5-3 a change in pH between 6 and 9.5 does not have a significant effect on the zeta potential of silica particles in AGW. The similarity in zeta potential for input and output silica particles in AGW might therefore be expected. With KCl the zeta potential decrease with pH might be expected to be more pronounced, as seen with sandstone particles in Chapter 4. Ion exchange introducing Ca^{2+} into solution during the KCl injection might then cause an increase in zeta potential, counteracting the effect of the overall increase in pH.
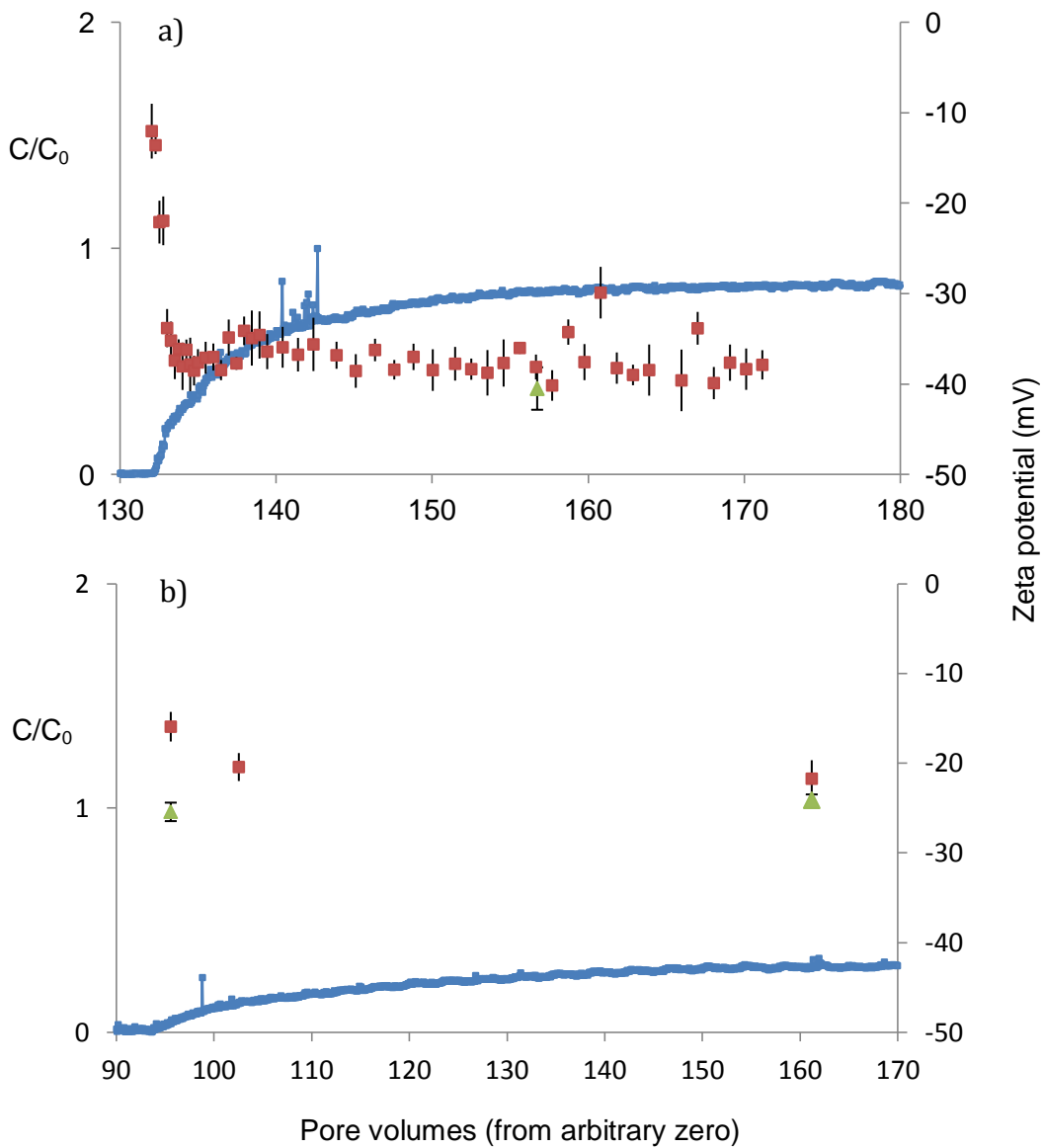
Figure 5-16 Average zeta potential of effluent particles during main silica nanoparticle input stage for a) KCl and b) AGW, error bars show standard deviation for five measurements. Green triangle points are input zeta potential and the blue trace is C/C_0. pH is stable at approximately a) 9.4, b) 9.0 and for $CaCl_2$ (not shown as there is no breakthrough and no zeta potential measurements were taken) pH8.8.

The zeta potential distributions for the input silica dispersion are also very similar to those of the comparable effluent solution (Figure 5-17), which is in agreement with the size data suggesting that the effluent is largely made up of the applied silica dispersion. The zeta potential for the KCl effluent remains relatively stable throughout the silica particle input stage, and the more limited data for the AGW experiments indicate the same.
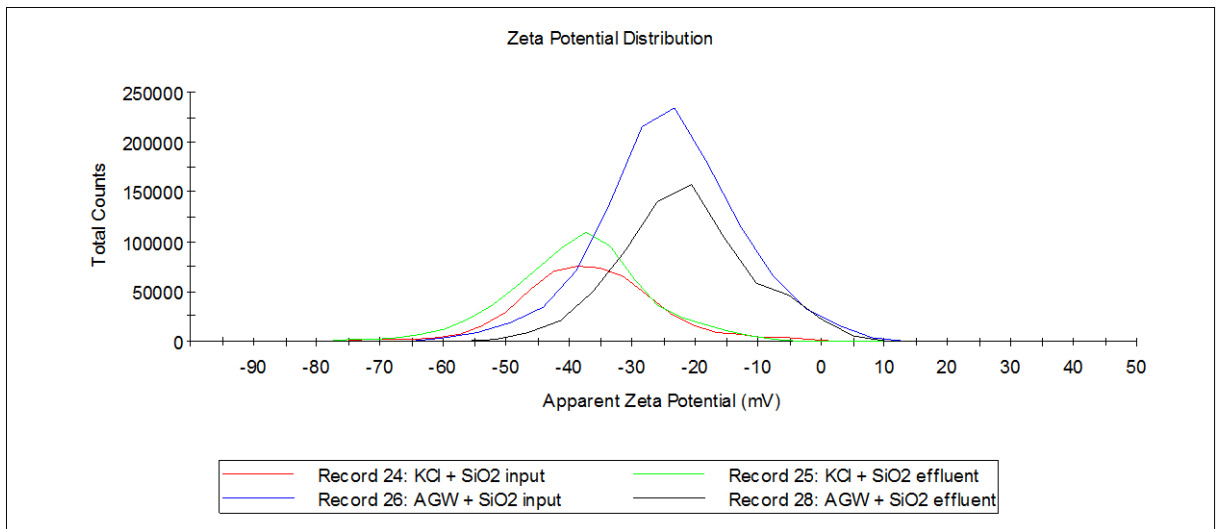
Figure 5-17 Zeta potential distributions for the input silica and effluent particles for KCl and AGW

5.5.6   Change input solution to electrolyte solution only

Once the input of silica particles has ceased, the columns were flushed through with the same chemistry solution to monitor removal of particles. The pH remains constant but the C/C_0 for both KCl and AGW begins to drop off quite quickly (Figure 5-18). Mass balance calculations show there is not significant removal by a particle free solution of the same chemistry in AGW; however 20% of the retained material is released during this stage of the KCl experiment (Table 5-8). A release of particles under the same chemical conditions as deposition suggests that some attachments were very weak and reversible, which could indicate deposition in a secondary minimum.

134

	C'/C₀	Input particle mass (mg)	Particle mass retained during the experiment (mg / %)	Particles released in electrolyte flush (mg)	% particle mass released in electrolyte flush
KCl	0.89	17.50	3.25 / 19	0.65	20
AGW	0.42	33.87	21.88 / 65	0.24	1
CaCl₂	0	18.08	18.08 / 100	0	0

**Table 5-8 Partial mass balance calculations for column experiments with KCl, AGW and CaCl₂**
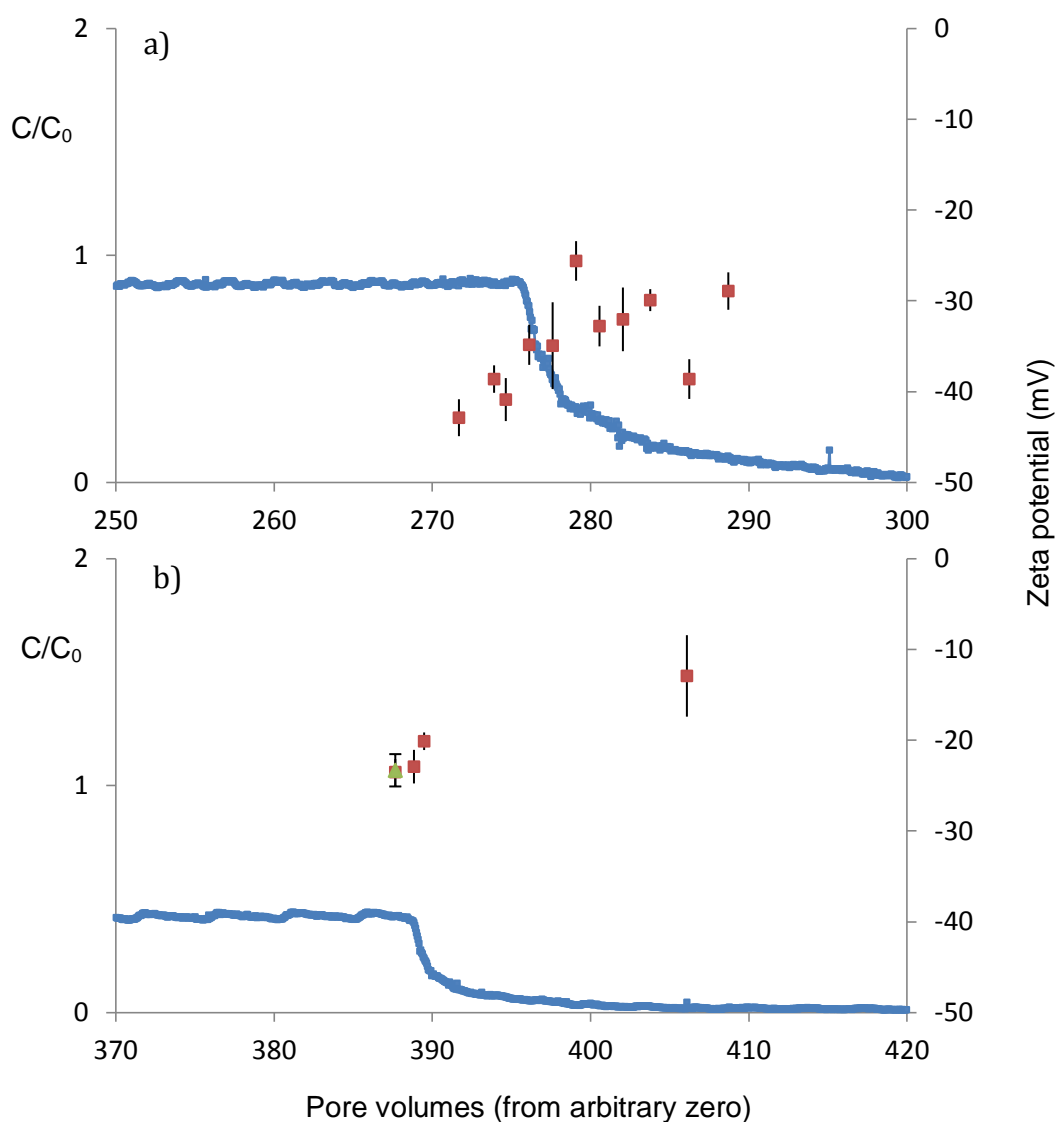
Figure 5-18 Average zeta potential of effluent particles during the electrolyte flush for a) KCl and b) AGW, error bars show standard deviation for five measurements. Green triangle points are input zeta potential and the blue trace is C/C₀. The pH is stable at approximately a) 9.4, b) 9.0 and for CaCl₂ pH8.8.

135

During the nanoparticle-free electrolyte solution flushes in both the KCl and AGW solutions, the zeta potential starts off with a slightly less negative value than that seen during silica input (-35mV and -20mV respectively) and the effluent particle zeta potential then becomes less negative with time (Figure 5-18). This is consistent with the more mobile particles (more negative zeta potential values) being removed first, followed up by less mobile particles as time goes on. The zeta potential distributions, particularly for AGW, seem to support this; with the distribution narrowing and moving towards lower magnitude values with time (Figure 5-19).

Particle size measurements for effluent from the KCl experiment (Figure 5-20a) show that after the input of silica is stopped, particles are initially the same size as the silica (~ 118-120nm) but gradually increase in size to 170nm over a period of 15 pore volumes.

Size and zeta potential measurements indicate that the most 'available' particles, those which are smaller in size with more negative zeta potential, are released first. Relatively less mobile particles are then released later. These particles are most likely to still be silica given the near coincidence of size and zeta potential, and are perhaps small aggregates with higher zeta potential.
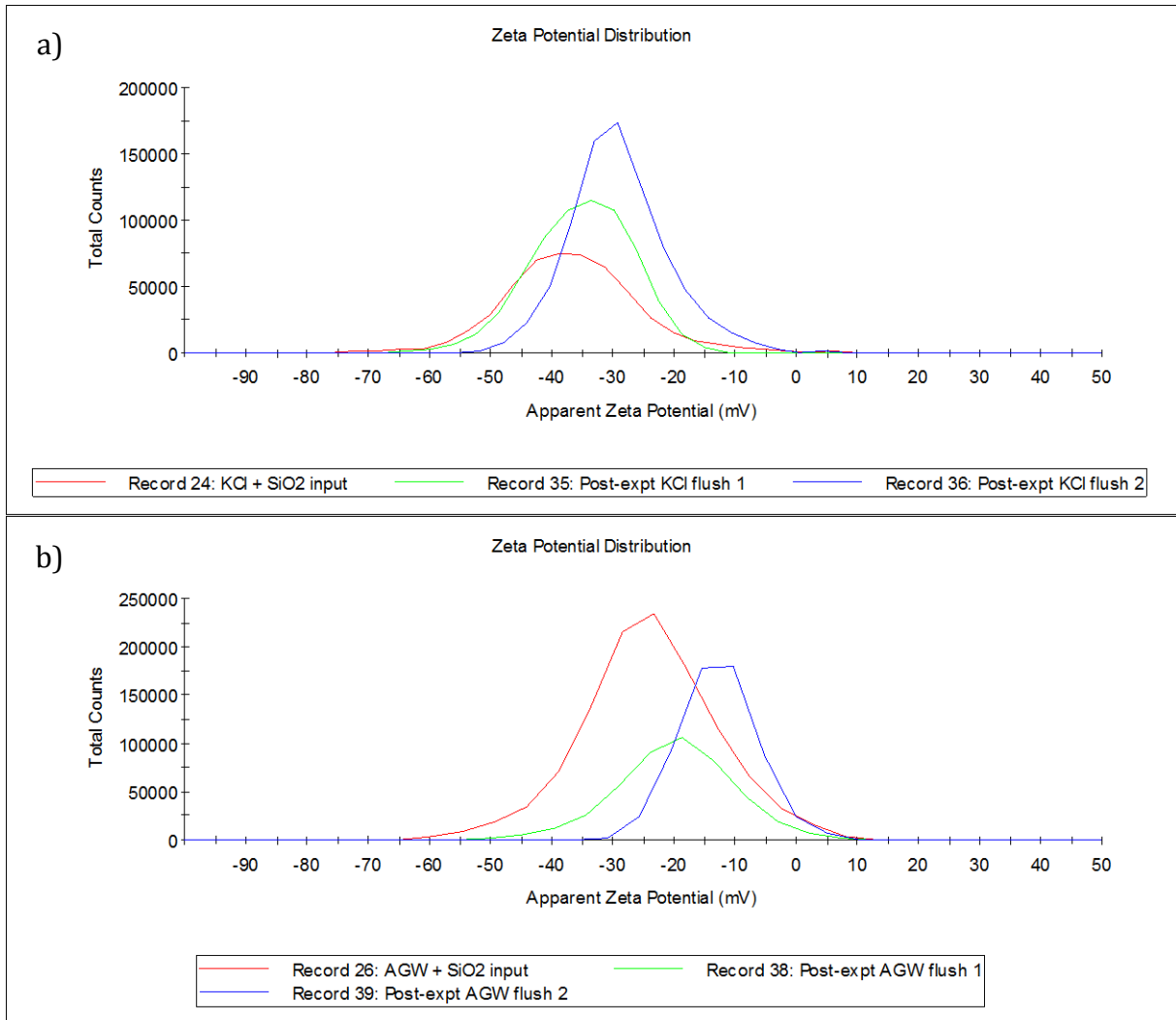
Figure 5-19 Zeta potential distributions for effluent particles following the stage change to electrolyte solution only for a) KCl and b) AGW. There is an initial time result (1) and a later time value (2) and these are compared to the silica input dispersion zeta potential distribution. For KCl (1) is at 276 pv and (2) 289 pv and for AGW (1) 390 pv and (2) 406 pv.
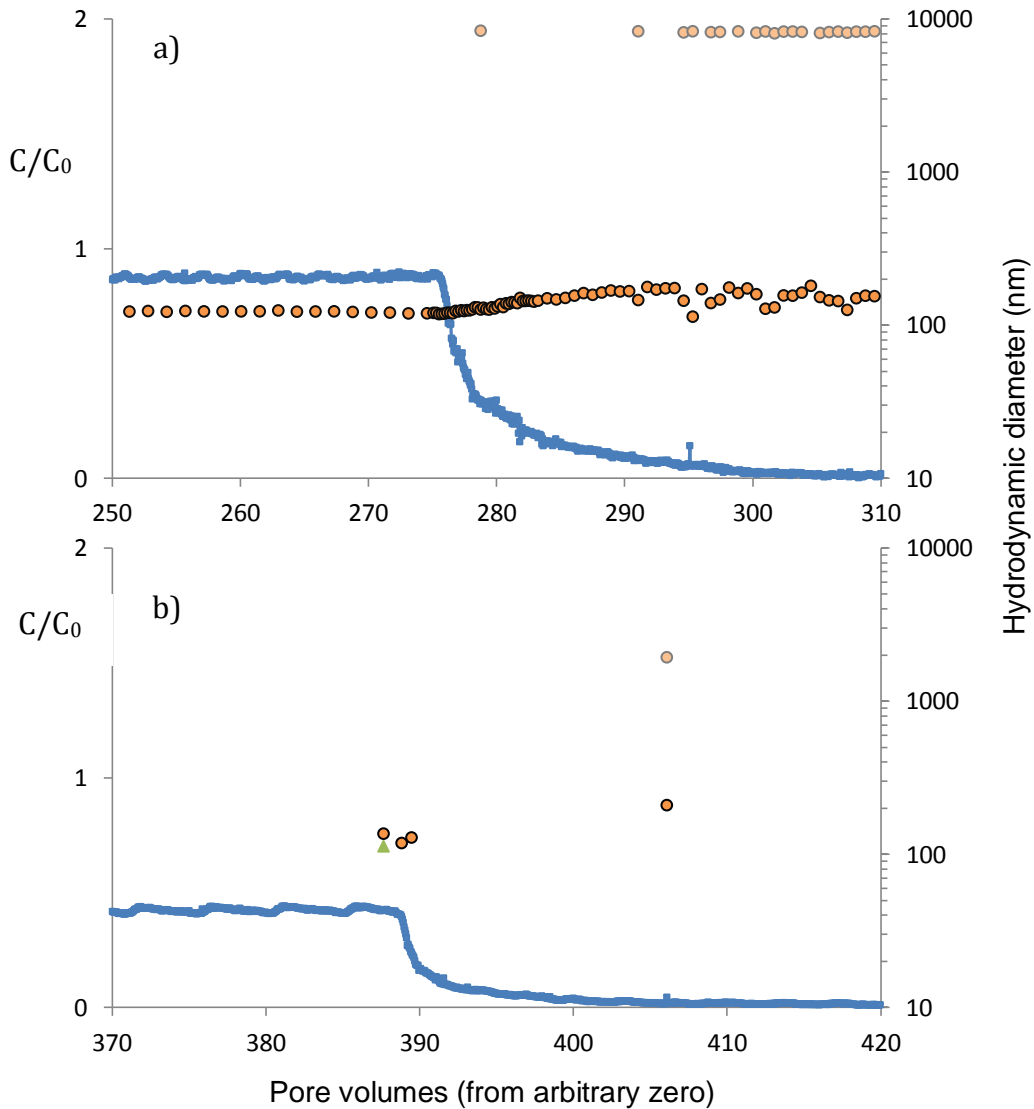
Figure 5-20 Size measurements of effluent particles during the electrolyte flush for a) KCl and b) AGW. The major peak (by percentage intensity) is shown with a dark orange circle, the secondary peak is in pale orange and green triangle points are input particle size. The blue trace is C/C₀

Approximately 15 pore volumes after silica particle input is stopped a polydisperse population develops in both KCl and AGW, perhaps indicating some indigenous particle release, or more probably being the result of concentrations getting too low for reliable measurements.

The size distribution curves for three points during the KCl electrolyte only flush (Figure 5-21) illustrate this pattern. The major peak has the same width and is just shifted towards larger particle sizes with time. The final measurement at 304 pore volumes has a second small population at around 8000-9000nm. This is a very small peak and, as intensity values are more influenced by larger particles, could just represent a very small number of particles.
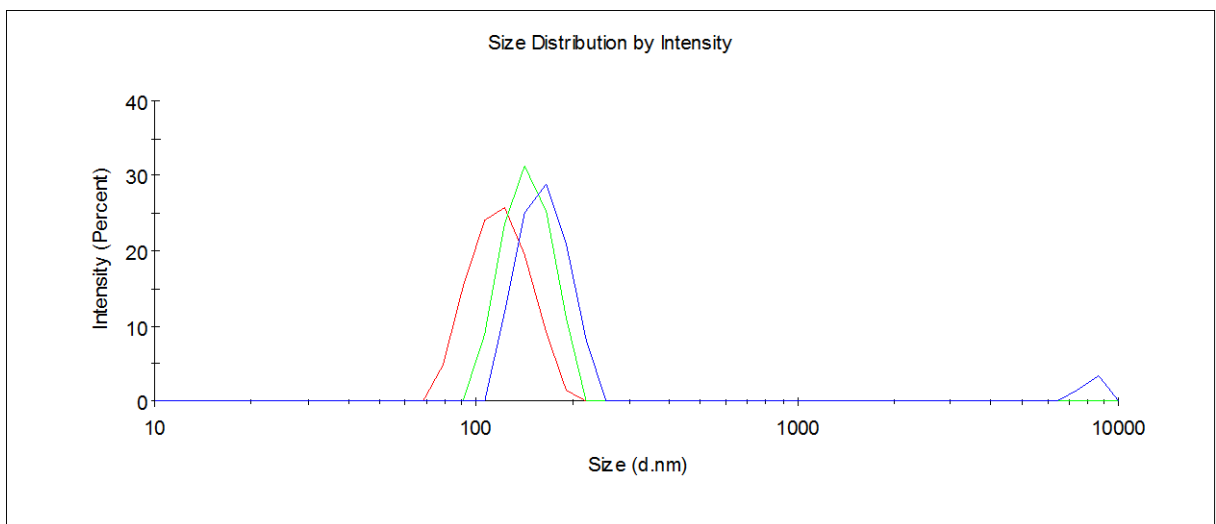
Figure 5-21 Size distribution of effluent particles during the KCl electrolyte flush. The curves represent different stages in the flush, at 275 pore volumes (red), 283 pore volumes (green) and 304 pore volumes (blue).

While there are fewer measurements available for the AGW experiment, the pattern is the same as that seen for a system equilibrated with KCl (Figure 5-20b).

5.5.7 Half strength electrolyte solution

In the AGW experiment an electrolyte solution with ionic strength half of that used in the bulk experiment is applied prior to flushing with low ionic strength DIW. This led to a small bump in particle concentration (C/C_0 changed from 0.004 to 0.025), but no significant loss of mass from the column, indicating that detachment of previously attached particles in AGW is unlikely with small changes in ionic strength.

5.5.8 Post-experiment DIW flush

5.5.8.1 Following the KCl experiment

Effluent particle zeta potential and size measurements for the KCl experiment are shown in Figure 5-22. The high initial zeta potential (-10mV) of the effluent particles is measured just as the particle breakthrough is occurring, suggesting that once again there is a release of indigenous particles at the initial point of this stage. Following this there is a decrease in conductivity, as the KCl is replaced by DIW, and zeta potential quickly decreases to approximately -48mV. This is lower than the input silica particle zeta potential, but the increase in pH could explain this difference (as seen in Section 4.4.5). After this the concentrations are low, so the results have larger standard deviations, but zeta potential values lie close to that of the input silica particles.
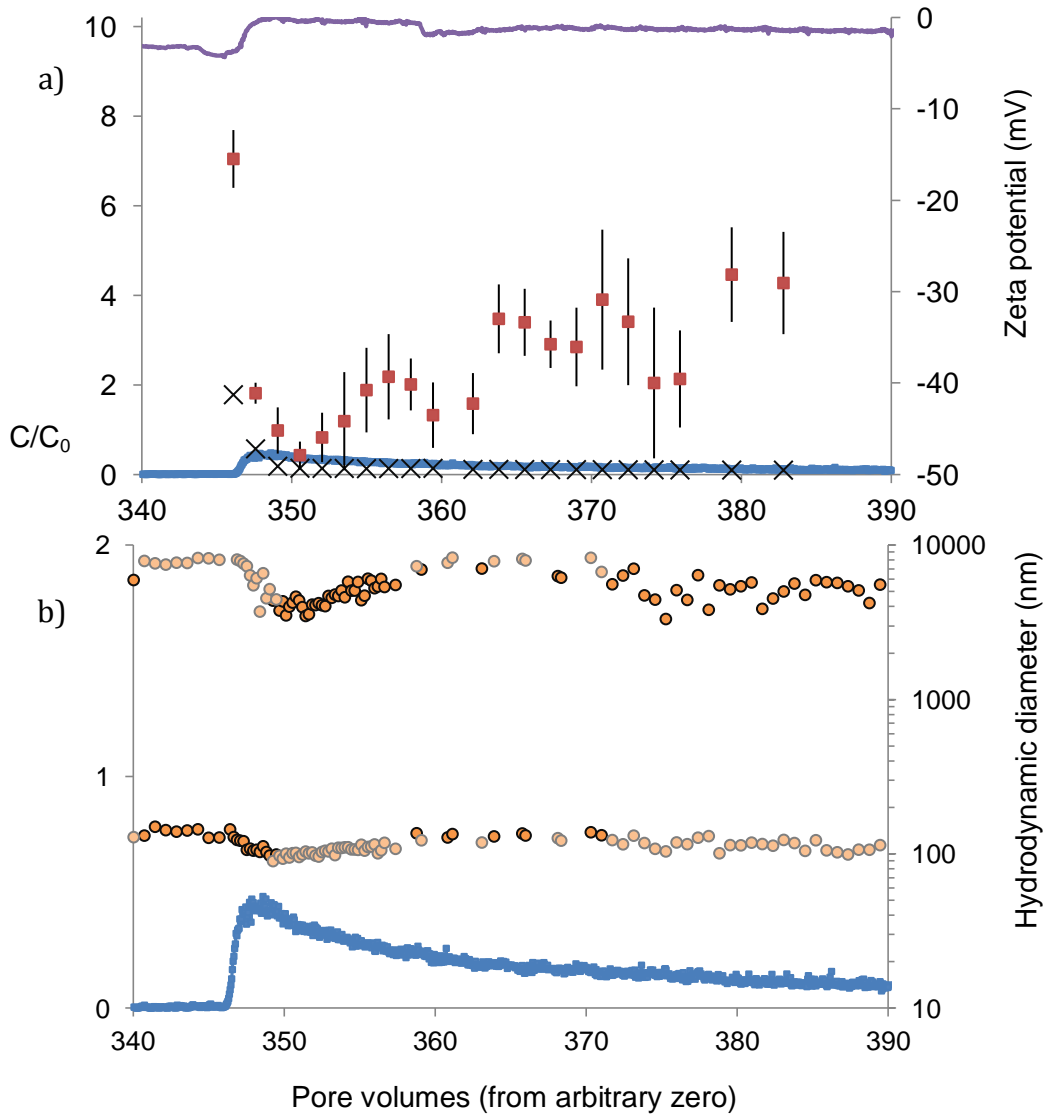
Figure 5-22 Average a) zeta potential (red squares), conductivity (crosses) and b) size of effluent particles during post-experiment DIW flush for the KCl experiment. Nephelometer measured concentrations are indicated in blue, and pH is the uppermost trace in a). Error bars for zeta potential show standard deviation for five measurements. The particles are usually polydisperse in terms of size, so the major peak (by percentage intensity) is shown with a dark orange circle, while the secondary peak is in pale orange.

The size measurements indicate that at the over the peak C/C_0 the particles are the same size as the silica (Figure 5-22b). After this point there is an increasing importance of larger size particles, similar in size to the indigenous particles released at the initial DIW flush, which can also be seen in the size distribution curves (Figure 5-23). While there are an increasing number of larger size particles, the intensity bias of size measurements

towards these larger particles will mean that the actual number of large particles is still

likely to be low, as shown by the number distribution in Figure 5-23.
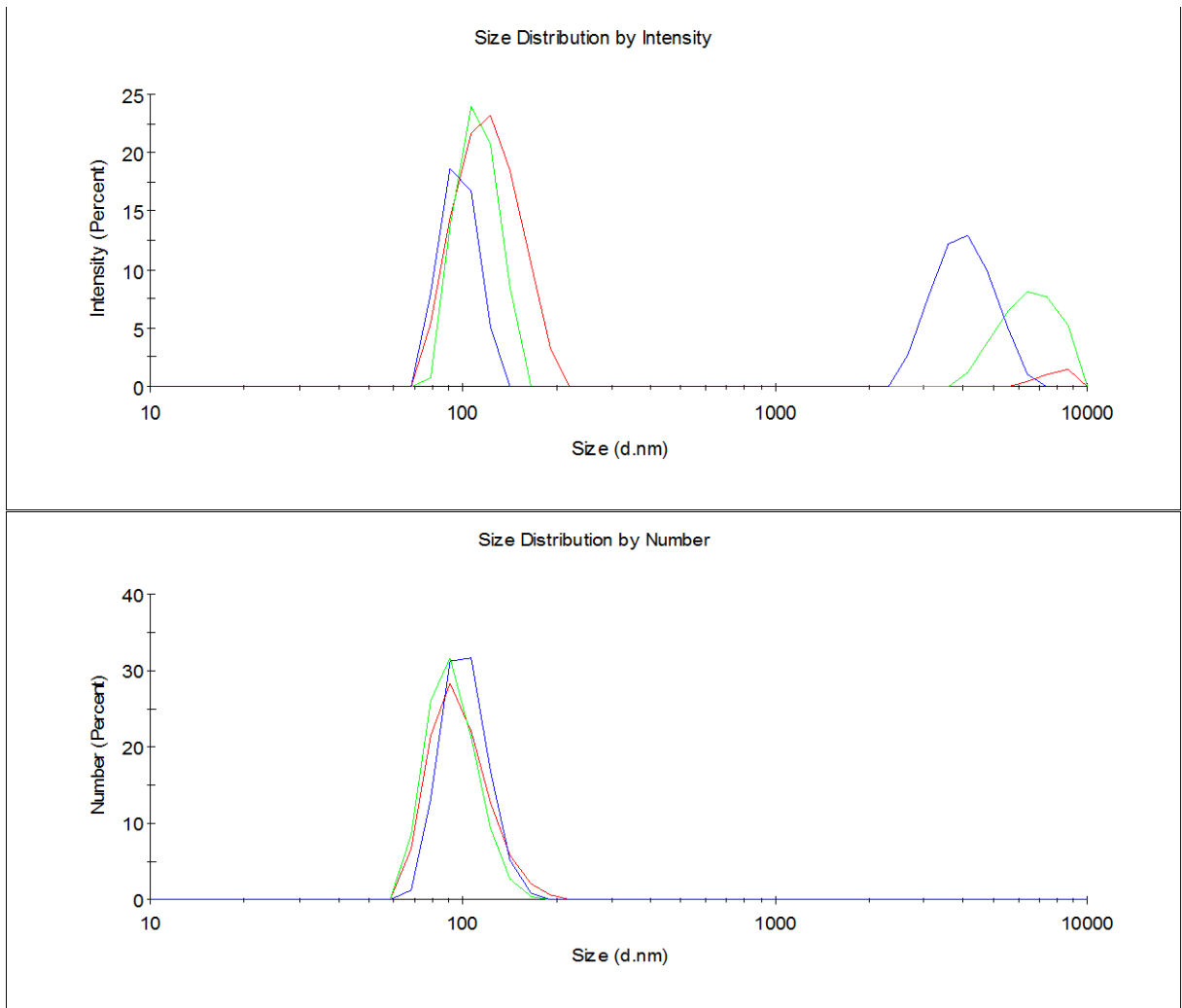
Figure 5-23 Size distribution curves for effluent particles from post-experiment DIW flush for particles at the peak concentration (347 pv, red) and two times after this (347.5 pv, green then 348.5 pv, blue)

A comparison of zeta potential distribution curves for input silica particles, effluent

particles from the initial DIW flush and effluent particles for this post-experiment DIW

flush is shown in Figure 5-24. The distribution for this later DIW flush (taken after the

concentration peak at 354 pore volumes) has two populations, the most dominant of

which has a distribution similar to that of the input silica particles, but also to that of

silica in DIW. From these distributions it is clear that a significant proportion of the effluent particles is silica, however the surface chemistry is not discernible due to the similarities in the zeta potential of silica in KCl and DIW.

The very negative component of the particle population is present in zeta potential measurements for 15 pore volumes from the start of the DIW injection. Zeta potential values this low have not been observed in any other part of the experiment, and are not seen in this DIW flush stage of the other experiments carried out. The reason for this very negative value is not known, it could perhaps be the high pH at this point particularly affecting a subsection of the particles.
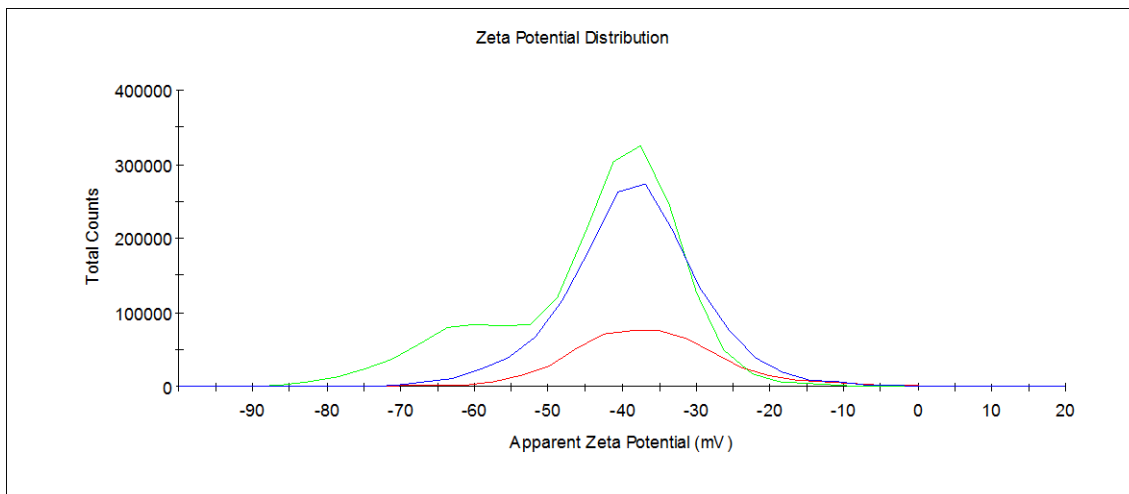
Figure 5-24 Zeta potential distribution curves for input silica particles in KCl (red), effluent particles for this post-experiment DIW flush at 354 pore volumes (green) and silica in DIW (blue).

5.5.8.2 Following the AGW experiments

Particle sizes in the effluent during the post-AGW experiment DIW flush are very stable at 121-125nm (Figure 5-25b), which is similar to the input silica particle diameter using DLS. The zeta potential is also similar to the zeta potential of input silica particles in AGW, within the error margin indicated (-24mV, Figure 5-25a), and perhaps lowers

slightly in line with the increase in pH. The values become less negative around 8 pore volumes after starting the DIW injection, but the concentration by this point is very low which could affect the accuracy of the results.
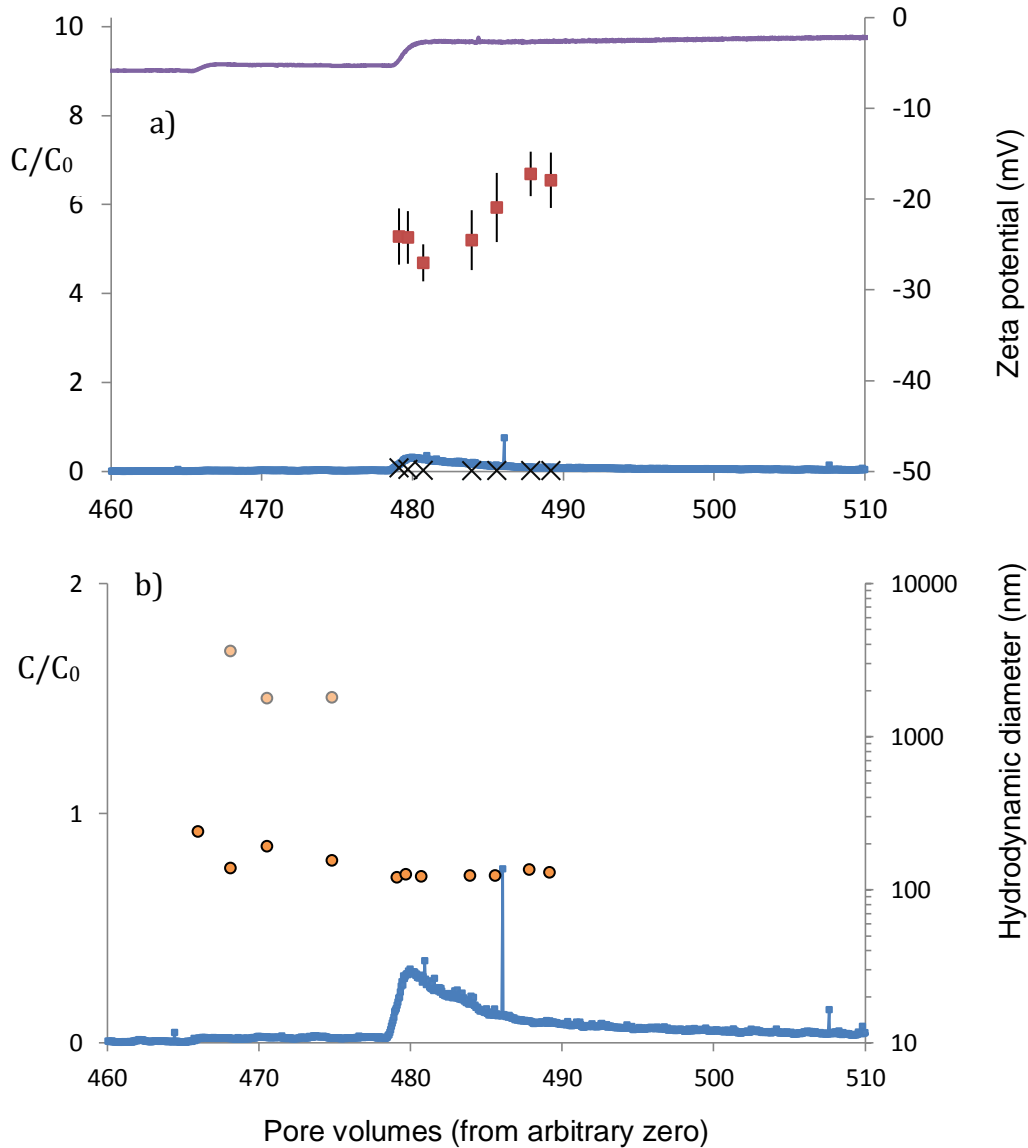

Figure 5-25 Average a) zeta potential (red squares), conductivity (crosses) and b) size of effluent particles during post-experiment DIW flush for the AGW experiment. Error bars for zeta potential show standard deviation for five measurements. The major size peak (by percentage intensity) is shown with a dark orange circle, while the secondary peak is in pale orange. The traces are C/C_0 (blue) and pH (purple).

Zeta potential distribution curves indicate that the value for the effluent particles during this stage is not similar to silica in DIW, but instead has a distribution the same as that of

144

the silica particles in equilibrium with AGW (Figure 5-26). The later zeta potential

distribution, at 488 pore volumes, indicates a narrowing of the zeta potential population

distribution. This suggests that more negative particles are released first, followed by

the less mobile particles with higher zeta potentials.

Size and zeta potential values both suggest that the particles released are the silica

nanoparticles injected during the experiment. The low zeta potential measurements also

suggest that the surface chemistry of the particles remains dominated by the ions from

AGW components (Ca^{2+} and Mg^{2+}) rather than releasing these as the DIW flush

commences. pH rises as the flush occurs, and this may encourage the divalent cations to

be retained on the silica surface if silica sorption is analagous to iron oxide sorption.
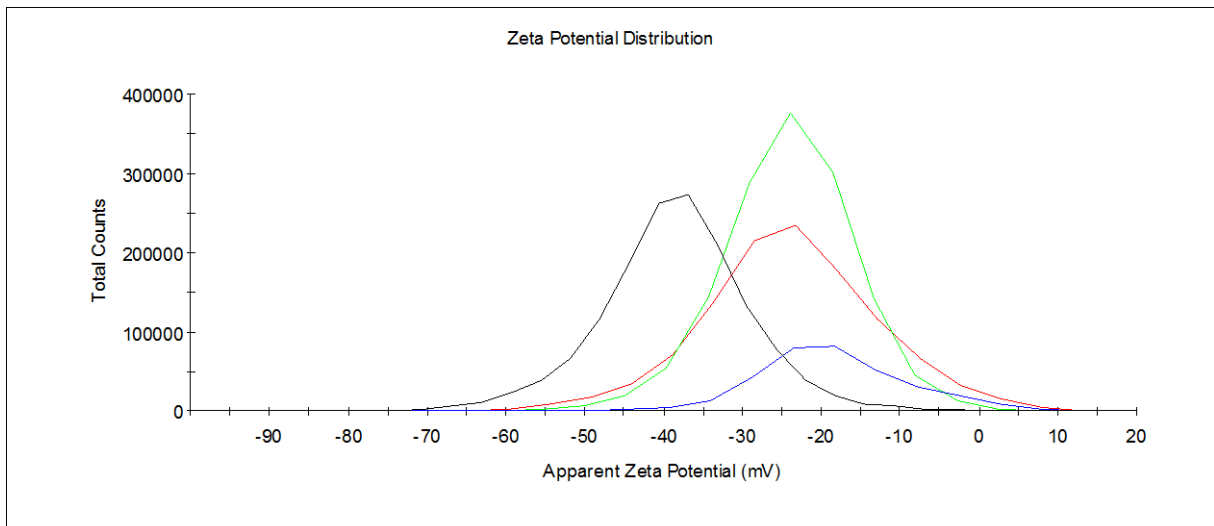
Figure 5-26 Zeta potential distribution curves for input silica particles in AGW (red) and effluent particles for this post-experiment DIW flush at 480 pore volumes (green) and 488 pore volumes (blue). A zeta potential distribution for 100ppm silica particles in DIW is also shown (black).

5.5.8.3 Following $CaCl_2$ experiments

The effluent particles in the DIW flush following the $CaCl_2$ experiment are initially

monodisperse with a diameter of 133-135nm (Figure 5-27b). The particle size remains

monodisperse but gradually increases over 27 pore volumes to approximately 150nm. While this particle diameter is slightly larger than the silica in equilibrium with $CaCl_2$ which was injected (119nm), it is still more likely to be slightly aggregated silica than indigenous material, which typically has a much larger dominant particle size.

At approximately 30 pore volumes after the start of the DIW flush the size measurements begin to show consistently two size populations, the second in the 8000-9000nm size range. Size distribution curves show that this population remains relatively small, and most likely consists of indigenous material.

Zeta potential measurements before the point where size measurements represent those of silica are high, at -10 to -12mV (Figure 5-27a). As seen before, these could indicate the presence of indigenous particles arriving before the main breakthrough of silica. After this the zeta potential returns to around -20mV, with a slight drop to more negative values of around -22mV with pH. This range is similar to the input zeta potential of -21mV and not characteristic of silica particles in DIW, as indicated by the zeta potential distribution curves in Figure 5-28. This is in good agreement with the findings at the same stage of the AGW experiment.
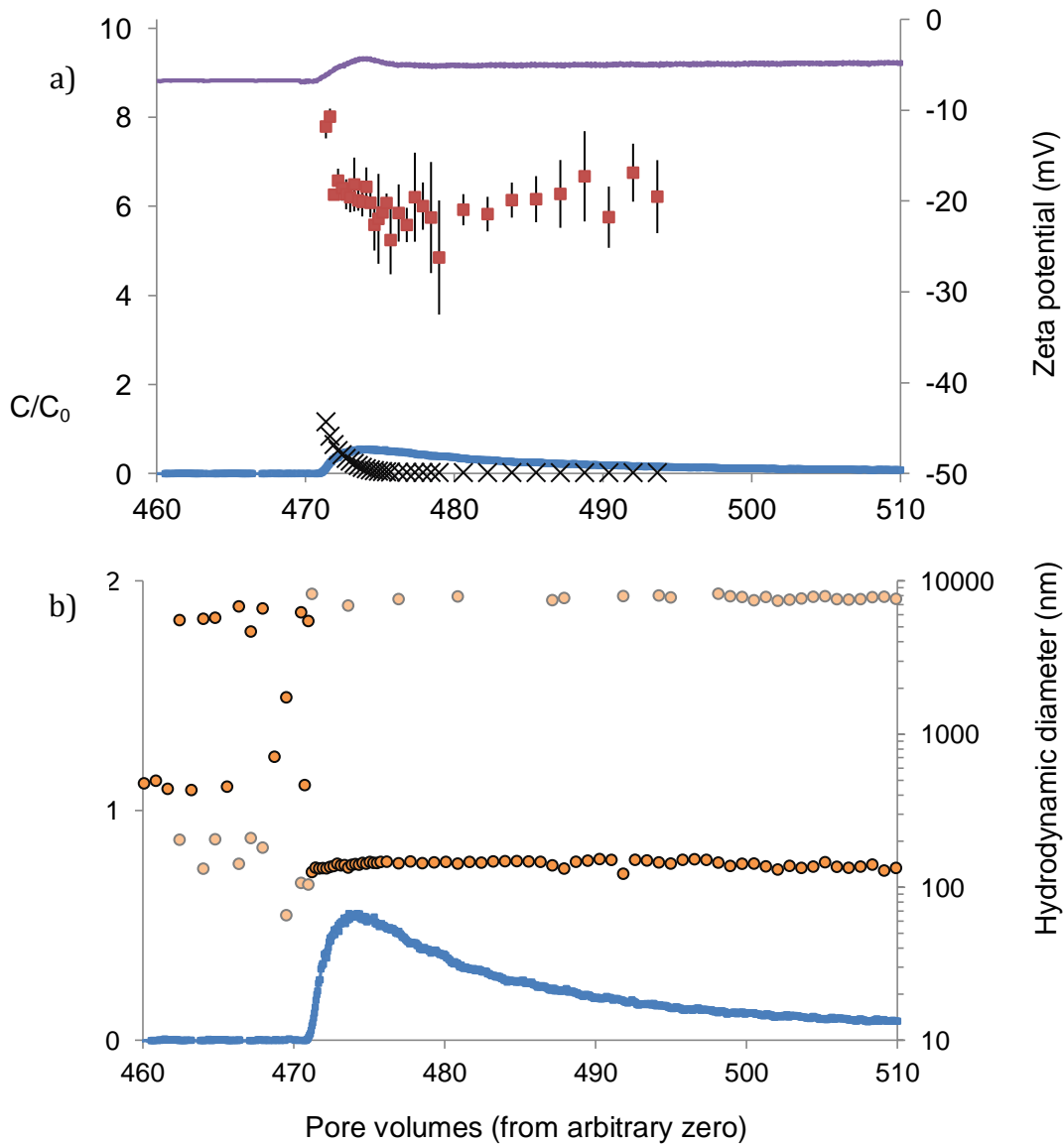
Figure 5-27 Average a) zeta potential (red squares), conductivity (crosses) and b) size of effluent particles during post-experiment DIW flush for the CaCl₂ experiment. Error bars for zeta potential show standard deviation for five measurements. The major size peak (by percentage intensity) is shown with a dark orange circle, while the secondary peak is in pale orange. The traces are C/C₀ (blue) and pH (purple).
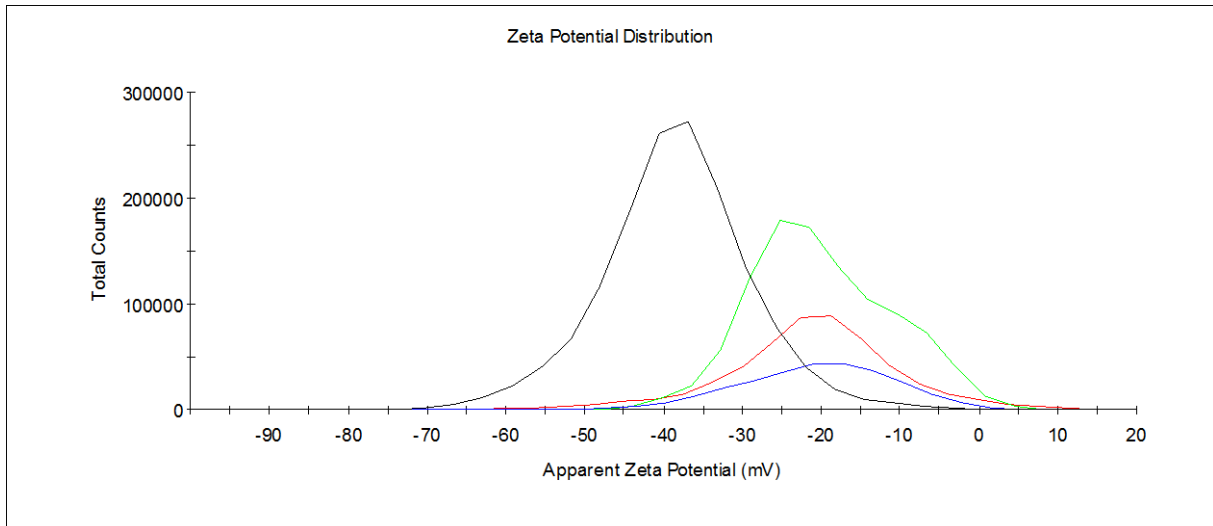
Figure 5-28 Zeta potential distribution curves for input silica particles in CaCl$_2$ (red) and effluent particles for this post-experiment DIW flush at 473.5 pore volumes (green) and 485 pore volumes (blue). A zeta potential distribution for 100ppm silica particles in DIW is also shown (black).

Similarly to the AGW results, the particles in the effluent of the DIW flush following the CaCl$_2$ experiment retain a zeta potential similar to that of silica in CaCl$_2$ rather than in DIW. The dominant ion on the particle surface must continue to be Ca^{2+}, suggesting a slow release of this ion from surface sites. Again, pH is higher than before the flush started which may encourage divalent cations to be retained here.

5.5.9   Mass balance calculations

Mass balance calculations were carried out assuming effluent particle concentration was composed just of silica and the results are presented in Table 5-9. This is a fair assumption as the number distributions of particle sizes indicate very little input from particle sizes much larger than those of the input silica. The values here will be the maximum possible however (with the final retained percentage being a minimum); as there could be a contribution to the C/C$_0$ of indigenous particles and these, along with aggregates, could also cause size bias in nephelometer measurements.

148

These mass balance calculations indicate that there is very little attachment in monovalent KCl, with approximately 50% of the relatively small volume of attached particles being released. Only 6% of the total input silica particles were retained by the end of the KCl column experiment.

Overall, 62% of the silica particles injected into the sandstone column are retained and 89% are retained during the $CaCl_2$ experiment. With AGW and $CaCl_2$ there was a small volume release of particles during the post-experiment DIW flush, but nothing which significantly altered the overall retention.

Roy and Dzombak (1996) and Hahn et al. (2004) both observed a similar response from latex particles attached to glass bead surfaces under equilibrium with solutions of different chemical composition. Particles showed 100% attachment and then very little release with $CaCl_2$, compared to significant release of particles attached under a monovalent ion solution. Roy and Dzombak (1996) attributed this behaviour to the porous medium surface remaining characterised by Ca^{2+} ions, their release being limited by a small amount of Ca^{2+} in the fluid phase. Hahn et al. (2004), however, understood it to be a result of reversible secondary and permanent primary minimum attachments being made by the particles under KCl and $CaCl_2$ respectively.

	C'/C₀	Input particles (mg)	Particles retained [P_r] during injection phase (mg/% input)	Retained particles released in electrolyte flush (mg/% P_r)	Retained particles released in 1/2 ionic strength electrolyte (mg/% P_r)	Retained particles released in DIW (mg/% P_r)	Total particles retained (mg/% P_r)	Total % of input particles retained
KCl	0.89	17.50	3.25/19	0.65/20	-	1.54/47	1.05/32	6
AGW	0.42	33.87	21.88/65	0.24/1	0.03/0.1	0.29/1	21.35/98	62
CaCl₂	0	18.08	18.08/100	0/0	-	1.95/11	16.19/89	89

Table 5-9 Mass balance calculations for the full KCl, AGW and CaCl₂ experiments

In the KCl experiment retained particles are released during flushes of both the same ionic strength solution and DIW. This behaviour suggests there is some reversible attachment in a secondary minimum. However, if DLVO interaction energy curves give an approximate representation of the system, then there would need to be an increase in particle size, ionic strength and the Hamaker constant before a secondary minimum is observed.

There are a small number of particles which are attached permanently in this system. Physical heterogeneities, such as grain roughness, and mineralogical or geochemical heterogeneity causing a variation in zeta potential (and Hamaker constant) below the scale of the SS-EFM measurements, could also provide points of attachment where an energy barrier can be overcome.

In the case of AGW and $CaCl_2$, where divalent cations are present, there is increased attachment during the experiment and then limited particle release by flushing with solutions of the same ionic strength, a low ionic strength of the same chemistry (in the case of AGW) or DIW. This is particularly the case in AGW where only 2% of particles are released after retention. The attachments made in the presence of divalent ions are therefore considered to be permanent.

There is evidence, in the zeta potential measurements of the effluent particles in the DIW flush, of slow release of divalent ions from the silica surface. The particle zeta potential remains at, or close to, the value of the silica particles equilibrated with AGW and $CaCl_2$, rather than changing to the zeta potential of silica in DIW. This would mean there was no change in conditions compared to those under which the particles attached

to the surface, especially so if the same effect were to be found in the sandstone zeta potential. This could offer an explanation for the lack of particle release in these systems.

The effects of sandstone heterogeneity, as described for the KCl experiment, could also be in effect here, just overshadowed by the effect of divalent ions on the surface chemistry.

5.6 Conclusions

Column studies have been undertaken to understand the effect of fluid phase chemical composition on manufactured nanoparticle mobility, and in particular to address the questions posed at the start of this chapter:

1. Do the changes in zeta potential with different chemical conditions seen in Chapter 4 significantly affect breakthrough of particles in intact sandstone?

2. Do the interactions between nanoparticles and surfaces result in significant particle fractionation by zeta potential during passage through these columns?

3. Can breakthrough be estimated using a DLVO/CFT approach using zeta potential as measured here and in Chapter 4?

4. Are the attachments permanent?

The experimental C'/C_0 is dependent upon chemical composition, with increasing proportions of divalent ions causing increasing nanoparticle deposition in the sandstone column. The zeta potential values measured in Chapter 4 give a good qualitative description of this behaviour.

There is little evidence of particle fractionation in the zeta potential during the silica input stage. Instead the input and effluent particle zeta potential during this stage remain the same, within the margins of measurement error. However, when the input of silica has ceased and the columns are flushed with particle-free solutions of the same chemistry an increase in zeta potential observed with time perhaps indicates more mobile particles with more negative zeta potentials are released first.

Calculations of C'/C_0 using CFT in the presence of repulsive DLVO forces give a reasonable indication of the mobility of silica nanoparticles over short distances in sandstone. Collision efficiency (α) has been calculated in two ways, from the Fuchs equation with unequally sized particles and from experimental data, and it is assumed that these two definitions of α are comparable. If this is the case, then the α for silica in KCl is considerably underestimated in theoretical calculations. This leads to an under-prediction of particle attachment when the particles and sandstone are equilibrated with KCl.

The CFT model is very sensitive to the value of the Hamaker constant (A_{132}), as shown in Chapter 2 and Section 5.5.2. Within a small range of A_{132} the theory can predict either complete breakthrough or no breakthrough at all for the AGW system. This is due to the theoretical attachment efficiency being directly related to the size of the energy barrier, which in turn is reliant upon the A_{132}, as this determines the magnitude of the attractive van der Waals forces.

At the calculated A_{132} for silica-water-chlorite, the zeta potential of the silica and sandstone would need to be less negative than that measured with KCl for the α value

and C'/C$_0$ to agree with what is observed experimentally. The ionic strength under which the sandstone zeta potential measurements were taken was lower than that of the column experiment solutions. This could mean that the sandstone zeta potential used in the calculation of α and C'/C$_0$ is more negative than it should be. This will have a small effect on the calculated values, however the zeta potential of both the sandstone and the silica need to be less negative to provide the necessary interaction energy profile to describe the experimental results.

A less negative zeta potential could be possible if there was zeta potential heterogeneity or patchiness below the scale of the electrophoresis and SS-EFM measurements, like that seen in mica measurements in Chapter 3.

The sensitivity to the Hamaker constant and zeta potential, and the observation that only relatively small changes in these values can affect C'/C$_0$ considerably, suggests that the calculations could be used as a screening tool for nanoparticle mobility if the variables are more closely constrained. Further work is needed to estimate Hamaker constant values between nanoparticles and sandstone or other rock material. Zeta potential heterogeneity needs to be investigated at a smaller scale than the measurement techniques in this study have allowed.

Under chemical conditions closest to those in the environment (AGW), the attachments made between silica and sandstone are permanent, at least over the limited time scales of the experiments. The particles which have been equilibrated with divalent ions appear to remain characterised by high zeta potentials associated with these ions, even under low ionic strength conditions. This is encouraging if the manufactured

nanoparticles in question are considered a contaminant, as permanent attachments reduce long term mobility. However, sorption on oxide surfaces is usually considered reversible, and over field time scales it is likely that the particles will become progressively more mobile with time, and thus such particles may become more prone to release subsequently.

In previous work on nanoparticle transport through intact sandstone columns interactions between the attached particles and freely moving particles have been observed. These have been seen to both encourage further attachment through more favourable particle-particle interactions and to increase particle mobility through blocking further attachment. These processes both have impacts on the overall surface zeta potential of the rock, on zeta potential heterogeneity and on the system Hamaker constant. To understand long-term mobility of manufactured nanoparticles in rock these issues must also be addressed.

6 CONCLUSIONS

6.1 Aim

The overall aim was to determine if zeta potential can be used as the basis for assessing the mobility of nanoparticles in sandstone groundwaters, with five main objectives defined to achieve this as follows:

1. to evaluate the dependence of nanoparticle mobility on zeta potential according to current theories

2. to assess the applicability to rocks of a new Malvern Instruments method for measuring the zeta potentials of surfaces

3. to measure the variation in rock surface zeta potential through an example rock

4. to determine the dependencies of particle and rock surface zeta potentials on chemical conditions

5. to test traditional nanoparticle transport theory on transport of nanoparticles through rock intact rock columns using measured zeta potential and other properties.

This chapter summarises the progress made towards each of the objectives (Section 6.2) before discussing the achievement of the overall aim (Section 6.3). A final section (Section 6.4) lists recommendations for further research.

6.2 Thesis Summary

6.2.1   Dependence of nanoparticle mobility on zeta potential according to traditional theories

Zeta potential is the potential at the shear plane between a solid surface and an electrolyte solution, and considered to be the best description of the potential which will

most directly affect particle-particle and particle-surface interactions. It is used in DLVO theory as a contributor to the electric double layer interaction energy and so plays an important role in the calculation of energy barrier height, which determines the theoretical value of the collision efficiency. The collision efficiency describes the likelihood of particle attachment following a collision with another particle or a surface, so determines the predicted equilibrium concentration (C'/C_0).

A small change in zeta potential of 5-10mV in systems where both surfaces are similarly charged (most surfaces are negatively charged in groundwater systems) can have a large impact on the height of the energy barrier.

The C'/C_0 calculated using colloid filtration theory (CFT) is also very sensitive to the zeta potential. If all other calculation parameters remain constant only a small change in the zeta potential of the particle or surface (or both) can cause a prediction of complete particle breakthrough to change to no breakthrough at all. As the zeta potential changes, the sensitivity of the C'/C_0 value to other input parameters also changes. With a more negative zeta potential there is more sensitivity to particle and collector grain size and less sensitivity to the Hamaker constant and ionic strength.

6.2.2 *Use of a new Malvern Instruments zeta potential measurement technique (SS-EFM) on rocks*

The use of intact aquifer rock in particle transport studies was considered to be important, and to represent more closely field conditions when field studies, as is the case currently in the UK, cannot be undertaken. The most common method for measuring porous media zeta potential is currently electrophoresis, which uses

disaggregated samples and would destroy natural rock fabrics which could impact on the results. A new technique for measuring the zeta potential of surfaces was developed by Malvern Instruments just before the current project was undertaken. The SS-EFM technique allowed zeta potential measurements on intact samples of a few millimetres in size.

To carry out the SS-EFM measurement, a stable probe particle suspension was required which would not interact with the sample surface. An aqueous suspension of silica nanoparticles were used, in low ionic strength solutions they do no attach to the redbed sandstone. The particles had a diameter of 100nm (115-120nm when measured using DLS) and were used at 100mg/L concentrations for the measurements. The same silica nanoparticles were also used later in the column experiments.

It was necessary for the SS-EFM method to be tested on rock surfaces before it was used further. Within the uncertainties associated with differences in sample preparation, storage and aging between different studies, good agreement with published results from established techniques was found using mica as an initial test of a mineralogical surface. The effects of roughness and equilibration volume were investigated, and found not to impact on the average surface zeta potential measurement using SS-EFM.

Surface zeta potential measurements of sandstone were successfully undertaken. An assessment of the repeatability of measurements on a single sandstone surface sample gave an average standard deviation of 3.1mV which is equivalent to an RSD of 9% of the absolute value, within the 10% found by Corbett et al. (2012) in well behaved systems. Variability in the absolute value of surface zeta potential is caused by various factors: the

technique in locating the sample surface; through the need for multiple measurements at several distances to calculate one value; the removal of the sample to clean the electrodes; and the possibility of air bubbles at the sample surface or from the sample contaminating the probe particle fluid. Protocols were developed to minimise the impact of these factors, and to remove data which did not meet a certain quality criteria.

SS-EFM measurements of intact sandstone were comparable with measurements on disaggregated sandstone samples using electrophoresis. Mudstone surfaces, however gave a much more negative zeta potential than sandstone when measured using SS-EFM. When the mudstones were disaggregated and measured using electrophoresis zeta potentials equivalent to the sandstone, and so very different from the intact mudstone, were measured.

6.2.3   Variation of surface zeta potential through an example rock sequence

There is little variation in sandstone zeta potential along a 50m length of core using either SS-EFM measurements of intact samples or electrophoresis measurements on disaggregated samples. An average surface zeta potential of -36.2±2.76mV (69 measurements) was measured for sandstone in 1mM KCl with SS-EFM and -37.9±2.36mV (28 samples) with electrophoresis. The similarities in sandstone zeta potential may be scale dependent, and variability may be present below the few millimetre scale of SS-EFM.

Both haematite-coated and naturally bleached sandstone samples have similar surface zeta potential values, indicating that the major control on the surface properties is not simply the coating of iron oxide. A simple quantification of the surface zeta potential

159

seems to be found in a surface-area modified linear mixing model. This is a relationship which has been observed in simpler bi-mineral systems (Johnson, 1999) but has been transferable to a more complex multi-mineral intact rock. Using this method, clay minerals become important in this sandstone due to their large surface area to volume ratio.

Despite the close agreement for sandstone samples, in the measurement of mudstone zeta potential, SS-EFM has indicated a much more negative value for the intact surface than is found for the disaggregated mudstone material using electrophoresis. Using SS-EFM the zeta potential is measured at -67.6mV, with a standard deviation of 24.2mV due to variation between different mudstone samples (there is only a small error on individual samples). In electrophoresis the same zeta potential is found for both disaggregated mudstone (-37.9±0.8mV) and sandstone. This is thought to be due to the platy clay minerals in mudstone, which have been observed to have a much less negative zeta potential on the crystal edges compared to the crystal faces (Zhao et al., 2008). In the intact mudstone these clay minerals may form more continuous layers, with the zeta potential dominated by that of the more negative crystal face. When the clays are disaggregated more edges are exposed and these control the overall zeta potential of the sample. The viability of this explanation was confirmed by examining the zeta potentials of mica cleavage planes and crushed mica.

Electrophoresis provides a simple way to measure the zeta potential of many samples very quickly, as long as the sample is disaggregated easily. The SS-EFM method, while more time-consuming and demanding, provides the zeta potential of an intact sample

perhaps more representative of the surface a nanoparticle in groundwater would interact with.

6.2.4   Dependency of particle and rock surface zeta potential on chemical conditions

The chemical composition of the fluid has a strong effect on the zeta potential, as the percentage of divalent ions increases from 0 to 100 (KCl<artificial groundwater (AGW)<$CaCl_2$) the zeta potential of both the silica particles used and the sandstone surface shifts closer to zero. In the electrical double layer model, divalent ions more effectively balance the surface charge of a solid body in an aqueous solution, causing a reduction in double layer thickness and a greater rate of decrease in potential with distance from that surface. Unfortunately full quantification of this will have to wait until an appropriate model of sorption on the solid phase surface is available (in the case of the rock this may mean effectively a model of the clay mineral surface – see Section 6.2.3).

Changing pH also influences the sandstone zeta potential; when the pH is increased using NaOH the zeta potential of samples under four different solution chemical compositions becomes more negative. With the same change in pH, there is a more significant change in zeta potential for samples in monovalent ion solutions than in divalent solutions, with the result for mixed-valence AGW lying in between.

The sandstone system is very sensitive; changes in chemistry through carbonate dissolution and ion exchange affect both pH and ionic composition such that zeta potential is significantly altered.

6.2.5 Testing of traditional nanoparticle transport theory on nanoparticle transport in intact rock using measured zeta potential

The measured zeta potential of both sandstone and silica particles in KCl, AGW and CaCl$_2$ give a good qualitative description of the mobility behaviour of silica nanoparticles (NPs) in sandstone column experiments. The most negative zeta potential and the highest mobility are found in KCl, with the least negative zeta potential and lowest mobility in CaCl$_2$. AGW is made up of a mixture of mono- and divalent ions, and silica NP mobility in sandstone is intermediate to the two end members.

A good prediction of experimental C'/C$_0$ in the AGW and CaCl$_2$ systems can be found using CFT calculations; however the theoretical results, particularly that for AGW, are very sensitive to both the zeta potential and the Hamaker constant (A$_{123}$). The theoretical collision efficiency is under-predicted in KCl, so CFT predicts a complete breakthrough, which is not observed experimentally. The model predictions still provide a good indication of whether particle mobility is likely, so is a good starting point for assessment of particle transport in groundwater systems. Due to the sensitivity of DLVO-theory estimated attachment, and therefore CFT, to zeta potential and A$_{123}$, these parameters would need to be carefully measured under precisely the correct chemical conditions.

The shape of the experimental breakthrough curve is not well matched by the CFT modelling as tailing occurs in the experimental data following a change in concentration which is not predicted by the theory. This suggests a non-equilibrium, NP-concentration dependent process is involved, something which is not included in CFT.

Mass balance calculations show that in the KCl column experiments there is some release of previously retained material, but with 50% of the initially retained silica particles remaining in the column after a deionized water (DIW) flush. This may suggest that some particles are not held in primary minima, instead are possibly in secondary minima. In the AGW and $CaCl_2$ experiments the silica particle retention appears to be largely permanent, consistent with primary minimum attachment. Zeta potential measurements on the particles which are released indicate that the NP surfaces are still dominated by the divalent ions of the initial chemistry.

6.3   Can zeta potential be used as the basis for assessing the mobility of nanoparticles in sandstone groundwaters?

With increasing nanoparticle development and use, a method of easily assessing the likely nanoparticle mobility in groundwaters, without individual testing of each nanoparticle and aquifer combination, is required. The aim of this work has been to test whether zeta potential can be used for this purpose.

Zeta potential has been successfully used in assessing the stability of particle dispersions and a similar approach is considered here in the attempt to predict the attachment of nanoparticles to rock surfaces. This method has been investigated in coincidence with the use of a new technique for measuring surface zeta potential (SS-EFM) developed by Malvern Instruments. While it is generally important to particle mobility, aggregation has not been considered due to the stability of the silica particles over time and with various chemistries. Physical straining of particles has not been directly assessed as a consequence, as the ratio of nanoparticle size to pore throat diameter is such that aggregation would be needed before straining would occur.

The simplest method of quantitatively representing nanoparticle mobility in porous media using zeta potential is by a combination of DLVO and CFT calculations. The zeta potential of sandstone was found to vary little between samples taken from a 50m sandstone core, so a single value could potentially represent the full sequence. The zeta potential is, however, sensitive to the chemical composition of the electrolyte solution. The equilibrium concentration (C'/C_0) reached in column experiments have indicated that zeta potential can be used to indicate the relative mobility of nanoparticles under these different chemical conditions.

Application of the DLVO and CFT models was less successful overall. Although CFT calculations were found to reproduce the most important feature, C'/C_0, it is shown here, as in previous studies, not to represent the tailing observed in the experimental data. This suggests there are some processes important to the transport and attachment behaviour in this system that are not represented in the CFT model.

In CFT calculations the probability of particle attachment following a collision with another particle or surface is included using the collision efficiency, α. This factor, and therefore the breakthrough predicted by CFT, is very sensitive to the zeta potential, and also to the Hamaker constant (A_{132}). Estimating the degree of mobility, from C'/C_0 using CFT, with any certainty is difficult, as A_{132} quantification for a complex system such as rock would be a significant challenge. Also, while little variability has been observed in sandstone zeta potential (with the same chemical conditions), variation in this property may be seen below the measurement scale which could impact on the particle-surface interactions.

A useful step forward, however, would be to simply determine whether there would be breakthrough or not in a system. Application of the DLVO and CFT calculations using measured zeta potential values and A_{132} values derived from literature provides a prediction of the mobility of the three systems presented here that is broadly correct. The models correctly predict that particles in KCl and AGW are likely to be mobile and in $CaCl_2$ that there will be no breakthrough. Overall, for simple systems results are consistent with the suggestion that DLVO and CFT could be used to screen the mobility risk, however a great deal more work is needed to fully demonstrate this.

Main findings:

1. Calculations to predict particle breakthrough are very sensitive to zeta potential and the Hamaker constant;

2. Sandstone zeta potential varies little with rock unit, under the same chemical conditions;

3. There could, however, be variation in zeta potential below the few millimetre scale of the measurement.

4. Sandstone zeta potential is a function of the solution cation composition and pH (dependence on anion composition and ionic strength have not been specifically investigated here);

5. It has been suggested that the clays determine the zeta potential of this system, although an in-depth investigation of the zeta potential and surface area of sandstone mineral components is necessary;

6. Particles are not fractionated by zeta potential while passing through the sandstone columns;

7. DLVO and CFT calculations cannot predict the tailing observed in particle breakthrough;

8. Release of nanoparticles following attachment only reaches a maximum of 50%, even in DIW;

9. DLVO and CFT calculations can be used to broadly distinguish between mobile and immobile nanoparticles.

6.4 Recommendations for further work

Further work in this field can be split into two approaches; to quantify the breakthrough of particles in intact rock to include the mechanisms which cause tailing and to further investigate and develop the use of DLVO and CFT-type calculations as a simple screening tool for predicting nanoparticle mobility.

The experimental breakthrough curves could be modelled using a kinetics approach to try and quantify the tailing which has been observed. This will require investigation and quantification of kinetic attachment mechanisms.

As intact rock surfaces have been used in the column experiments, it will be important to understand the effect of the rock properties on attachment and mobility. Exploration of the effects of morphology, organic surface coatings and chemical interaction processes will be important. While an attempt has been made to understand the chemical interactions between the sandstone and the fluid using zeta potential measurements alone, elemental analysis of the effluent fluid and comparison of this with the input fluid would improve quantification of the importance of ion exchange. Analysis

of the sandstone and particle surfaces to identify the dominant ion species could also provide confirmation for the interpretation of the effluent particle zeta potential.

Characterisation of the nanoparticle dispersion properties will continue to be necessary, particularly if a stabiliser has been used to alter the particle surface properties for its designated purpose. Interaction of particles in the environment with natural stabilisers, such as humic and fulvic acids, could also alter particle behaviour, so surface property transformation over time should also be considered.

To interpret the mobility of nanoparticles quantitatively using DLVO and CFT requires knowledge of both the zeta potential and the Hamaker constant under the experimental conditions used.

A surface-area modified linear mixing model was found to reproduce the bulk zeta potential value for the sandstone samples. However, the literature values for the individual mineral zeta potential were taken from a wide range of studies using different preparation and storage methods, which are understood to have significant effects on the absolute value. In order to interpret the surface heterogeneity of the sandstone fully, and potentially other rock types, the relationship between bulk rock zeta potential, individual mineral zeta potential and mineral surface area and pore wall exposure needs to be further investigated. This would allow the transferability of the SS-EFM technique to other rock types to be tested, along with the interpretation of the results using a simple mixing model.

The value of zeta potential is limited by the scale at which the measurement can be taken. While SS-EFM measurements represent a reduction in the scale of the measurement to a few millimetres, the particles will interact with the sandstone surface at a much smaller scale. Heterogeneity below the millimetre scale could therefore be important, but not currently measureable.

While the DLVO and CFT calculations are sensitive to the Hamaker constant this has not been a focus for this work. An attempt at calculating the A_{132} has been made using literature values for individual minerals and assuming importance of clay minerals, as found for zeta potential. If traditional particle deposition theory is to be used further in the study of manufactured nanoparticles in aquifer rocks then an investigation of the Hamaker constant in various rock types and the effects of the use of an electrolyte solution rather than water need to be addressed.

In modelling nanoparticle transport using DLVO and CFT, the zeta potential and A_{132} are assumed to be constant. With particle attachment over time however the zeta potential and A_{132} could change, affected by the surface coverage of nanoparticles. The retention of particles could also impact on the hydraulic conductivity of the porous material. The interaction of manufactured nanoparticles with indigenous nanoparticles could also cause their initial properties to change. These are important considerations for future work.

7 LIST OF REFERENCES

Nanoscience and nanotechnologies: opportunities and uncertainties. London: The Royal Society & The Royal Academy of Engineering, 2004.

Malvern Instruments Ltd. 2013. Zetasizer Nano User Manual.

ACKLER, H. D., FRENCH, R. H. & CHIANG, Y. M. 1996. Comparisons of Hamaker constants for ceramic systems with intervening vacuum or water: From force laws and physical properties. *Journal of Colloid and Interface Science,* 179**,** 460-469.

ADAMCZYK, Z., NATTICH, M. & WASILEWSKA, M. 2010a. Irreversible adsorption of latex particles on fibrinogen covered mica. *Adsorption-Journal of the International Adsorption Society,* 16**,** 259-269.

ADAMCZYK, Z., ZAUCHA, M. & ZEMBALA, M. 2010b. Zeta Potential of Mica Covered by Colloid Particles: A Streaming Potential Study. *Langmuir,* 26**,** 9368-9377.

ALKAFEEF, S. F. & ALAJMI, A. F. 2006. Streaming potentials and conductivities of reservoir rock cores in aqueous and non-aqueous liquids. *Colloids and Surfaces A - Physicochemical and Engineering Aspects,* 289**,** 141-148.

ALKAFEEF, S. F. & ALAJMI, A. F. 2007. The electrical conductivity and surface conduction of consolidated rock cores. *Journal of Colloid and Interface Science,* 309**,** 253-261.

ALKAFEEF, S. F., GOCHIN, R. J. & SMITH, A. L. 1999. Measurement of the electrokinetic potential at reservoir rock surfaces avoiding the effect of surface conductivity. *Colloids and Surfaces A - Physicochemical and Engineering Aspects,* 159**,** 263-270.

ALKAN, M., DEMIRBAS, O. & DOGAN, M. 2005. Electrokinetic properties of kaolinite in mono- and multivalent electrolyte solutions. *Microporous and Mesoporous Materials,* 83**,** 51-59.

ALLEN, D. J., BREWERTON, L. J., COLEBY, L. M., GIBBS, B. R., LEWIS, M. A., MACDONALD, A. M., WAGSTAFF, S. J. & WILLIAMS, A. T. 1997. *The physical properties of major aquifers in England and Wales,* Keyworth, Nottingham, British Geological Survey.

ALVAREZ-SILVA, M., URIBE-SALAS, A., MIRNEZAMI, M. & FINCH, J. A. 2010. The point of zero charge of phyllosilicate minerals using the Mular-Roberts titration technique. *Minerals Engineering,* 23**,** 383-389.

ANDERSON, B. J. 2008. The mobility of colloids in red sandstone: the effect of flow rate and ionic strength. Unpublished MSc Thesis. University of Birmingham.

ANDREWS, M. 2007. Colloid Mobility Through the Wildmoor Sandstone Formation of the Permo-Triassic Red Bed Sequence. University of Birmingham.

AVENA, M. J. & DE PAULI, C. P. 1998. Proton adsorption and electrokinetics of an Argentinean montmorillonite. *Journal of Colloid and Interface Science,* 202**,** 195-204.

BALES, R. C., LI, S. M., YEH, T. C. J., LENCZEWSKI, M. E. & GERBA, C. P. 1997. Bacteriophage and microsphere transport in saturated porous media: Forced-gradient experiment at Borden, Ontario. *Water Resources Research,* 33**,** 639-648.

BASHAR, K. & TELLAM, J. H. 2011. Sandstones of unexpectedly high diffusibility. *Journal of Contaminant Hydrology,* 122**,** 40-52.

BERGSTROM, L. 1997. Hamaker constants of inorganic materials. *Advances in Colloid and Interface Science,* 70**,** 125-169.

BERGSTROM, L., MEURK, N., ARWIN, H. & ROWCLIFFE, D. J. 1996. Estimation of Hamaker constants of ceramic materials from optical data using Lifshitz theory. *Journal of the American Ceramic Society,* 79**,** 339-348.

BERNHARDT, C. 1988. Preparation of Suspensions for Particle-Size Analysis - Methodical Recommendations, Liquids and Dispersing Agents. *Advances in Colloid and Interface Science,* 29**,** 79-139.

BESRA, L., SENGUPTA, D. K. & ROY, S. K. 2000. Particle characteristics and their influence on dewatering of kaolin, calcite and quartz suspensions. *International Journal of Mineral Processing,* 59**,** 89-112.

BHATTACHARJEE, S., KO, C. H. & ELIMELECH, M. 1998. DLVO interaction between rough surfaces. *Langmuir,* 14**,** 3365-3375.

BLOOMFIELD, J. P., GOODDY, D. C., BRIGHT, M. I. & WILLIAMS, P. J. 2001. Pore-throat size distributions in Permo-Triassic sandstones from the United Kingdom and some implications for contaminant hydrogeology. *Hydrogeology Journal,* 9**,** 219-230.

BRADFORD, S. A., BETTAHAR, M., SIMUNEK, J. & VAN GENUCHTEN, M. T. 2004. Straining and attachment of colloids in physically heterogeneous porous media. *Vadose Zone Journal,* 3**,** 384-394.

BURLEY, S. D. 1984. Patterns of Diagenesis in the Sherwood Sandstone Group (Triassic), United-Kingdom. *Clay Minerals,* 19**,** 403-440.

CARLSON, J. J. & KAWATRA, S. K. 2011. Effects of CO(2) on the zeta potential of hematite. *International Journal of Mineral Processing,* 98**,** 8-14.

CARLSON, J. J. & KAWATRA, S. K. 2013. Factors Affecting Zeta Potential of Iron Oxides. *Mineral Processing and Extractive Metallurgy Review,* 34**,** 269-303.

CICERONE, D. S., REGAZZONI, A. E. & BLESA, M. A. 1992. Electrokinetic Properties of the Calcite Water Interface in the Presence of Magnesium and Organic-Matter. *Journal of Colloid and Interface Science,* 154**,** 423-433.

CORBETT, J. C. W., MCNEIL-WATSON, F., JACK, R. O. & HOWARTH, M. 2012. Measuring surface zeta potential using phase analysis light scattering in a simple dip cell arrangement. *Colloids and Surfaces,* 396**,** 169-176.

DAS, M. R., BORDOLOI, D., BORTHAKUR, P. C. & MAHIUDDIN, S. 2005. Kinetics and adsorption of benzoate and salicylate at the natural hematite–water interface. *Colloids and Surfaces A: Physicochemical and Engineering Aspects,* 254**,** 49-55.

DEBACHER, N. & OTTEWILL, R. H. 1992. An Electrokinetic Examination of Mica Surfaces in Aqueous Media. *Colloids and Surfaces,* 65**,** 51-59.

DELGADO, A., GONZALEZCABALLERO, F. & BRUQUE, J. M. 1986. On the Zeta Potential and Surface Charge Density of Montmorillonite in Aqueous Electrolyte Solutions. *Journal of Colloid and Interface Science,* 113**,** 203-211.

DELGADO, A. V., GONZALEZ-CABALLERO, F., HUNTER, R. J., KOOPAL, L. K. & LYKLEMA, J. 2007. Measurement and interpretation of electrokinetic phenomena. *Journal of Colloid and Interface Science,* 309**,** 194-224.

DEMIR, C., ABRAMOV, A. A. & CELIK, M. S. 2001. Flotation separation of Na-feldspar from K-feldspar by monovalent salts. *Minerals Engineering,* 14**,** 733-740.

DEMIR, C., BENTLI, I., GULGONUL, I. & CELIK, M. S. 2003. Effects of bivalent salts on the flotation separation of Na-feldspar from K-feldspar. *Minerals Engineering,* 16**,** 551-554.

DOGAN, A. U., DOGAN, M., ONAL, M., SARIKAYA, Y., ABURUB, A. & WURSTER, D. E. 2006. Baseline studies of The Clay Minerals Society source clays: Specific surface area by the Brunauer Emmett Teller (BET) method. *Clays and Clay Minerals,* 54**,** 62-66.

DUBOIS, I., HOLGERSSON, S., ALLARD, S. & MALMSTRÖM, M. Correlation between particle size and surface area for chlorite and K-feldspar. 2010.

DURAN, J. D. G., RAMOS-TEJADA, M. M., ARROYO, F. J. & GONZALEZ-CABALLERO, F. 2000. Rheological and electrokinetic properties of sodium montmorillonite suspensions - I. Rheological properties and interparticle energy of interaction. *Journal of Colloid and Interface Science,* 229**,** 107-117.

ELIMELECH, M. 1991. Kinetics of Capture of Colloidal Particles in Packed Beds Under Attractive Double Layer Interactions. *Journal of Colloid and Interface Science,* 146**,** 337-352.

ELIMELECH, M., GREGORY, J., JAI, X. & WILLIAMS, R. A. 1995. *Particle Deposition and Aggregation: Measurement, Modelling and Simulation,* Woburn, MA, USA, Butterworth-Heinemann.

ELIMELECH, M., NAGAI, M., KO, C. H. & RYAN, J. N. 2000. Relative insignificance of mineral grain zeta potential to colloid transport in geochemically heterogeneous porous media. *Environmental Science & Technology,* 34**,** 2143-2148.

ELIMELECH, M. & O'MELIA, C. R. 1990a. Effect of Electrolyte Type on the Electrophoretic Mobility of Polystyrene Latex Colloids. *Colloids and Surfaces,* 44**,** 165-178.

ELIMELECH, M. & O'MELIA, C. R. 1990b. Effect of Particle-Size on Collision Efficiency in the Deposition of Brownian Particles with Electrostatic Energy Barriers. *Langmuir,* 6**,** 1153-1163.

ELIMELECH, M. & O'MELIA, C. R. 1990c. Kinetics of Deposition of Colloidal Particles in Porous Media. *Environmental Science & Technology,* 24**,** 1528-1536.

FARMAKIS, L., LIORIS, N., KOHADIMA, A. & KARAISKAKIS, G. 2006. Estimation of the Hamaker constants by sedimentation field-flow fractionation. *Journal of Chromatography A,* 1137**,** 231-242.

FAURE, B., SALAZAR-ALVAREZ, G. & BERGSTROM, L. 2011. Hamaker Constants of Iron Oxide Nanoparticles. *Langmuir,* 27**,** 8659-8664.

FRANCHI, A. & O'MELIA, C. R. 2003. Effects of natural organic matter and solution chemistry on the deposition and reentrainment of colloids in porous media. *Environmental Science & Technology,* 37**,** 1122-1129.

FRENCH, R. H., CANNON, R. M., DENOYER, L. K. & CHIANG, Y. M. 1995. Full Spectral Calculation of Nonretarded Hamaker Constants for Ceramic Systems from Interband Transition Strengths. *Solid State Ionics,* 75**,** 13-33.

FRIEL, J. J. 2000. *Practical Guide to Image Analysis,* USA, ASM International.

GENCE, N. & OZBAY, N. 2006. pH dependence of electrokinetic behavior of dolomite and magnesite in aqueous electrolyte solutions. *Applied Surface Science,* 252**,** 8057-8061.

GREENWOOD, R., LAPČÍKOVÁ, B., SURÝNEK, M., WATERS, K. & LAPČÍK, L. 2007. The zeta potential of kaolin suspensions measured by electrophoresis and electroacoustics. *Chemical Papers,* 61**,** 83-92.

GREGORY, J. 1981. Approximate Expressions for Retarded Van der Waals Interaction. *Journal of Colloid and Interface Science,* 83**,** 138-145.

GRESWELL, R. B., RAHMAN, S. H., CUTHBERT, M. O. & TELLAM, J. H. 2010. An inexpensive flow-through laser nephelometer for the detection of natural colloids and manufactured nanoparticles. *Journal of Hydrology,* 388**,** 112-120.

HAHN, M. W., ABADZIC, D. & O'MELIA, C. R. 2004. Aquasols: On the role of secondary minima. *Environmental Science & Technology,* 38**,** 5915-5924.

HAHN, M. W. & O'MELIA, C. R. 2004. Deposition and reentrainment of Brownian particles in porous media under unfavorable chemical conditions: Some concepts and applications. *Environmental Science & Technology,* 38**,** 210-220.

HARVEY, R. W., KINNER, N. E., MACDONALD, D., METGE, D. W. & BUNN, A. 1993. Role of Physical Heterogeneity in the Interpretation of Small-Scale Laboratory and Field Observations of Bacteria, Microbial-Sized Microsphere, and Bromide Transport Through Aquifer Sediments. *Water Resources Research,* 29**,** 2713-2721.

HIEMENZ, P. C. & RAJAGOPALAN, R. 1997. *Principles of Colloid and Surface Chemistry,* New York, Marcel Dekker.

HIGGO, J. J. W., WILLIAMS, G. M., HARRISON, I., WARWICK, P., GARDINER, M. P. & LONGWORTH, G. 1993. Colloid Transport in a Glacial Sand Aquifer - Laboratory and Field Studies. *Colloids and Surfaces A-Physicochemical and Engineering Aspects,* 73**,** 179-200.

HOGG, R., HEALY, T. W. & FUERSTEN.DW 1966. Mutual Coagulation of Colloidal Dispersions. *Transactions of the Faraday Society,* 62**,** 1638-&.

HORIKAWA, Y., MURRAY, R. S. & QUIRK, J. P. 1988. The Effect of Electrolyte Concentration on the Zeta Potentials of Homoionic Montmorillonite and Illite. *Colloids and Surfaces,* 32**,** 181-195.

HUNTER, R. J. 1981. *Zeta Potential in Colloid Science*, Academic Press Inc. (London) Ltd.

HUNTER, R. J. 1993. *Introduction to Modern Colloid Science*, Oxford University Press.

HUNTER, R. J. 2001. *Foundations of Colloid Science,* Oxford, UK, Oxford University Press.

ISRAELACHVILI, J. N. 2011. *Intermolecular and Surface Forces,* USA, Academic Press.

JACOBASCH, H. J., SIMON, F. & WEIDENHAMMER, P. 1998. Adsorption of ions onto polymer surfaces and its influence on zeta potential and adhesion phenomena. *Colloid and Polymer Science,* 276**,** 434-442.

JOHNSON, P. R. 1999. A comparison of streaming and microelectrophoresis methods for obtaining the zeta potential of granular porous media surfaces. *Journal of Colloid and Interface Science,* 209**,** 264-267.

JOHNSON, P. R., SUN, N. & ELIMELECH, M. 1996. Colloid transport in geochemically heterogeneous porous media: Modeling and measurements. *Environmental Science & Technology,* 30**,** 3284-3293.

JOHNSON, W. P. & TONG, M. P. 2006. Observed and simulated fluid drag effects on colloid deposition in the presence of an energy barrier in an impinging jet system. *Environmental Science & Technology,* 40**,** 5015-5021.

KAYA, A. & YUKSELEN-AKSOY, Y. 2005. Zeta potential of clay minerals and quartz contaminated by heavy metals. *Canadian Geotechnical Journal,* 42**,** 1280-1289.

KOSMULSKI, M., MACZKA, E., JANUSZ, W. & ROSENHOLM, J. B. 2002. Multiinstrument study of the electrophoretic mobility of quartz. *Journal of Colloid and Interface Science,* 250**,** 99-103.

LEE, S. & SIGMUND, W. M. 2001. Repulsive van der Waals forces for silica and alumina. *Journal of Colloid and Interface Science,* 243**,** 365-369.

LI, H. C. & DEBRUYN, P. L. 1966. Electrokinetic and Adsorption Studies on Quartz. *Surface Science,* 5**,** 203-&.

LI, X. Q., SCHEIBE, T. D. & JOHNSON, W. P. 2004. Apparent decreases in colloid deposition rate coefficients with distance of transport under unfavorable deposition conditions: A general phenomenon. *Environmental Science & Technology,* 38**,** 5616-5625.

LI, Y. S., WANG, Y. G., PENNELL, K. D. & ABRIOLA, L. M. 2008. Investigation of the transport and deposition of fullerene (C60) nanoparticles in quartz sands under varying flow conditions. *Environmental Science & Technology,* 42**,** 7174-7180.

LOGAN, B. E., JEWETT, D. G., ARNOLD, R. G., BOUWER, E. J. & O'MELIA, C. R. 1995. Clarification of Clean-Bed Filtration Models. *Journal of Environmental Engineering-Asce,* 121**,** 869-873.

LOVELAND, J. P., BHATTACHARJEE, S., RYAN, J. N. & ELIMELECH, M. 2003. Colloid transport in a geochemically heterogeneous porous medium: aquifer tank experiment and modeling. *Journal of Contaminant Hydrology,* 65**,** 161-182.

LYONS, J., FURLONG, D. & HEALY, T. 1981. The electrical double-layer properties of the mica (muscovite)-aqueous electrolyte interface. *Australian Journal of Chemistry,* 34**,** 1177-1187.

MACHT, F., EUSTERHUES, K., PRONK, G. J. & TOTSCHE, K. U. 2011. Specific surface area of clay minerals: Comparison between atomic force microscopy measurements and bulk-gas (N-2) and -liquid (EGME) adsorption methods. *Applied Clay Science,* 53**,** 20-26.

MAROUF, R., MAROUF-KHELIFA, K., SCHOTT, J. & KHELIFA, A. 2009. Zeta potential study of thermally treated dolomite samples in electrolyte solutions. *Microporous and Mesoporous Materials,* 122**,** 99-104.

MCMILLAN, L. 2010. Characterisation of Manufactured Nanoparticle Migration in Sandstone Aquifers. Unpublished MSc Thesis. University of Birmingham.

MEDOUT-MARERE, V. 2000. A simple experimental way of measuring the Hamaker constant A(11) of divided solids by immersion calorimetry in apolar liquids. *Journal of Colloid and Interface Science,* 228**,** 434-437.

MICHAEL, H. L. & WILLIAMS, D. J. A. 1984. Electrochemical Properties of Quartz. *Journal of Electroanalytical Chemistry,* 179**,** 131-139.

NANTHAKUMAR, B., ARINAITWE, E. & PAWLIK, M. 2010. Adsorption of sodium lignosulfonates on hematite. *Adsorption-Journal of the International Adsorption Society,* 16**,** 447-455.

NAVARRO, E., BAUN, A., BEHRA, R., HARTMANN, N. B., FILSER, J., MIAO, A. J., QUIGG, A., SANTSCHI, P. H. & SIGG, L. 2008. Environmental behavior and ecotoxicity of engineered nanoparticles to algae, plants, and fungi. *Ecotoxicology,* 17**,** 372-386.

NELSON, K. E. & GINN, T. R. 2005. Colloid filtration theory and the Happel sphere-in-cell model revisited with direct numerical simulation of colloids. *Langmuir,* 21**,** 2173-2184.

NELSON, K. E. & GINN, T. R. 2011. New collector efficiency equation for colloid filtration in both natural and engineered flow conditions. *Water Resour. Res.,* 47**,** W05543.

NEUKUM, C., BRAUN, A. & AZZAM, R. 2014. Transport of stabilized engineered silver (Ag) nanoparticles through porous sandstones. *Journal of Contaminant Hydrology,* 158**,** 1-13.

NISHIMURA, S., SCALES, P. J., TATEYAMA, H., TSUNEMATSU, K. & HEALY, T. W. 1995. Cationic Modification of Muscovite Mica - an Electrokinetic Study. *Langmuir,* 11**,** 291-295.

NISHIMURA, S., TATEYAMA, H., TSUNEMATSU, K. & JINNAI, K. 1992. Zeta Potential Measurement of Muscovite Mica Basal Plane Aqueous Solution Interface by Means of Place Interface Technique. *Journal of Colloid and Interface Science,* 152**,** 359-367.

NYSTROM, R., LINDEN, M. & ROSENHOLM, J. B. 2001. The influence of Na+, Ca2+, Ba2+, and La3+ on the zeta potential and the yield stress of calcite dispersions. *Journal of Colloid and Interface Science,* 242**,** 259-263.

OGATA, A. & BANKS, R. B. 1961. A solution of the differential equation of longitudinal dispersion in porous media. USGS Professional Paper: 411-A.

OVERBEEK, J. T. G. 1977. Recent developments in the understanding of colloid stability. *Journal of Colloid and Interface Science,* 58**,** 408-422.

PASHLEY, R. M. 1985. Electromobility of Mica Particles Dispersed in Aqueous-Solutions. *Clays and Clay Minerals,* 33**,** 193-199.

PATTENDEN, O. 2007. Colloid Facilitated Virus Transport through a saturated sandstone column. Unpublished MSc Thesis. University of Birmingham.

PELLEY, A. J. & TUFENKJI, N. 2008. Effect of particle size and natural organic matter on the migration of nano- and microscale latex particles in saturated porous media. *Journal of Colloid and Interface Science,* 321**,** 74-83.

PETOSA, A. R., JAISI, D. P., QUEVEDO, I. R., ELIMELECH, M. & TUFENKJI, N. 2010. Aggregation and Deposition of Engineered Nanomaterials in Aquatic Environments: Role of Physicochemical Interactions. *Environmental Science & Technology,* 44**,** 6532-6549.

PLANT, J. A., JONES, D. G. & HASLAM, H. W. (eds.) 1999. *The Cheshire Basin: Basin evolution, fluid movement and mineral resources in a Permo-Triassic rift setting,* Keyworth, Nottingham: The British Geological Survey.

PLAZA, R. C., GONZALEZ-CABALLERO, F. & DELGADO, A. V. 2001. Electrical surface charge and potential of hematite/yttrium oxide core-shell colloidal particles. *Colloid and Polymer Science,* 279**,** 1206-1211.

PREDALI, J. J. & CASES, J. M. 1973. Zeta Potential of Magnesian Carbonates in Inorganic Electrolytes. *Journal of Colloid and Interface Science,* 45**,** 449-458.

RAHMAN, S. H. 2006. Colloid Movement Through Saturated Sandstone Matrix. PhD Thesis. University of Birmingham.

RAJAGOPALAN, R. & TIEN, C. 1976. Trajectory Analysis of Deep-Bed Filtration with Sphere-in-Cell Porous-Media Model. *Aiche Journal,* 22**,** 523-533.

ROCO, M. C. & BAINBRIDGE, W. S. 2005. Societal implications of nanoscience and nanotechnology: Maximizing human benefit. *Journal of Nanoparticle Research,* 7**,** 1-13.

ROY, S. B. & DZOMBAK, D. A. 1996. Na+-Ca2(+) exchange effects in the detachment of latex colloids deposited in glass bead porous media. *Colloids and Surfaces A - Physicochemical and Engineering Aspects,* 119**,** 133-139.

RYAN, J. N. & ELIMELECH, M. 1996. Colloid mobilization and transport in groundwater. *Colloids and Surfaces a-Physicochemical and Engineering Aspects,* 107**,** 1-56.

RYAN, J. N., ELIMELECH, M., ARD, R. A., HARVEY, R. W. & JOHNSON, P. R. 1999. Bacteriophage PRD1 and silica colloid transport and recovery in an iron oxide-coated sand aquifer. *Environmental Science & Technology,* 33**,** 63-73.

SAIERS, J. E., HORNBERGER, G. M. & HARVEY, C. F. 1994. Colloidal Silica Transport Through Structured, Heterogeneous Porous-Media. *Journal of Hydrology,* 163**,** 271-288.

SAIERS, J. E. & RYAN, J. N. 2005. Colloid deposition on non-ideal porous media: The influences of collector shape and roughness on the single-collector efficiency. *Geophysical Research Letters,* 32.

SCALES, P. J., GRIESER, F. & HEALY, T. W. 1990. Electrokinetics of the Muscovite Mica Aqueous Solution Interface. *Langmuir,* 6**,** 582-589.

SCHRAMM, L. L., MANNHARDT, K. & NOVOSAD, J. J. 1991. Electrokinetic Properties of Reservoir Rock Particles. *Colloids and Surfaces,* 55**,** 309-331.

SCOWN, T. M., VAN AERLE, R. & TYLER, C. R. 2010. Review: Do engineered nanoparticles pose a significant threat to the aquatic environment? *Critical Reviews in Toxicology,* 40**,** 653-670.

SHAW, D. J. 1992. *Colloid and Surface Chemistry,* Oxford, UK, Butterworth-Heinemann.

SHELLENBERGER, K. & LOGAN, B. E. 2002. Effect of molecular scale roughness of glass beads on colloidal and bacterial deposition. *Environmental Science & Technology,* 36**,** 184-189.

SHEPHERD, K. A. 2003. *Contamination and groundwater quality in the Birmingham aquifer.* PhD, University of Birmingham.

SIDES, P. J., FARUQUI, D. & GELLMAN, A. J. 2009. Dynamics of Charging of Muscovite Mica: Measurement and Modeling. *Langmuir,* 25**,** 1475-1481.

SIDES, P. J., NEWMAN, J., HOGGARD, J. D. & PRIEVE, D. C. 2006. Calculation of the streaming potential near a rotating disk. *Langmuir,* 22**,** 9765-9769.

SIFFERT, B. & FIMBEL, P. 1984. Parameters Affecting the Sign and the Magnitude of the Electrokinetic Potential of Calcite. *Colloids and Surfaces,* 11**,** 377-389.

SONDI, I., BISCAN, J. & PRAVDIC, V. 1996. Electrokinetics of pure clay minerals revisited. *Journal of Colloid and Interface Science,* 178**,** 514-522.

SONDI, I., BISCAN, J., VDOVIC, N. & SKAPIN, S. D. 2009. The electrokinetic properties of carbonates in aqueous media revisited. *Colloids and Surfaces A - Physicochemical and Engineering Aspects,* 342**,** 84-91.

SONDI, I., MILAT, O. & PRAVDIC, V. 1997. Electrokinetic potentials of clay surfaces modified by polymers. *Journal of Colloid and Interface Science,* 189**,** 66-73.

SONG, L. F. & ELIMELECH, M. 1994. Transient Deposition of Colloidal Particles in Heterogeneous Porous Media. *Journal of Colloid and Interface Science,* 167**,** 301-313.

SONG, L. F., JOHNSON, P. R. & ELIMELECH, M. 1994. Kinetics of Colloid Deposition onto Heterogeneously Charged Surfaces in Porous Media. *Environmental Science & Technology,* 28**,** 1164-1171.

STEPHAN, E. A. & CHASE, G. G. 2001. A preliminary examination of zeta potential and deep bed filtration activity. *Separation and Purification Technology,* 21**,** 219-226.

STEVENTON-BARNES, H. 2001. *Solid organic carbon in UK aquifers: its role in sorption of organic contaminants.* PhD, University of London.

STUMM, W. & MORGAN, J. J. 1996. *Aquatic chemistry: chemical equilibria and rates in natural waters*, Wiley.

STUMM, W., SIGG, L. & SULZBERGER, B. 1992. *Chemistry of the Solid-Water Interface: Processes at the Mineral-Water and Particle-Water Interface in Natural Systems*, Wiley.

TELLAM, J. H. 1995. Hydrochemistry of the Saline Groundwaters of the Lower Mersey Basin Permo-Triassic Sandstone Aquifer, UK. *Journal of Hydrology,* 165**,** 45-84.

TELLAM, J. H. & BARKER, R. D. 2006. Towards prediction of saturated-zone pollutant movement in groundwaters in fractured permeable-matrix aquifers: the case of the UK Permo-Triassic sandstones. *Fluid Flow and Solute Movement in Sandstones: The Onshore UK Permo-Triassic Red Bed Sequence,* 263**,** 1-48.

THOMPSON, D. W. & POWNALL, P. G. 1989. Surface Electrical Properties of Calcite. *Journal of Colloid and Interface Science,* 131**,** 74-82.

TUFENKJI, N. 2007. Modeling microbial transport in porous media: Traditional approaches and recent developments. *Advances in Water Resources,* 30**,** 1455-1469.

TUFENKJI, N. & ELIMELECH, M. 2004a. Correlation equation for predicting single-collector efficiency in physicochemical filtration in saturated porous media. *Environmental Science & Technology,* 38**,** 529-536.

TUFENKJI, N. & ELIMELECH, M. 2004b. Deviation from the classical colloid filtration theory in the presence of repulsive DLVO interactions. *Langmuir,* 20**,** 10818-10828.

TUFENKJI, N., REDMAN, J. A. & ELIMELECH, M. 2003. Interpreting deposition patterns of microbial particles in laboratory-scale column experiments. *Environmental Science & Technology,* 37**,** 616-623.

VAN GENUCHTEN, M. T. & ALVES, W. J. 1982. *Analytical Solutions of the One-Dimensional Convective-Dispersive Solute Transport Equation*, U.S. Department of Agriculture, Agricultural Research Service.

VANE, L. M. & ZANG, G. M. 1997. Effect of aqueous phase properties on clay particle zeta potential and electro-osmotic permeability: Implications for electro-kinetic soil remediation processes. *Journal of Hazardous Materials,* 55**,** 1-22.

VDOVIC, N. 2001. Electrokinetic behaviour of calcite - the relationship with other calcite properties. *Chemical Geology,* 177**,** 241-248.

VDOVIC, N. & BISCAN, J. 1998. Electrokinetics of natural and synthetic calcite suspensions. *Colloids and Surfaces A - Physicochemical and Engineering Aspects,* 137**,** 7-14.

VISSER, J. 1972. On Hamaker constants: A comparison between Hamaker constants and Lifshitz-van der Waals constants. *Advances in Colloid and Interface Science,* 3**,** 331-363.

WANG, Y. M., FORSSBERG, E. & PUGH, R. J. 1992. The Influence of Ph on the High-Gradient Magnetic Separation of Less-Than-10-Mu-M Particles of Hematite and Quartz. *International Journal of Mineral Processing,* 36**,** 93-105.

YAO, K. M., HABIBIAN, M. M. & O'MELIA, C. R. 1971. Water and Waste Water Filtration - Concepts and Applications. *Environmental Science & Technology,* 5**,** 1105-&.

YUKSELEN-AKSOY, Y. & KAYA, A. 2003. Zeta potential of kaolinite in the presence of alkali, alkaline earth and hydrolyzable metal ions. *Water Air and Soil Pollution,* 145**,** 155-168.

YUKSELEN-AKSOY, Y. & KAYA, A. 2011. A study of factors affecting on the zeta potential of kaolinite and quartz powder. *Environmental Earth Sciences,* 62**,** 697-705.

ZHANG, J. W. & BUFFLE, J. 1995. Kinetics of Hematite Aggregation by Polyacrylic-Acid - Importance of Charge Neutralization. *Journal of Colloid and Interface Science,* 174**,** 500-509.

ZHAO, H. Y., BHATTACHARJEE, S., CHOW, R., WALLACE, D., MASLIYAH, J. H. & XU, Z. H. 2008. Probing Surface Charge Potentials of Clay Basal Planes and Edges by Direct Force Measurements. *Langmuir,* 24**,** 12899-12910.

ZHUANG, J., QI, J. & JIN, Y. 2005. Retention and transport of amphiphilic colloids under unsaturated flow conditions: Effect of particle size and surface property. *Environmental Science & Technology,* 39**,** 7853-7859.